Spring 2011

Regional pulmonary function analysis using image registration

Kaifang Du
University of Iowa

REGIONAL PULMONARY FUNCTION ANALYSIS

USING IMAGE REGISTRATION

by

Kaifang Du

A thesis submitted in partial fulfillment of the
requirements for the Master of Science
degree in Biomedical Engineering
in the Graduate College of
The University of Iowa

May 2011

Thesis Supervisor: Professor Joseph M. Reinhardt

Graduate College
The University of Iowa
Iowa City, Iowa

CERTIFICATE OF APPROVAL

MASTER'S THESIS

This is to certify that the Master's thesis of

Kaifang Du

has been approved by the Examining Committee for the thesis requirement for the Master of Science degree in Biomedical Engineering at the May 2011 graduation.

Thesis Committee: _____
Joseph M. Reinhardt, Thesis Supervisor

_____
John E. Bayouth

_____
Gary E. Christensen

_____
Madhavan L. Raghavan

_____
Edwin L. Dove

ACKNOWLEDGEMENTS

First of all, I would like to thank my advisor Prof. Reinhardt for his elaborate instructions and patient guidance. I have being impressed and inspired by his serious attitude to science, meticulous research spirit and excellence of work style.

I would like to express sincere respect to Dr. Bayouth, who is also my advisor, for his support and encouragement on my research. I am very grateful to Prof. Christensen for his wise advice on image registration. I would like to thank Prof. Raghavan and his student Ryan Amelon for their talented suggestions on lung mechanical analysis. I would like to express my sincere gratitude to Kai Ding, Who was also a phD student of Prof. Reinhardt and my collaborator. Kai lead me to the gate of lung research and helped me a lot in both work and life, with his aggressive research spirit, profound knowledge and optimistic life attitude. I enjoyed working with him. I would like to give special thanks to Kunlin Cao, who is a phD candidate of Prof. Christensen, for her selfless help on image registration. I benefitted a lot from the bright discussion with Kunlin. Thanks to Divya Maxwell for her outstanding assistance in landmark picking. Thanks to my labmates Lijun Shi, Xiayu Xu, Panfang Hua, Vinayak Joshi, Sandeep Bodduluri and Richard Amendola for being helpful and hanging out.

This word was supported in part by grants 2009 Carver Collaborative Pilot Grant and EB004126 from the National Institutes of Health.

Finally, this thesis is dedicated to my loved parents and family. Their silent

support behind me is my biggest motivation.

The contributions of all people are greatly appreciated.

ABSTRACT

Lung function depends on the expansion and contraction of lung tissue during the respiratory cycle. The measurement of regional pulmonary function is of great interest and importance since many lung diseases can cause changes in biomechanical or material properties. It is also significant to study the radiation-induced changes in pulmonary function following radiation therapy.

In this thesis, we propose a technique that uses four-dimensional (3D+time) CT imaging (4DCT), 3D non-rigid image registration to estimate regional lung function. Lung images reconstructed at different inflation levels are analyzed for dynamic lung function development during a breath cycle. We demonstrate local pulmonary function can be reproducibly measured using 4DCT in human subjects prior to RT. The image registration accuracy is validated using semi-automatic anatomic landmark picking system.

The major contributions of this thesis include: 1) demonstrating the robustness and reproducibility of regional pulmonary function measurement using 4DCT in both sheep and human subjects, 2) developing approaches to improve the measurement reproducibility by dynamic lung volume matching and Jacobian normalization, 3) development and comparison four cubic metrics for reproducibility analysis, 4) research on time-varying lung ventilation in different breathing phases in both sheep and human subjects. Our contributions in this thesis are useful for diagnosis and assessment of lung diseases, useful for qualifying radiation induced changes in pul-

monary function in irradiated and non-irradiated lung tissue.

TABLE OF CONTENTS

LIST OF TABLES

LIST OF FIGURES

CHAPTER 1
INTRODUCTION

1.1 Regional Lung Function Measurement

The primary function of the lung is gas exchange. During each respiratory cycle, the lung undergoes tissue expansion and contraction, which in turn depends on the material and mechanical properties of lung parenchyma. The breathing action and timing are ensured by the cooperation of the lung, diaphragm and other parts of respiratory system. Many lung diseases affect pulmonary function by changing the tissue material and mechanical properties. For example, pulmonary emphysema, a component of chronic obstructive pulmonary disease (COPD), results from tissue elasticity decline (increased tissue compliance) with the destruction of structures supporting the alveoli and the destruction of capillaries feeding the alveoli [35]. In the other direction, one interstitial lung disease called idiopathic pulmonary fibrosis (IPF) can cause lung inflammation and fibrosis by making lung tissue thicker and stiffer (reduced tissue compliance). Lung breathing ability and breath pattern can also be impacted and influenced by lung cancers [39]. For lung undergoing radiation therapy (RT), radiation pneumonitis is a common treatment-related toxicity and alters pulmonary function, although radiotherapy improves locoregional control and survival in patients with non-small-cell lung cancer [32]. Since lung diseases and treatment are all associated with lung tissue mechanics changes, it would be very helpful to develop a method to look into the regional mechanics which determine pulmonary function.

Various methods have been developed for lung function analysis. Invasive methods, such as percutaneously or surgically implanted parenchymal markers or inhaled fluorescent microspheres, are not possible for translation to humans [23, 27, 37]. Nuclear medicine imaging such as positron emission tomography (PET) and single photon emission CT (SPECT) can be used to assess lung function [21], but their application cannot ensure the high spatial resolution of pulmonary image across several respiratory cycles. Traditional 3D CT image can provide high-resolution images for lung disease diagnosis but cannot provide ventilation information because it is static. Hyperpolarized noble gas MR imaging such as Helium (He^3) has been developed for lung pulmonary function assessment [33, 42, 26]. But this method has a bad reputation due to insufficient signal from airway walls and lung tissues in spite of the advantage of avoiding radiation to human body. The xenon-enhanced CT (Xe-CT) is another technique to directly assess regional lung function by observing the gas wash-in and wash-out rate on temporal image series [30, 41, 8]. Whereas the requirement of high temporal resolution limits the axis coverage about 2.5 cm to 12 cm while the typical z-axis extent of human lung is on the order of 25 cm. No specialized papers have involved the reproducibility of assessment of regional pulmonary function with Xenon-CT.

With the development of 4DCT imaging technique and 3D non-rigid image registration, many groups have turned to pulmonary function analysis in the perspective of lung tissue mechanics, since lung function is determined by the inherent material and mechanical properties of lung tissue. Guerrero et al. used optical-flow

registration to compute ventilation map from 4DCT [19, 18]. After identifying corresponding voxels across the 4DCT data set by optical flow image registration, the local ventilation (represented by change in fraction of air per voxel) was calculated from local averaged CT values. The calculated ventilation is summed and then compared to global lung volume change for validation. Christensen et al. applied image registration to cine-CT sequences and estimate local lung tissue expansion and contraction rate by Jacobian determinant [9]. Their study shows regional pulmonary measurements match well with spirometry test. In four of five individuals, over multiple breathing periods, the average log-Jacobian value and the air flow rate correlates well ($r^2 = 0.858$ on average for the entire lung). The correlation of the average log-Jacobian value and the air flow rate for images near the diaphragm correlated well in all five individuals ($r^2 = 0.943$ on average). Reinhardt et al. [36] compared this registration-based estimation on regional lung function to Xenon-CT and the average r^2 reaches 0.73. Fuld et al. [15] validated regional specific volume change against Xenon-CT specific ventilation in four anesthetized, ventilated sheep. Yamamoto et al. [48] demonstrated the strong correlation between the HU-based 4D-CT ventilation and emphysema, which indicates the potential for HU-based 4D-CT ventilation imaging to achieve high physiologic accuracy.

4DCT-based regional pulmonary function is also of great use when it comes to the applications like instructions on RT planning to reduce tissue irradiation and assessment of lung function change following RT courses. Recently Yaremko et al. [50] proposed a method incorporating image registration with 4DCT images to identify

regions of highly functional lung for avoidance in IMRT planning in non-small-cell lung cancer. Ding et al. [11] quantitatively measured the regional changes in lung tissue function following a course of radiation therapy by using 4DCT and image registration techniques. Keall et al. [49] also quantified the dosimetric impact of 4DCT and image registration derived pulmonary ventilation map on functional treatment planning to avoid high-functional lung regions. But the reproducibility of the method of pulmonary function using 4DCT and image registration is still uncertain. It is cloudy how much the measurement is affected by uncertainties in breath pattern and effort, image acquisition, reconstruction and image registration other than reflecting real pulmonary function change. We need to establish the robustness of this method for significant pulmonary function measurement.

1.2 Pulmonary 4D CT Imaging

The lung at different volumes and air pressure is studied for different pulmonary CT imaging protocol. Figure 1.1 shows an illumination of global lung capacities recorded on a spirometer. The definitions are:

Tidal Volume (TV): Volume inspired or expired with each normal breath.

Inspiratory Reserve Volume (IRV): Maximum volume that can be inspired over the inspiration of a tidal volume/normal breath. Used during exercise/exertion.

Expiratory Reserve Volume (ERV): Maximal volume that can be expired after the expiration of a tidal volume/normal breath.

Residual Volume (RV): Volume that remains in the lungs after a maximal expiration. It cannot be measured by spirometry.

Inspiratory Capacity (IC): Volume of maximal inspiration: IRV + TV.

Functional Residual Capacity (FRC): Volume of gas remaining in lung after normal expiration, cannot be measured by spirometry because it includes residual volume: ERV + RV.

Vital Capacity (VC): Volume of maximal inspiration and expiration: IRV + TV + ERV = IC + ERV.

Total Lung Capacity (TLC): The volume of the lung after maximal inspiration. The sum of all four lung volumes, cannot be measured by spirometry because it includes residual volume: IRV+ TV + ERV + RV = IC + FRC.

Static breath-hold scans are acquired at lung volumes near FRC or TLC and the 4DCT dynamic scan is at the tidal breathing volumes in the middle of figure 1.1 somewhere between FRC and FRC+TV. While the regional lung density information can be evaluated by static breath-hold images at well-controlled pressure [25, 24], the advantage of 4DCT-based regional ventilation study is in that we can reconstruct 3D lung images at any breathing phase of interest within a breathing cycle using retrospective gating methods. But the subject is going to receive more radiation dose than common 3D CT.

4D (3D + time) multi-detector CT imaging technology provides lung images

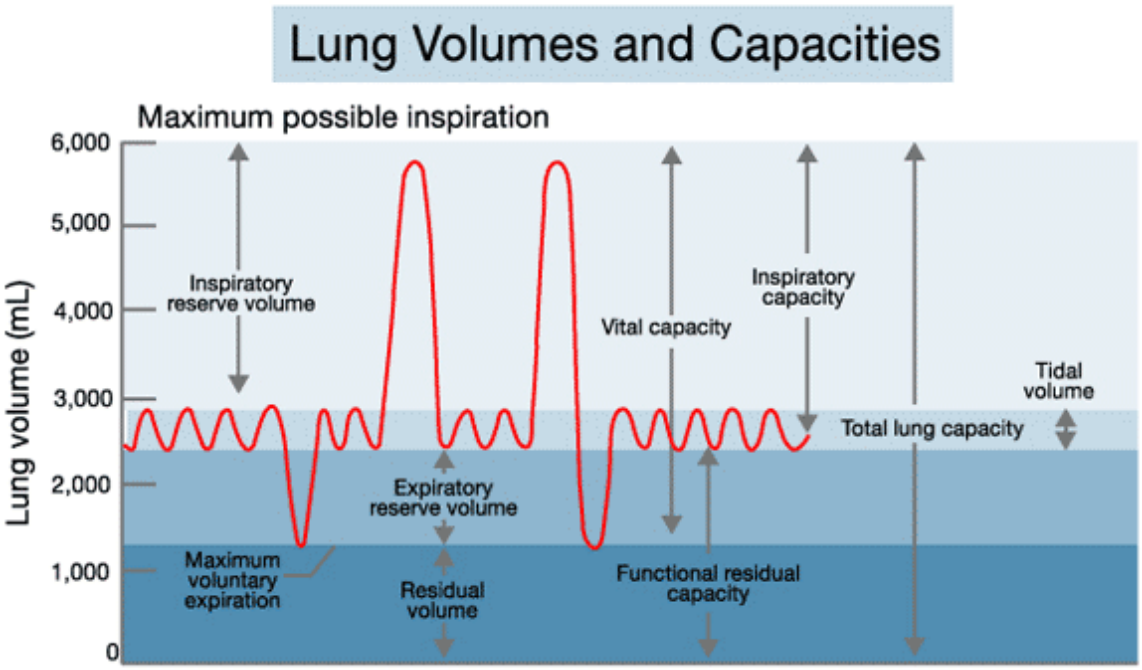

Figure 1.1: Lung volumes and capacities recorded on a spirometer, an apparatus for measuring inspired and expired volumes. Figure from [1].

at different respiratory phases of the breathing lung. Due to current spatio-temporal limitations of CT scanners, the entire lung cannot be imaged in a single respiratory cycle. One widely used alternative method is to acquire a 4DCT image using CT scanner in helical mode, which means the image data in adjacent couch positions are continuously acquired in sequence. To obtain time-resolved image data during the whole respiratory cycle, multiple image slices must be reconstructed at each couch positions in a time interval equal to the duration of a full cycle. During imaging the couch moves at a speed low enough so that a sufficient number of slices are acquired for a full respiratory cycle. If the CT tube rotation time is short compared to the period of motion, CT data acquisition can be achieved over several tube rotations. Because of the multi-detector scanner in data collection, the 2D image slices acquired at each couch position form an image stack, covering only part of the lung at a certain respiratory phase. Then in the post-processing stage, the stacks from all respiratory periods associated with a same specific respiratory phase are stacked and combined together to form a 3D CT image at that phase. By viewing temporally the 3D images in all sequential phases, the reconstruction of a 4DCT image is complete (see figure 1.2). If we use the multi-detector CT scanner in cine mode, the couch does not move during data acquisition. To summarize, this process includes two steps. The first is to acquire a set of CT images per slice through the volume; the second step is to resort the images and assemble spatio-temporally coherent data from acquired data, which are most certainly shuffled and out of order.

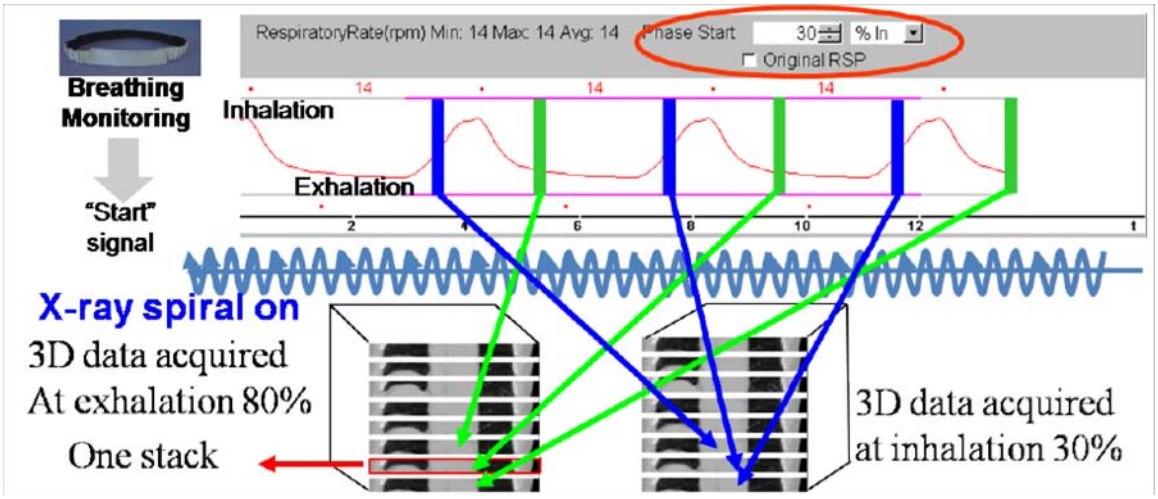

Figure 1.2: Illustration of 4DCT imaging. 4DCT image consists of a series of multiple 3D CT volume datasets at different respiratory phases. Each phase-specific 3D CT image is made of several groups of 2D slices (stacks), which are reconstructed from each period of respiration during acquisition. Figure from [20].

1.3 Basic Concepts in Image Registration

Lung mechanics and regional pulmonary function information can be extracted from the motion of all lung tissue from one breathing stage to another. Therefore first we need to map each image voxel to the corresponding voxel in the associated image. The problem can be solved by image registration whose task is to find the spatial transform for mapping between one image and another as shown in figure 1.3. Although various image registration algorithm have been developed, the basic components of the registration framework is basically the same, as shown in figure 1.4 [28, 10].

Images: The registration framework requires two input images. One is defined as the *moving* or *template* image I_1 and the other as the *fixed* or *target* image I_2. The

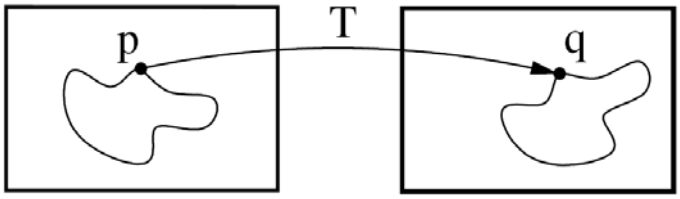

Figure 1.3: Image registration is the task of finding a spatial transformation mapping one image to another. Figure adapted from [28].

registration process can be treated as a optimization problem to find the best spatial mapping that align the moving image to the fixed image.Usaully, a multi-resolution strategy is employed to speed up the registration and enhance algorithm robustness. The multi-resolution strategy started from registering low resolution images of original input images. Then the acquired transform at low resolution will be used as the initial input transform of the next higher resolution level. In this way, the transform is computed step by step from coarse to fine until reaching the last level. The final transform is computed with composition and combination of transforms at all levels.

Transform: We use $\mathbf{h}(\mathbf{x})$ to indicate the transformation model which deforms each point in one image to its corresponding point in another image. The vector $\mathbf{x} = (x_1, x_2, x_3)^T$ is the voxel coordinate in one image. In order of increasing flexibility, the transformation models are the translation, the rigid, the similarity, the affine, the nonrigid B-spline and the nonrigid thin-plate spline like transformations. Among the non-rigid transformation models, B-splines [38] is widely used in deformable registration of medical imaging process like lung CT images. If we use $\phi_i = [\phi_x(\mathbf{x}_i), \phi_y(\mathbf{x}_i), \phi_z(\mathbf{x}_i)]^T$ to represent the coefficients of the i-th control point $\mathbf{x}_i$

on the spline grid G in each direction, then the transformation is represented as

$$\mathbf{h}(\mathbf{x}) = \mathbf{x} + \sum_{i \in G} \phi_i \beta^{(3)}(\mathbf{x} - \mathbf{x}_i), \tag{1.1}$$

Where ϕ_i describes the displacement information of control nodes on the image grid and $\beta^{(3)}(\mathbf{x})$ is a three-dimensional tensor product of cubic B-spline basis functions defined as

$$\beta^{(3)}(\mathbf{x}) = \beta^{(3)}(x)\beta^{(3)}(y)\beta^{(3)}(z). \tag{1.2}$$

Where $\beta^{(3)}(\mathbf{x})$ is a separable convolution kernel. In the uniform cubic B-Spline the basis function is defined as

$$\beta^{(3)}(x) = \begin{cases} (4 - 6x^2 + 3|x|^3)/6, & 0 \leq |x| < 1 \\ (2 - |x|)^3/6, & 1 \leq |x| < 2 \\ 0, & |x| \geq 2 \end{cases} . \tag{1.3}$$

Similar cases for $\beta^{(3)}(y)$ and $\beta^{(3)}(z)$.

Cost Function: The cost function measures how well the moving image is matched with the fixed image based on current transformation. A simple and common cost function metric is the sum of squared difference (SSD), which measures the intensity difference between two images at paired corresponding points. It is defined as

$$C_{\text{SSD}} = \int_{\mathbf{\Omega}} \left\{ [I_2(\mathbf{x}) - I_1(\mathbf{h}(\mathbf{x}))]^2 \right\} d\mathbf{x}. \tag{1.4}$$

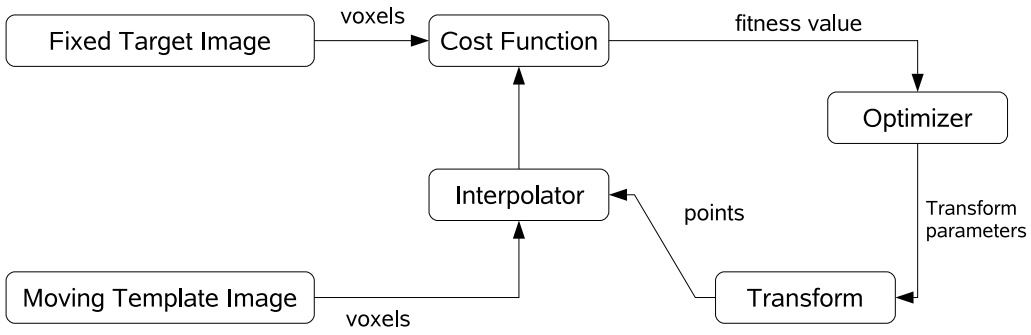

Figure 1.4: The basic components of the registration framework are two input images, a transform, a cost function, an interpolator and an optimizer. Adapted from [28].

A more complicated similarity metric, the sum of squared tissue volume difference (SSTVD) [51, 16, 52, 3] is specially designed to account for the intensity change in lung CT images. This cost function metric minimizes the local difference of tissue volume inside the lungs scanned at different air pressure levels. Assume the Hounsfield units (HU) of CT lung images are primarily contributed by tissue and air. Then the tissue volume in a voxel at position $\mathbf{x}$ can be estimated as $V(\mathbf{x}) = v(\mathbf{x})\frac{HU(\mathbf{x})-HU_{air}}{HU_{tissue}-HU_{air}}$ where $v(\mathbf{x})$ is the volume of voxel $\mathbf{x}$. It is assumed that $HU_{air} = -1000$ and $HU_{tissue} = 55$. The intensity similarity metric SSTVD is defined as

$$\begin{aligned} C_{\text{SSTVD}} &= \int_{\mathbf{\Omega}} [V_2(\mathbf{x}) - V_1(\mathbf{h}(\mathbf{x}))]^2 \, d\mathbf{x} \\ &= \int_{\mathbf{\Omega}} \left[v_2(\mathbf{x}) \frac{I_2(\mathbf{x}) + 1000}{1055} - v_1(\mathbf{h}(\mathbf{x})) \frac{I_1(\mathbf{h}(\mathbf{x})) + 1000}{1055} \right]^2 d\mathbf{x} \end{aligned} \quad (1.5)$$

Optimization: The solve of optimization problem is to obtain the optimal transformation parameter after the transformation in the last iteration moves in an optimized direction with a controlled step size. A limited-memory, quasi-Newton minimization method with bounds (L-BFGS-B) [2] algorithm is commonly used in B-spline based registration. By constraining the search space of parameters, certain properties are preserved during the optimization process. Based on the sufficient conditions to guarantee the local injectivity of functions parameterized by uniform cubic B-Splines proposed by Choi and Lee [7], the B-Splines coefficients can be constrained so that the transformation maintain the topology of two images.

Interpolator: The intensity interpolation is needed for evaluation at non-voxel position after intermediate transformations. Several methods for interpolation exist, varying in quality and speed. The nearest neighbor is the most simple technique and requires little resources, but low in quality. The returned value of linear interpolator is a weighted average of the surrounding voxels. For the B-spline interpolator, the higher the order, the better the quality, but also requiring more computation time. In fact, nearest neighbor (N=0) and linear interpolation (N=1) also fall in this category. To generate the final deformed result of the registration, a higher-order interpolation is usually required, for which we recommend N=3.

After the image registration, we should have obtained the voxel-by-voxel transformation. Based on the transformation matrix, many mechanical and mathematical analysis are performed tracking the regions of interest of the lung at difference conditions.

1.4 Organization of the Thesis

This thesis is divided into 4 chapters, which are organized as follows:

Chapter 2 presents our research on time-varying lung ventilation analysis of 4DCT using image registration. In this paper, we propose an image registration-based technique for assessing regional pulmonary function using multiple 4DCT phase images, which aims at measuring the regional ventilation within the respiratory cycle. Using data from four anesthetized mechanically-ventilated sheep, we showed the variation of ventilation at different phase and the ratio of the total lung volume that reaches the maximum ventilation during all respiratory phases. In specific, regional lung function during the first period of expiration immediately after the maximum inhalation was discussed. Ventral to dorsal regional expiration volume ratio patterns were compared. This chapter is based on:

1. Du, K., Ding, K., Cao, K., Bayouth, J.E., Christensen, G.E., Reinhardt, J.M.: Registration-based measurement of regional expiration volume ratio using dynamic 4DCT imaging. 2011 IEEE International Symposium on Biomedial Engineering (ISBI)

2. Ding, K., Du, K., Cao, K., Christensen, G.E., Reinhardt, J.M.: Time-varying lung ventilation analysis of 4DCT using image registration. 2011 International Conference on Acoustics, Speech and Signal Processing (ICASSP)

Chapter 3 talks about the reproducibility of 4DCT-based pulmonary function measurement using image registration. Data from nine patients about to undergo

radiation therapy and three mechanically respiratory-gated sheep were used for this analysis. We also propose a method to normalize Jacobian using the high correlation between mean of Jacobian and global lung volume change. This chapter has not been published.

Chapter 4 presents four metrics for the reproducibility of pulmonary function measurement including Jacobian ratio map, displacement vector area, displacement vector subtract and gamma index comparison of two Jacobian maps. Repeated 4DCT scans prior to RT are analyzed in this chapter with tissue volume preserving image registration. This chapter has not yet been published.

Chapter 5 concludes the thesis and proposes interesting potential improvements in future research.

CHAPTER 2
DYNAMIC LUNG VENTILATION ANALYSIS OF 4DCT USING IMAGE REGISTRATION

2.1 Introduction

With the development of CT imaging technique and respiratory gating methods, 4D CT imaging and 3D image registration were employed to locally estimate lung tissue expansion and contraction to obtain a lung function map over the whole lung [36, 6]. This technique has the advantages of increased resolution, reduction in time, and avoidance of agent exposure, compared to other image-based regional lung function methods such as positron emission tomography (PET) [40], single photon emission CT (SPECT) [31] and hyperpolarized noble gas MRI with helium (^{3}He) or xenon (^{129}Xe) [26]. Reinhardt et al. [36] compared registration-based estimation of regional lung function to Xenon-CT and the average r^2 reaches as high as 0.73. Marcucci et al [30] studied the distribution of pulmonary ventilation using Xe-enhanced CT in prone and supine dogs. In the supine position, ventilation increased with dependent location, with a mean slope of 7.3%/cm lung height, whereas no ventilation gradients were found at any location in the prone position. Unlike static CT scans, the import of 4D CT imaging can compensate the deficiency of low temporal resolution. 4D CT has become a routine imaging in many institutions as part of standard treatment planning for thoracic diseases. With image registration, we could utilize the images reconstructed at any time point of the respiratory circle to analyze regional

pulmonary function over a certain period of time.

During 4D CT imaging, subjects are scanned with simultaneous monitoring of breathing by the technique of respiratory tracing and gating. Then CT images are typically selected from a sequence of acquired images according to breathing phases, which are defined by depth of breathing. Theoretically images can be reconstructed at any breathing time point with the respiratory trace signal. A breathing circle should contain a series of breathing phases from end exhalation to end inhalation then return to end exhalation as a periodic process. Image registration is used to register the images in the breathing circle voxel-by-voxel and get a deformation field which stores the transformation information from one scan to another scan. The end expiration and end inspiration phases were used a lot to measure regional lung function [18, 11]. However, the other respiratory phases also contain abundant clinical information that can be exploited.

This chapter describes a new scheme to measure instantaneous regional ventilation from image registration of multiple 4DCT phases. We also show that the ventilation change during the respiratory cycle are region and phase dependent. In addition, we look into a specific breathing phases from maximum inhalation to the first expiration phase. Distributions of regional expiration ratio are analyzed in blocks from dorsal to ventral at two ROIs. The registration accuracy are evaluated using anatomical landmarks. These results may provide insight into the regional ventilation change within the respiratory cycle and may be used to follow regional function changes of lung cancer patients following radiation therapy.

2.1.1 Data Acquisition

Four adult sheep were used for these experiments. Appropriate animal ethics approval was obtained for these protocols from the University of Iowa Animal Care and Use Committee and the study adhered to NIH guidelines for animal experimentation. The animals are anesthetized using intravenous pentobarbital (2 cc of 50 mg/ml bolus, 2.5-5 mg/kg/hr maintenance), intubated, monitored for ECG and arterial pressure, and mechanically ventilated during the experiments. All images are acquired on a Siemens Sensation 64 multi-detector CT scanner (MDCT) (Siemens Medical Solutions; Erlangen, Germany) with the animals in the supine position using a dynamic imaging protocol. Images are reconstructed retrospectively at 25, 50, 75, and 100% phase points of the inspiratory portion and 75, 50, 25 and 0% of the expiration portion of the respiratory cycle (herein denoted as the $T1$, $T2$, $T3$, $T4$, $T5$, $T6$, $T7$ and $T0$ images). All the eight phases are used for ventilation measurements. The respiratory rate (RR) for the four animals ranges from 15 to 18 breaths per minute. All of the 4DCT images are reconstructed using a matrix of 512 by 512 pixels. The in-plane pixel spacing is approximately 0.5 mm $\times$ 0.5 mm.

2.1.2 Image Registration

The regularized tissue volume and vesselness measure preserving nonrigid registration algorithm is used to estimate transforms between different respiration phases. The algorithm regularizes its transformation using the Laplacian regularization constraint (LAP) and minimizes the sum of squared tissue volume difference (SSTVD) [52] and vesselness measure difference (SSVMD), utilizing the rich image

intensity information and natural anatomic landmarks provided by the vessels. This method has been shown to be effective in a recent online competition [5] at registering lung CT images across changes in lung volume.

Let I_1 and I_2 represent two 3D image volumes to be registered and Ω is the union domain of the images I_1 and I_2. The vector $\mathbf{x}$ defines the voxel coordinate within an image. The algorithm find the optimal transformation $\mathbf{h}$ that maps the template image I_1 to the target image I_2 by minimizing the cost function

$$C_{\text{TOTAL}} = C_{\text{SSTVD}} + \rho_1 C_{\text{SSVMD}} + \rho_2 C_{\text{LAP}}, \tag{2.1}$$

where C_{SSTVD} is the SSTVD cost, C_{SSVMD} is the SSVMD cost, C_{LAP} is the Laplacian regularization constraint, and ρ_1 and ρ_2 are weighting constants that control how the individual costs are combined to form the total cost.

The SSTVD cost assumes that the measured Hounsfield units (HU) in the lung CT images is a function of tissue and air content. Following the findings by Hoffman et. al [22], from the CT value of a given voxel, the tissue volume can be estimated as

$$V(\mathbf{x}) = \nu(\mathbf{x}) \frac{I(\mathbf{x}) - HU_{air}}{HU_{tissue} - HU_{air}} = \nu(\mathbf{x}) \beta(I(\mathbf{x})), \tag{2.2}$$

where $\nu(\mathbf{x})$ denotes the volume of voxel $\mathbf{x}$ and $I(\mathbf{x})$ is the intensity of a voxel at position $\mathbf{x}$. HU_{air} and HU_{tissue} refer to the intensity of air and tissue, respectively. In this work, we assume that air is -1000 HU and tissue is 0 HU.

Given (2.2), we can then define the SSTVD cost:

$$C_{\text{SSTVD}} = \int_{\Omega} \left[\nu_2(\mathbf{x})\beta(I_2(\mathbf{x})) - \nu_1(\mathbf{h}(\mathbf{x}))\beta(I_1(\mathbf{h}(\mathbf{x})))\right]^2 d\mathbf{x}. \tag{2.3}$$

With the warping function $\mathbf{h}(\mathbf{x})$, $I_1(\mathbf{h}(\mathbf{x}))$ can be interpolated from the template image. $\nu_1(\mathbf{h}(\mathbf{x}))$ can be calculated from the Jacobian $J(\mathbf{h}(\mathbf{x}))$ of the deformation as $\nu_1(\mathbf{h}(\mathbf{x})) = J(\mathbf{h}(\mathbf{x}))\nu_2(\mathbf{x})$.

As the blood vessels branch to small diameters, the raw grayscale information from vessel voxels provide almost no contribution to guide the intensity-based registration. To better utilize the information of blood vessel locations, we use Frangi's vesselness measure $F((\mathbf{x}))$ which is based on the eigenvalues of the Hessian matrix of image intensity. The eigenvalues, ordered by magnitude $|\lambda_1| \leq |\lambda_2| \leq |\lambda_3|$, are geometrically interpreted as principal curvatures and can be used to indicate the shape of underlying object [14]. The vesselness measure is rescaled to [0, 1] and can be considered as a probability-like estimate of vesselness features and the SSVMD is:

$$C_{\text{SSVMD}} = \int_{\Omega} \left[F_2(\mathbf{x}) - F_1(\mathbf{h}(\mathbf{x}))\right]^2 d\mathbf{x}. \tag{2.4}$$

Enforcing constraints on the transformation helps generate physiologically more meaningful registration results. Continuum mechanical models such as linear elasticity can be used to regularize the transformations. In this paper, a Laplacian operator is used to regularize the displacement fields $\mathbf{u}$ where $\mathbf{u} = \mathbf{h}(\mathbf{x}) - \mathbf{x}$. This

regularization term is formed as

$$C_{\text{LAP}} = \int_{\mathbf{\Omega}} ||\nabla^2 \mathbf{u}(\mathbf{x})||^2 d\mathbf{x}. \tag{2.5}$$

where $\nabla^2 = \nabla \cdot \nabla = \left[\frac{\partial^2}{\partial x_1^2} + \frac{\partial^2}{\partial x_2^2} + \frac{\partial^2}{\partial x_3^2}\right]$. Using a linear elasticity differential operator can help smooth the transformation, and help eliminate abrupt changes in the displacement fields.

The transformation $\mathbf{h}(\mathbf{x})$ is a cubic B-splines transform. Note that the Jacobian value must be positive here, which can be achieved by using displacement constraints on the control nodes [5]. The total cost in equation 2.1 is optimized using a limited-memory, quasi-Newton minimization method with bounds (L-BFGS-B) algorithm. In our study, we register $T1$ to $T0$, $T2$ to $T0$, ..., and $T7$ to $T0$. A semi-automatic landmark system is then used for landmark detection and annotation [34].

2.1.3 Time-Varying Regional Ventilation Analysis from Image Registration

After obtaining the displacement field, we can estimate regional ventilation using the Jacobian measure. This approach is based on the assumption that local volume change is due to air volume change alone, and thus, any regional volume change is due only to local air volume change. Since the Jacobian tells us the local volume expansion (or contraction) between any two lung phase volumes, after

registration, the regional volume at voxel $\mathbf{x}$ and phase t is equal to:

$$J(h(\mathbf{x},t)) = \begin{vmatrix} \frac{\partial h_1(\mathbf{x},t)}{\partial \mathbf{x}_1} & \frac{\partial h_2(\mathbf{x},t)}{\partial \mathbf{x}_1} & \frac{\partial h_3(\mathbf{x},t)}{\partial \mathbf{x}_1} \\ \frac{\partial h_1(\mathbf{x},t)}{\partial \mathbf{x}_2} & \frac{\partial h_2(\mathbf{x},t)}{\partial \mathbf{x}_2} & \frac{\partial h_3(\mathbf{x},t)}{\partial \mathbf{x}_2} \\ \frac{\partial h_1(\mathbf{x},t)}{\partial \mathbf{x}_3} & \frac{\partial h_2(\mathbf{x},t)}{\partial \mathbf{x}_3} & \frac{\partial h_3(\mathbf{x},t)}{\partial \mathbf{x}_3} \end{vmatrix}. \tag{2.6}$$

where $t = T_i, i = 0, 1, \ldots 7$. $h(\mathbf{x}, t)$ is the transformation calculated from the registration method described above and maps the template image I_{T_i} to the target image I_{T_0}. $h_1(\mathbf{x}, t)$ is the x component of $h(\mathbf{x}, t)$, $h_2(\mathbf{x}, t)$ is the y component of $h(\mathbf{x}, t)$, and $h_3(\mathbf{x}, t)$ is the z component of $h(\mathbf{x}, t)$.

Assume the volume of voxel at T_0 phase is 1, we have $V(\mathbf{x}, T_0) = 1$. Then take T_1 as the example, the volume can be computed by the transformation from I_{T_1} to I_{T_0}. In Lagrangian coordinate system, $V(\mathbf{x}, T_1) = V(\mathbf{x}, T_0)J(h_{1,0}(\mathbf{x}))$. Therefore, the regional ventilation at any phase interval $[T_{i-1}, T_i)$ can be measured by taking the derivative of the air volume V:

$$\begin{aligned} \dot{V}(\mathbf{x}, T_i, T_{i-1}) &= \frac{V(\mathbf{x}, T_i) - V(\mathbf{x}, T_{i-1})}{T_i - T_{i-1}} && (2.7) \\ &= \frac{J(h(\mathbf{x}, T_i)) - J(h(\mathbf{x}, T_{i-1}))}{T_i - T_{i-1}} && (2.8) \\ &= \frac{J(h_{i,0}(\mathbf{x})) - J(h_{i-1,0}(\mathbf{x}))}{T_i - T_{i-1}}, && (2.9) \end{aligned}$$

where $V(\mathbf{x}, T_i)$ and $V(\mathbf{x}, T_{i-1})$ are air volumes in voxel $\mathbf{x}$ at two neighboring phases T_i and T_{i-1}. $[T_{i-1}, T_i)$ is the time step between two neighboring phases for the measured respiratory cycle. With the ability to measure the instantaneous ventilation within

the respiratory cycle at different phases, we can analyze the ventilation variation at different intervals within the respiratory cycle in a voxel-by-voxel basis. Let the $t_{MIV}(\mathbf{x})$ represent the phase when a local region reaches its highest inspiring ventilation and $t_{MEV}(\mathbf{x})$ represent the phase when a local region reaches its highest expiring ventilation. They can be calculated as:

$$t_{MIV}(\mathbf{x}) = \underset{t}{\text{argmax}}(\dot{V}(\mathbf{x}, T_i, T_{i-1})), \quad \text{for} \quad t = [T_0, T_1), [T_1, T_2), [T_2, T_3), [T_3, T_4), \quad (2.10)$$

$$t_{MEV}(\mathbf{x}) = \underset{t}{\text{argmax}}(-\dot{V}(\mathbf{x}, T_i, T_{i-1})), \quad \text{for} \quad t = [T_4, T_5), [T_5, T_6), [T_6, T_7), [T_7, T_0). \quad (2.11)$$

In spirometry, forced expiratory volume in one second(FEV1) is the amount of air which can be forcibly exhaled from the lung in the first second of a forced exhalation. The FEV1 is an important lung function parameter in clinical for diagnosis of obstructive and restrictive lung disease such as COPD [13] and airway obstruction. To look into the regional expiration at FEV1 interval, we can measure that regional step ventilation during the maximum inspiration and the first expiration phase by simply dividing voxel-by-voxel Jacobian from end inspiration (100%IN) phase to end expiration phase and Jacobian from the first expiration (75%EX) phase to end expiration phase. The reason why we use here Jacobian ratio rather Jacobian subtract is because of the nonlinear character of Jacobian map. Similar Jacobian ratio maps at other expiration intervals can be computed in the same way. To study the ratio map into details, we divide the lung into 15 equal height slabs from ventral to dorsal. For

each slab, two blocks were chose at locations near diaphragm and near the middle lung height. The cross sectional size for each block is 11 mm by 11 mm. The mean and standard deviation of Jacobian values in each block were evaluated and compared between inspiration ventilation and the ventilation at expiration intervals to study the ventilation change distribution pattern from ventral to dorsal.

2.2 Results

Approximately 200 automatic identified landmarks within the lungs are used to compute the registration accuracy. The landmarks are uniformly distributed in the lung regions. Figure 2.1 shows an example of the distribution of the landmarks in one animal for the T_4 (100% inspiration phase) images, viewed in both the anterior-posterior and right-left angles. For all four animals and all phases, before registration, the average landmark distance is 2.96 mm with standard deviation 2.61 mm. After registration, the average landmark distance is 0.62 mm with standard deviation 0.55 mm. The results demonstrate that the registration results are in good agreement with the landmark locations defined by the human expert.

Figure 2.2 shows landmark distances before and after image registration for FEV1 regional expiration study. The landmark distances before registration for pair 100%IN to 0%IN are higher than pair 75%EX to 0%IN, which reflects the average larger deformation of lung from end expiration to end inspiration, inducing larger difference of landmark locations. The landmark distance after registration are all reduced to the order of less than 0.8 mm, confirming with previous reported registration accuracy of SSTVD registration algorithm described by [4, 5]. The landmark

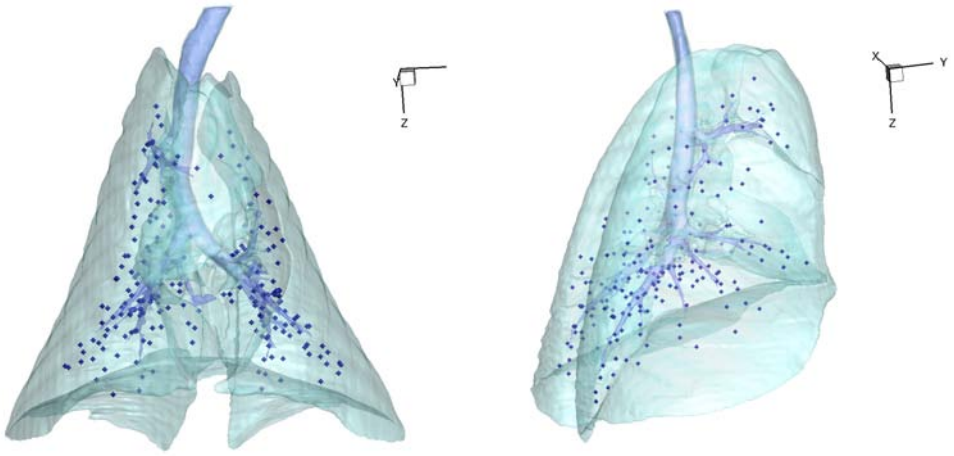

(a) (b)

Figure 2.1: 3D view of the landmarks in different angles: (a) anterior-posterior and (b) right-left. The spheres are the automatically defined landmarks.

distance analysis shows good image registration accuracy and guarantees the further regional lung function study.

Figure 2.3 shows the results based on the equation 2.10 (left column) and 2.11 (right column). The four rows (top to bottom) depict results for each of the four animals. To avoid the influence of noise, we overlay a significance map on the results. Every color region represents the breathing phase when the ventilation reaches its maximum, with significance larger than 2.0. To compute the significance, we subtract the chosen maximum ventilation with the geometrical average of the rest three, and then divide by the standard deviation. The grayscale regions are under significance 2.0. The results show that for all significant regions, during the inspiration portion of the respiratory cycle, the maximum ventilation is primarily at interval T_1 to T_2, while during the expiration portion, the maximum ventilation is mainly at interval

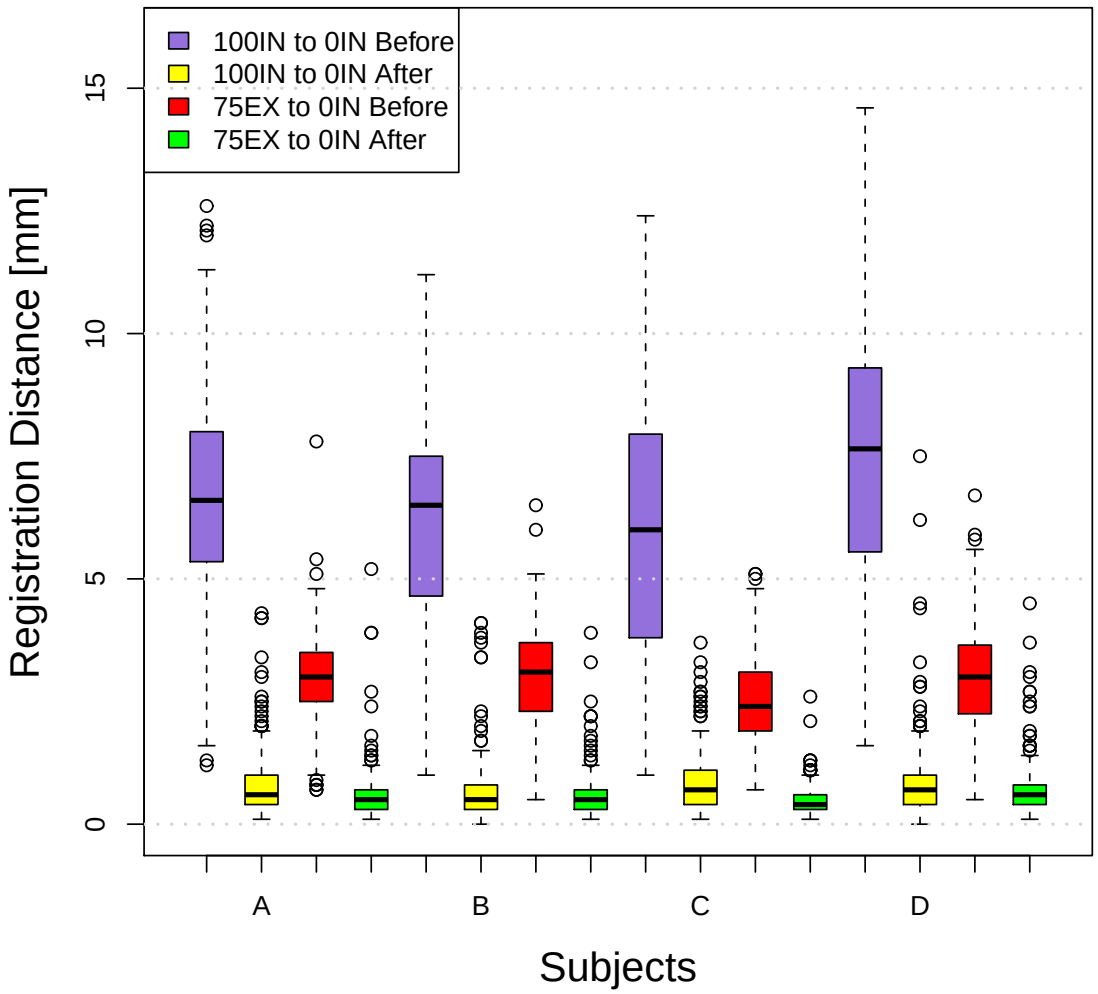

Figure 2.2: Lung landmark distance before and after registration of the two phase pairs (100%IN to 0%IN and 75%EX to 0%IN) for all four animals A, B, C, and D.

T_4 to T_5, which is at the beginning of expiration. From figure 2.4, 39% of the total lung volume reaches maximum ventilation at T_2 during inspiration and the 75% of the total lung volume reaches maximum ventilation at T_5 during expiration. The dynamic lung volumes ratio in figure 2.4 is calculated only at the significant regions. These results can be compared with the sheep mouth pressure versus time during imaging, as shown in figure 2.5 (a). We can notice the asymmetry of the curve that the mouth pressure during the first expiration intervals is much larger than the other three intervals.

Figure 2.6 shows color coded Jacobian maps in transverse view and coronal view representing regional lung function at different phases. All the color Jacobian maps are warped and overlapped onto end expiration phase. The color bars show color scale so different color represents different tissue expansion or contraction magnitude. Figure 2.7 and figure 2.8 show curves of statistical mean and standard deviation (showed as the error bars on marked points) across the 15 blocks from ventral to dorsal. As it shows in the illustration of figure 2.5 (b), the ROI blocks in figure 2.7 are near the diaphragm and the ROI blocks in figure 2.8 are at the middle height of the lung. The cross sectional area of the blocks is 11 mm by 11 mm at the coronal view. Inspiration ventilation from T_0 to T_4 and expiration ventilation for each expiration phases were compared. Since Jacobian represents expansion/contraction ratio which is non-linear, we use the natural logarithm of Jacobian as the vertical axis. Additionally, we flipped the T_4 to T_5 curve upside down by multiplying with -1, i.e. converting contraction to expansion symmetrically, in order to be compared with

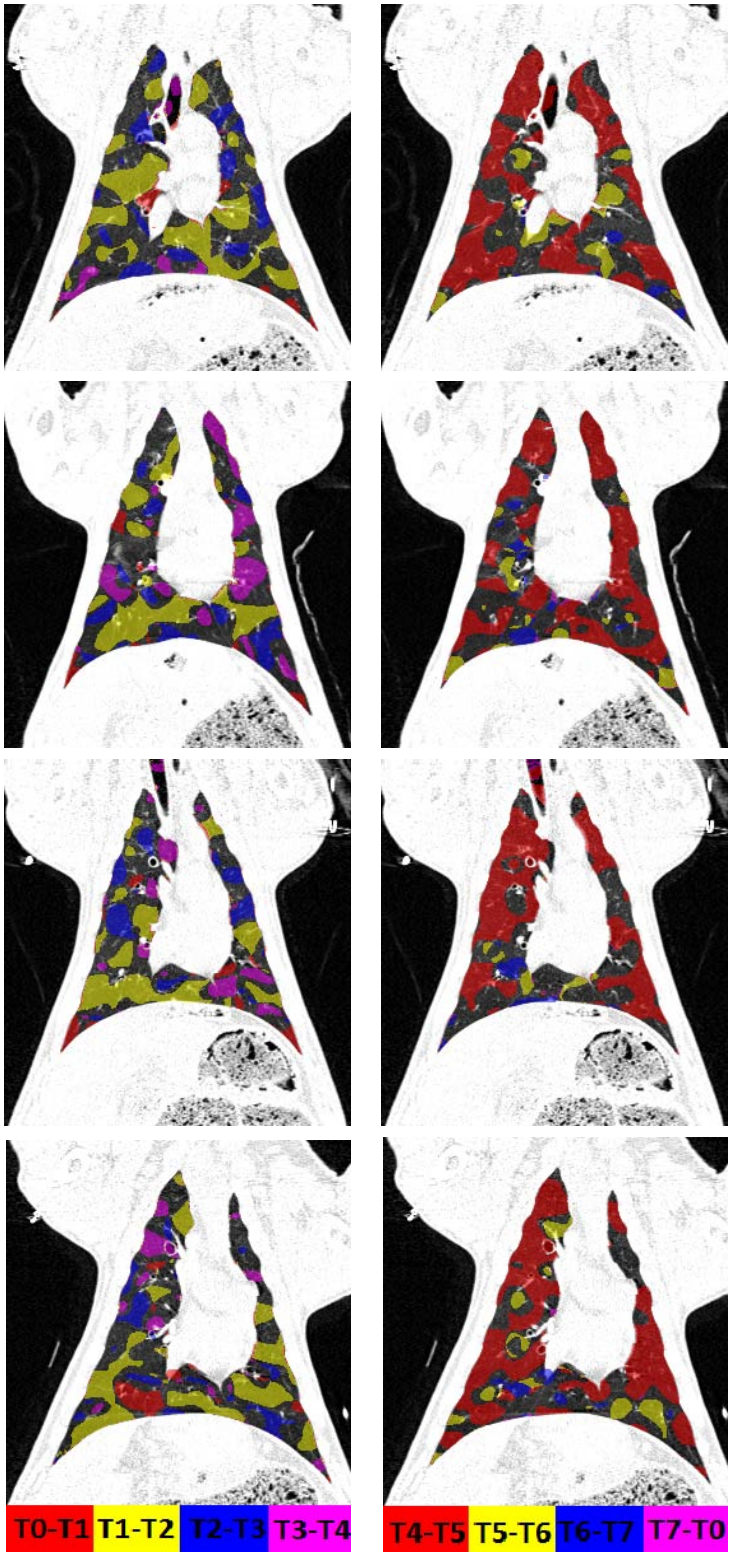

Figure 2.3: Color coded maps showing the variation of ventilation at different phase. Colors were overlaid only on the regions with large enough significance. From top to bottom, each row represent the t_{MIV} (left column) and the t_{MEV} from animals A, B, C and D. Note the color bars are different for two columns.

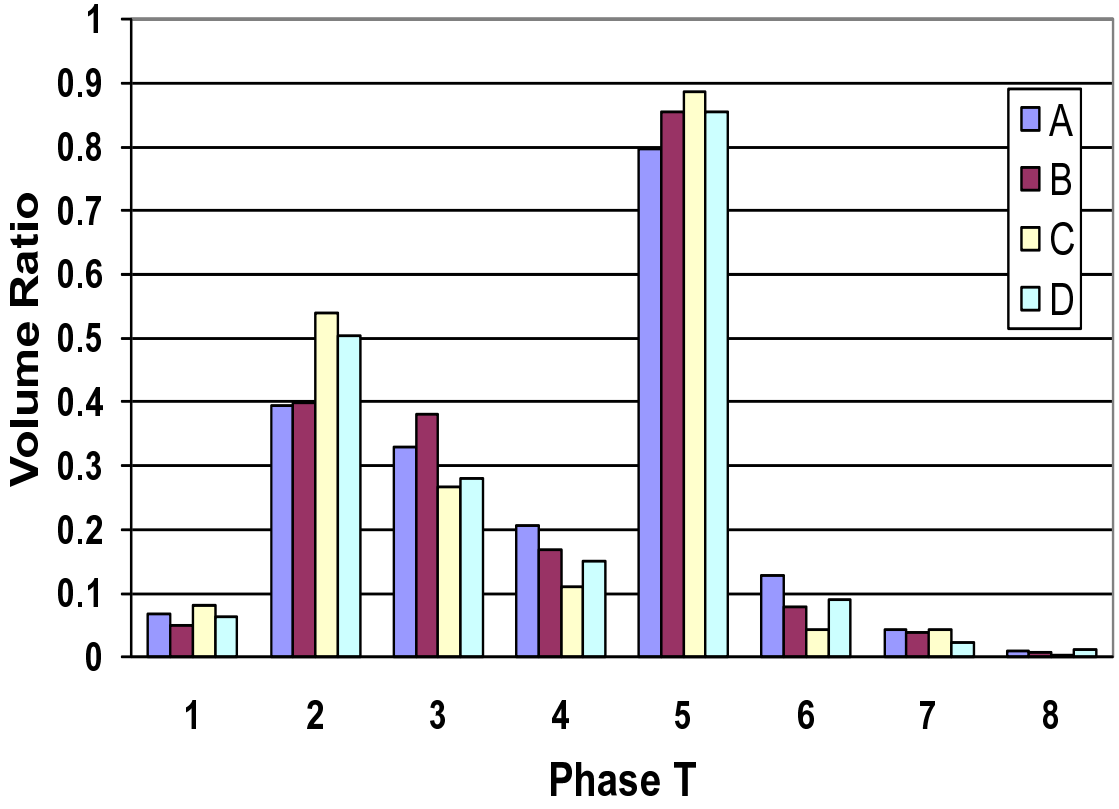

Figure 2.4: Ratio of the total lung volume that reaches the maximum ventilation during the inspiration phases T_1, T_2, T_3, T_4 and during the expiration phases T_5, T_6, T_7, T_0 for animals A, B, C, and D, at significant regions only.

the curve from T_0 to T_4.

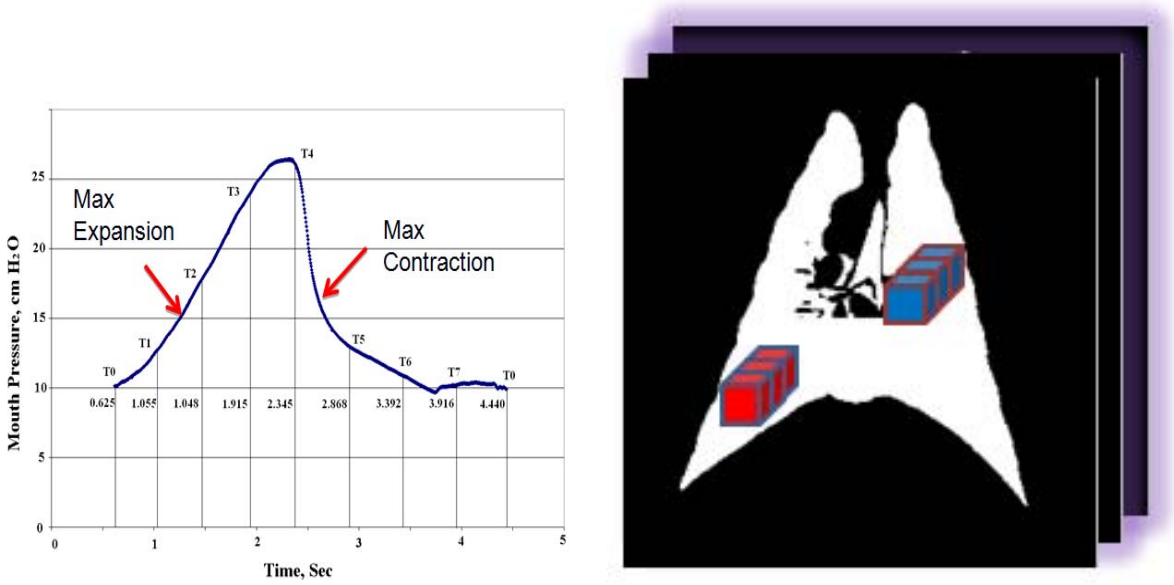

(a) (b)

Figure 2.5: (a) Sheep mouth pressure versus time during imaging; (b) Illustration of choosing ROI blocks for ventilation distribution in the dorsal-ventral direction.

2.3 Discussion

We have described a new scheme for measuring instantaneous ventilation at each phase within respiratory cycle from a regularized tissue volume and vesselness preserving image registration of 4DCT phase images. $t_{MIV}(\mathbf{x})$ and $t_{MEV}(\mathbf{x})$ are used to represent the phase when a local region reaches its highest inspiring ventilation and highest expiring ventilation separately. The maximum ventilation is verified by a significance check. The ventilation variation is quantified using the distribution of volume ratio of voxels that reach to $\dot{V}_{max}(\mathbf{x}, t_i)$ at different phase. 39% of the total

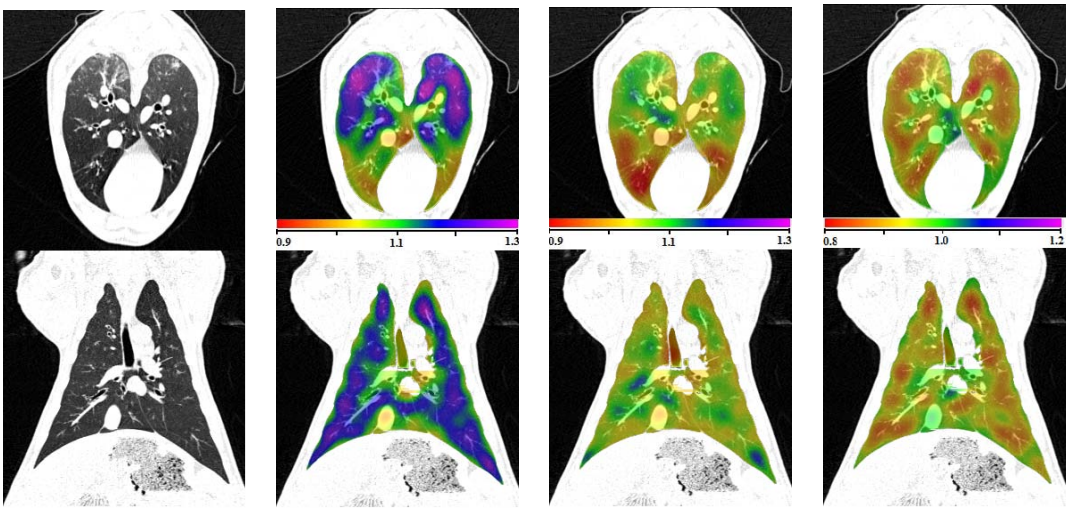

(a) (b) (c) (d)

Figure 2.6: Color coded Jacobian map in transverse view and coronal view showing the regional lung function at different phases. Different colors show regional expansion or contraction of lung tissue. (a) The intensity CT image end expiration phase; (b) Jacobian map from 100%IN to 0%IN; (c) Jacobian map from 75%EX to 0%IN; (d) Jacobian ratio map from 75%EX to 100%IN;

lung volume reaches maximum ventilation at T_1 to T_2 during inspiration and the 75% of the total lung volume reaches max ventilation at T_4 to T_5 during expiration. About 200 anatomical landmarks are identified and annotated to evaluate the registration accuracy. The average landmark error is on the order of 1 mm after registration.

The results show that by registering all the phase images to the T_0 image and taking the derivative with respect to the time step, we can estimate instantaneous regional ventilation. Moreover, by comparing the instantaneous ventilation change across the respiratory cycle, the time-varying regional ventilation effects can be examined. The distribution of phases at which regions reaches highest ventilation is more homogeneous at expiration than the inspiration. This is consistent with our

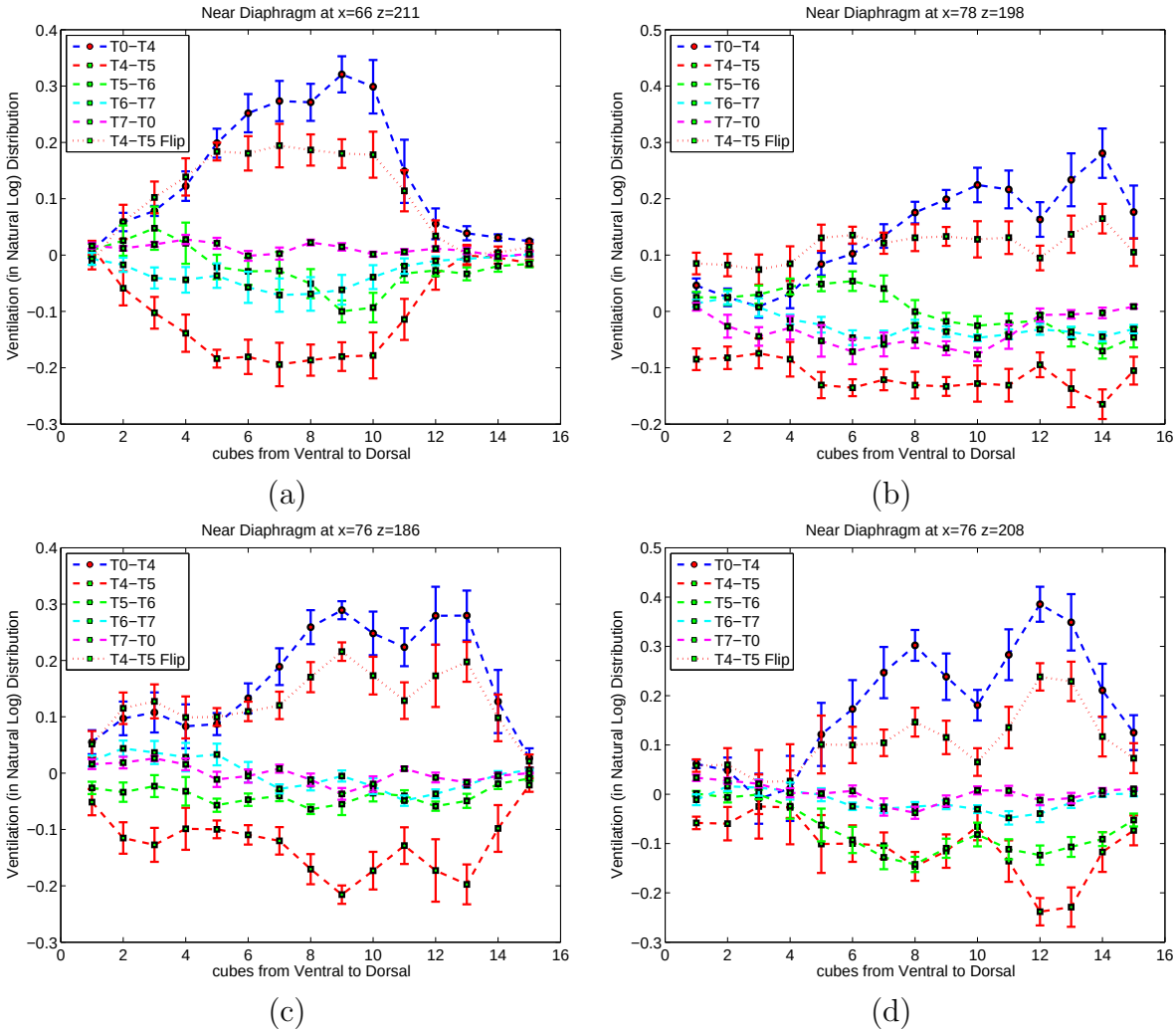

Figure 2.7: Mean and standard deviation distribution of logarithmic Jacobian near diaphragm from ventral block 1 to dorsal block 15. The error bar on each marked point shows standard deviation in the block.(a) Animal A; (b) Animal B; (c) Animal C; (d) Animal D;

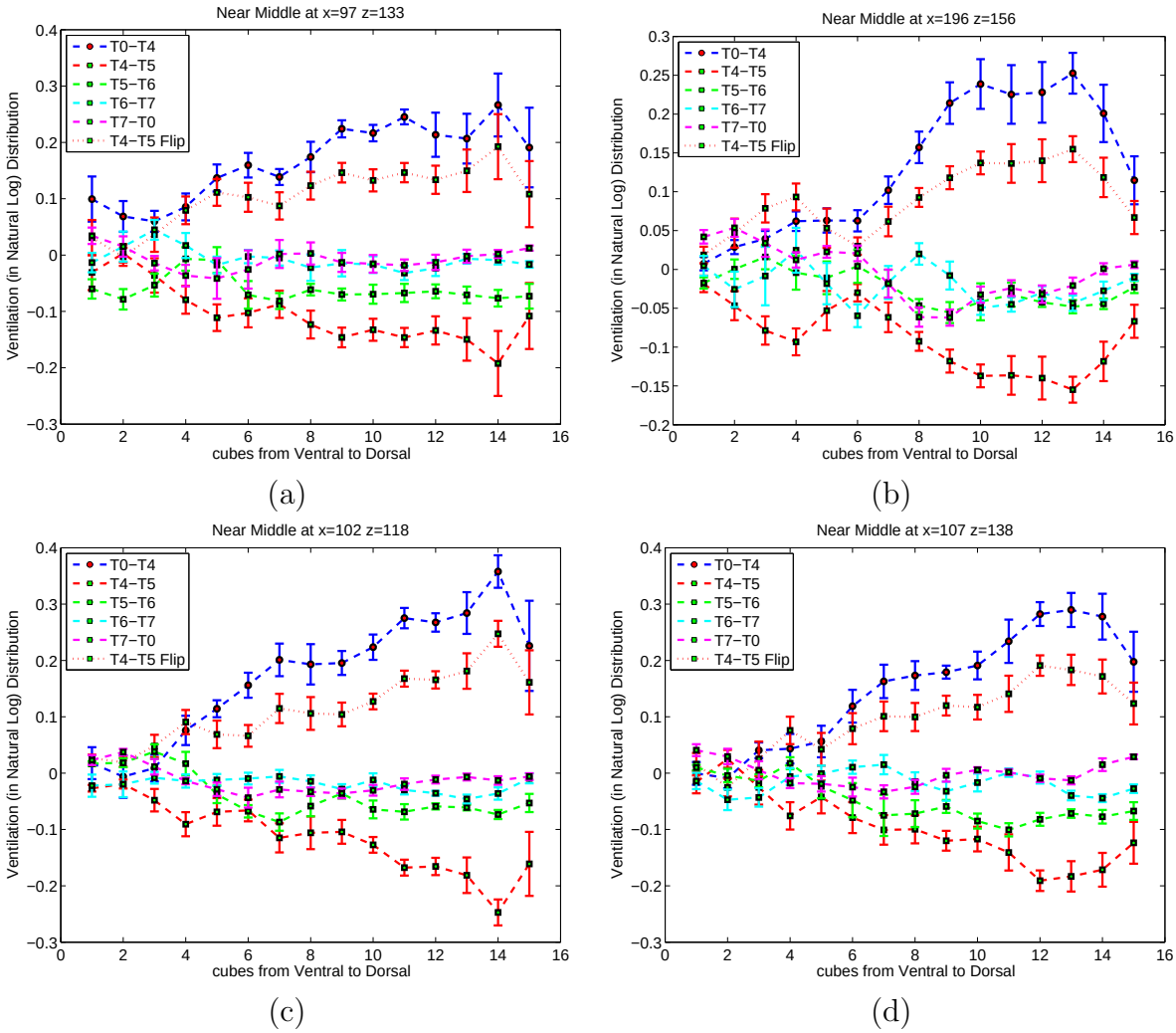

Figure 2.8: Mean and standard deviation distribution of logarithmic Jacobian near middle lung height from ventral block 1 to dorsal block 15. The error bar on each marked point shows standard deviation in the block.(a) Animal A; (b) Animal B; (c) Animal C; (d) Animal D;

expectation and global mouth pressure measurement since during tidal breathing, the lung usually releases most of the expired gas within the short time period at the beginning of the expiration while in inspiration it typically takes more time to reach to its tidal volume.

In the traditional pulmonary function test (also known as spirometry), forced expiratory volume in one second (FEV_1) is used for diagnosis of obstructive and restrictive lung disease. In Figure 2.6, it makes sense that Jacobian from 100%IN to 0%IN has more blue and purple area (meaning more expansion) than Jacobian from 75%EX to 0%IN. Intuitively we can also find that in both breathing phase pairs the dorsal lung expands more than the ventral lung, which is consistent with clinical discovery. Figure 2.6 (d) shows regional lung ventilation from 75%EX to 100%IN, which also appears that dorsal lung exhales more than ventral part. In Figure 2.6 (d) almost all lung tissue contracts though in various degrees. For all animals from dorsal to ventral, the contraction from 75%EX to 100%IN is the deepest among all four expiratory phases and is the most symmetric with the expansion from 0%IN to 100%IN, while the contraction at the other three expiratory intervals are relatively low and not obvious. The interesting symmetric curves from 75%EX to 100%IN and from 100%IN to 0%IN indicates the active regions are almost the same ones in the inspiration and the first expiratory phase. As the FEV_1 test in spirometry is important in lung diseases diagnosis like airway obstruction, these results show the first expiratory interval is probably an alternative way to analyze regional pulmonary function other than end-to-end breath interval. Basically larger standard deviation corresponds to

lower mean value, showing that lung tissue undergoing more ventilation would have larger lung function variance. At both ROIs near the diaphragm and near the middle lung, the results show the dorsal lung tissue is more active than the ventral. If we compare the ventral-dorsal distribution near the diaphragm and near the middle, the middle lung tissue looks more monotonous than lung tissue near the diaphragm.

These results could be useful for constructing distributed or lumped parameter models of the respiratory system (i.e., RLC networks) for computer simulation studies. Given such a model, the effects of mechanical ventilation strategies (such as high-frequency ventilation to treat acute respiratory distress syndrome) on the regional distribution of lung expansion could be studied, and such a model could be least partially validated using 4DCT measurements of lung expansion and contraction.

In conclusion, the use of multiple respiratory phase images from 4DCT allows instantaneous ventilation maps to be produced and the maximum ventilation phase to be identified regionally. The regional expiration volume ratio is also of significance in medical applications. These measurements may improve our understanding of dynamics and function in the normal lung, and increase our ability to identify and categorize abnormal behaviors in the diseased lung.

CHAPTER 3
REPRODUCIBILITY OF 4DCT PULMONARY FUNCTION MEASUREMENT USING IMAGE REGISTRATION

3.1 Introduction

The primary function of the respiratory system is gas exchange. Therefore ventilation performance is another interpretation of lung function which depends on lung mechanical motion as expansion and contraction during the respiratory circle. Since many diseases and injury conditions can affect directly or indirectly the lung condition, it is useful to understand lung function behavior in the global and/or regional level. Clinically, regional pulmonary function measurement is of greater significance especially for Radiation Therapy (RT) planning to avoid normal lung function loss, track the ventilation toxicity during RT and estimate the contribution of RT in the lung function improvement.

Regional pulmonary function is difficult to measure quantitatively in three dimensions. So far various methods have been made to assess regional lung function [23]. Invasive methods, such as percutaneously or surgically implanted parenchyma markers or inhaled fluorescent microspheres, are inaptitude for translation to humans [23, 37, 27]. Noninvasive measurement mainly refers to methods by mean of medical imaging. However, the measured pulmonary function by medical imaging methods may be strongly affected by the image acquisition, imaging agents and image processing. So far there are rare papers talking about the reproducibility of regional pulmonary func-

tion measurement. Nuclear medicine imaging, such as positron emission tomography (PET) and single photon emission computed tomography (SPECT) could provide a direct assessment of lung function [40, 45, 21, 43], but its application is limited by low spatial resolution. Additionally to obtain reasonable signal to noise ratio, the patient has to be imaged across multiple respiratory circles, which deteriorates the spatial resolution. This is also one reason why regional pulmonary function cannot be measured reproducibly by nuclear medicine imaging. Hyperpolarized noble gas (such as ^{129}Xe and ^{3}He) MR imaging has been developed for functional imaging of pulmonary ventilation [33, 46, 42, 47, 26]. Sufficient temporal resolution is guaranteed by hyperpolarized MRI so that we could observe the dynamics of gas flow through the lung. But currently it is partially quantitative and depicts only a few anatomic detail. In addition it requires tracer gases and associated special equipments. Finally, Xenon-enhanced CT (Xenon-CT) is another imaging modality to directly assess pulmonary ventilation by observing wash-in and wash-out rate of serial CT images [30, 41, 8]. Whereas the requirement of high temporal resolution limits the axis coverage about 2.5 cm to 12 cm while the typical z-axis extent of human lung is on the order of 25 cm. No specialized papers have involved the reproducibility of assessment of regional pulmonary function with Xenon-CT.

Respiratory-gated CT imaging and 3D image registration can be used to locally estimate lung tissue expansion and contraction (regional lung volume change) to obtain a ventilation map over the whole lung [36, 6]. This is of significance to functional lung imaging with the advantages of increased resolution, reductions in time,

and avoidance of agent exposure. Reinhardt et al. [36] compared this registration-based estimation on regional lung function to Xenon-CT and the average r^2 reaches 0.73. Even better, the deficiency of low temporal resolution can be compensated by the import of 4DCT imaging. 4DCT has become a routine imaging at many institutions as part of standard RT planning for thoracic diseases. We could utilize 3D CT images reconstructed at certain phases on the respiratory circle combining image registration to analyze regional pulmonary function over a certain period of time. The result regional pulmonary function is of great use when it comes to, for example, instructions on RT planning to reduce tissue irradiation and assessment of lung function change following RT courses. Recently Yaremko et al. [50] proposed a method incorporating image registration with 4DCT images to identify regions of highly functional lung for avoidance in IMRT planning in non-small-cell lung cancer. Ding et al. [11] quantitatively measured the regional changes in lung tissue function following a course of radiation therapy by using 4DCT and image registration techniques. Keall et al. [49] also quantified the dosimetric impact of 4DCT and image registration derived pulmonary ventilation map on functional treatment planning to avoid high-functional lung regions.

The advantages of using 4DCT images to assess local pulmonary function encourage the research on the measurement reproducibility of this method. Before the clinical applications of 4DCT derived regional pulmonary function, it is necessary to quantify and demonstrate that the pulmonary function can be reproducibly measured using 4DCT and image registration-based method. By 4DCT images acquired

at different time with other imaging parameters fixed, if the measurement result of pulmonary function could repeat its pattern and vary in a reasonable and small enough range, then we are able to say it is meaningful to utilize the pulmonary function to RT planning or lung function change analysis before and after RT. Otherwise, it is not convincing to incorporate this 4DCT ventilation map into RT planning; and for lung function change measurement, it may be due to the inaccuracy and unrepeatability of image acquisition or image processing algorithm rather than inherent lung function change.

There are many factors influencing the reproducibility in two 4DCT scans, even they were scanned in a short time. The baseline volume and tidal volume in the respiratory cycles of two scans may vary much, causing different magnitude and pattern of expansion and contraction of lung tissue. The various breathing patterns may also be a problem, especially for patients with seriously damaged lung who cannot control their breath easily. There may be inconformity of the imaging process in the two scans, for example the Hounsfield Units (HU) may be different. Image processing algorithm might also induce influences on the reproducibility. Finally, for scans got acquired in a long time interval, the internal change in lung tissue or lung function itself may reduce the reproducibility we are caring about.

In this paper, we evaluate and demonstrate the reproducibility of local pulmonary function using 4DCT images in human subjects prior to radiation therapy. As the control group, 4DCT images acquired from anesthetized and mechanically ventilated sheep are also analyzed. We found that regional pulmonary function from

human subjects shows good reproducibility in the two pre-RT 4DCT scans, while that from animal subjects shows better reproducibility. The high reproducibility of sheep data shows the importance of breath control and respiratory training during 4DCT. The reproducibility is measured by calculating the ratio of the Jacobian from two 4DCT scans. These results may provide insight into breath control during image acquisition and pulmonary function normalization in further study. We also propose methods to improve reproducibility by matching the tidal volume and head-and-tail volumes in two scans and to normalize Jacobian by total lung volume change to offset the different breath effort.

3.2 Material and methods

3.2.1 Method Overview

Figure 3.1 shows a block diagram of the entire process. 4DCT data from nine patients and three sheep are analyzed. For this study we mainly focus on two phases - maximum inspiration and maximum expiration (herein denoted as the 100%IN and 0%EX images). For each subject in this study, 100%IN and 0%EX images for both scans are reconstructed, while in section 3.3.3 intermediate breathing phases like 50%IN are also reconstructed for volume matching study. 3D deformable image registration is used to create a voxel-by-voxel displacement field map between 3 pairs, scan1 100%IN to scan1 0%EX (T1), scan2 100%IN to scan2 0%EX (T2), and scan2 0%EX to scan1 0%EX (T0). Local lung function is assessed via Jacobian of two scans that are calculated from the displacement field map of scan1 100%IN to scan1 0%EX and scan2 100%IN to scan2 0%EX (denoted as JAC_{T1} and JAC_{T2}). Since

there might be anatomical difference between the 2 baseline scans (0%EX) which impedes the comparison of Jacobian, scan1 0%EX is chosen as the reference data set, that is, JAC_{T2} will be later warped to the same coordinate system of JAC_{T1}. Table 3.1 summarizes these three transformations. Transformations T1 and T2 are defined between respiratory phase points on 4DCT and transformation T3 is used to convert the lung expansion map onto the same coordinate system. The ratio maps of regional lung function from the two scans (denoted as JAC_{RATIO}) are ready to be analyzed for reproducibility study.

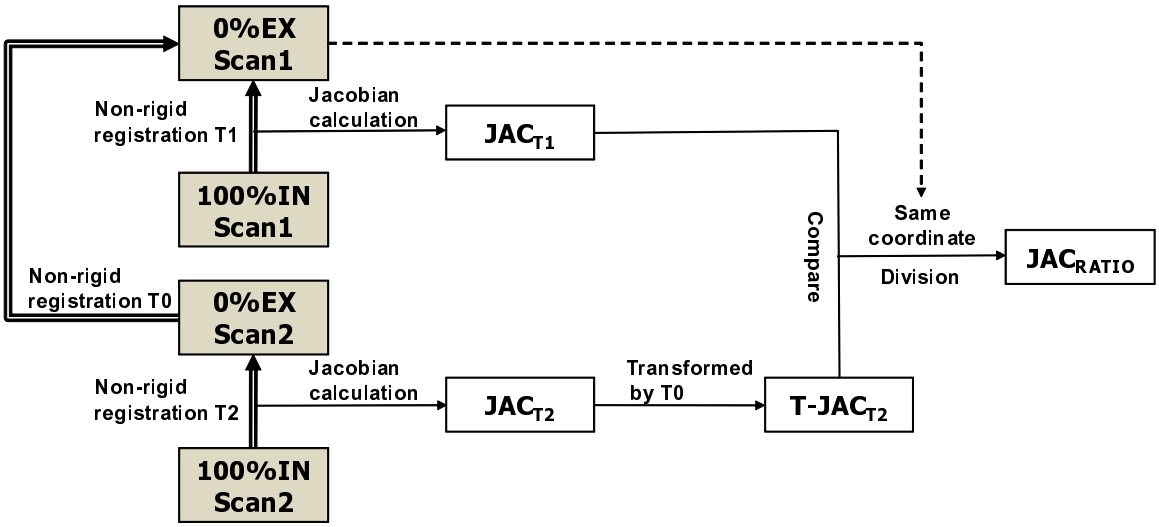

Figure 3.1: Block diagram shows the pipeline of the entire process. In the two 4DCT data sets from two "Coffee Break" scans. Scan1 0%EX and scan2 0%EX indicate end expiration while scan1 100%IN and scan2 100%IN indicate end inspiration. Jacobian is calculated registration displacement field. Besides the registration from end inspiration to end expiration in two scans, registration from scan2 0%EX to scan1 0%EX was also operated, from which the deformation field would be used to warp JAC_{T2} to the coordinate of scan1 0%EX, for direct comparison of two Jacobian. In the last step, division between transformed $T - JAC_{\mathrm{T2}}$ and JAC_{T1} is used for analysis of Jacobian reproducibility.

Transformation Name	Image Transformed	Used To
T0	Scan2 0%EX $\rightarrow$ Scan1 0%EX	Transform scan2 Jacobian into scan1 0%EX coordinate system for comparison ($T - JAC_{T2}$)
T1	Scan1 100%IN $\rightarrow$ Scan1 0%EX	Calculate pre-RT scan1 lung expansion map (JAC_{T1})
T2	Scan2 100%IN $\rightarrow$ Scan2 0%EX	Calculate pre-RT scan2 lung expansion map (JAC_{T2})

Table 3.1: Summary of image registrations performed to calculate lung function. Names of images and transformations refer to those given in Figure 3.1.

3.2.2 Image Data Sets

All human data sets were gathered under a protocol approved by the University of Iowa IRB and Animal Care approvals. These human subjects all have lung tumors ranging from mild to severe and are receiving RT in the Department of Radiation Oncology at the University of Iowa Hospitals and Clinics. Prior to each 4DCT scan, the patient will receive respiratory training using a biofeedback system (RESP@RATE, Intercure Ltd., Lod Israel) to identify their nominal breathing rate. Musical cues will used to pace respiration during imaging, a technique developed at our institution and shown to have high success and compliance [44]. Two 4DCT will be scanned during the patient's initial visit at around 30 minutes interval (called "coffee break scans"). The 4DCT datasets will also be used as usual to create the RT treatment plan for the consequent RT. Three sheep were anesthetized and mechanically ventilated during experiments. 4DCT images were acquired in supine position

with dynamic imaging protocol. Animal were not moved between scans. Respiratory rate (RR) for animals ranges from 15 to 18 breaths per minute. Both human and animal images were reconstructed with matrix of 512 × 512. In Z direction the slab thickness of human images is 2 mm and that of sheep is 0.5 mm. The in-plane pixel spacing of human images is approximately 0.97 mm × 0.97 mm and that of sheep images is 0.5 mm × 0.5 mm.

3.2.3 Data processing

Pre-processing After image acquisition, the respiratory trace data and 4DCT image data will firstly be examined for evidence of breathing artifacts or other acquisition problems, since acquisition artifacts may disrupt the image registration process and lead to erroneous lung function measurements. Before image registration, all the images were sampled to size 304 × 304 × 320 with resolution 1 mm × 1 mm × 1 mm. Pulmonary Workstation 2.0 (VIDA Diagnostics, Inc., Iowa City, IA) was applied to delineate lung voxel from surrounding tissue in CT images. The binary mask obtained from segmentation was subsequently used to limit the spatial domain of image registration and following lung function analysis. The lung volume is calculated by counting the non-zero voxel in the binary lung mask and multiplying with the spacing. Table 3.2 and table 3.3 list the lung volumes involved in this study.

Image Registration The tissue volume preserving nonrigid registration algorithm, combined with Laplacian Regularization Constraints (LAP), is used to match the lung structure across the respiratory circle, which provides a voxel-by-voxel displacement

field between the two images being matched. Based on cubic b-spline transformation model and multi-resolution procedure, this algorithm minimizes the sum of squared tissue difference (SSTVD) while at the same time regularizing LAP constraints as shown in equation 3.1. This method has been shown to be effective at registering lung CT images with high accuracy [53, 4].

$$C_{\text{TOTAL}} = C_{\text{SSTVD}} + \rho C_{\text{LAP}}, \tag{3.1}$$

where C_{SSTVD} is the SSTVD cost, C_{LAP} is the Laplacian regularization constraint, and ρ is a weighting parameter.

Suppose I_1 and I_2 are two images ready to be registered, I_1 as the template image and I_2 as the target image. Consider the vector displacement function $\mathbf{x} = (x_1, x_2, x_3)^T$ that transforms a voxel from I_1 into its corresponding point in I_2. The goal of registration algorithm is to solve the optimal correspondence mapping $\mathbf{h}$ which connects points at coordinate $\mathbf{x}$ in both template and target images.

As the main factor of the cost function in our registration algorithm, SSTVD serves as the intensity similarity criterion because it compensates the change in CT intensity as air inspired or expired in the respiratory process. Therefore it is especially useful when it comes to the registration of images acquired at different air pressure levels. The SSTVD cost function assumes Hounsfield Units (HU) of lung CT images is a function of tissue and air content. The factual tissue volume $V(\mathbf{x})$ at voxel

coordinate $\mathbf{x}$ can be estimated as

$$V(\mathbf{x}) = v(\mathbf{x})\frac{HU(\mathbf{x}) - HU_{air}}{HU_{tissue} - HU_{air}}, \tag{3.2}$$

Where v($\mathbf{x}$) is the total volume of voxel $\mathbf{x}$. HU_{air} and HU_{tissue} refer to the intensity of air and tissue respectively. We assume air intensity is -1000 and tissue intensity is 55 [22]. Then the intensity similarity metric becomes as [53]

$$\begin{aligned} C_{\text{SSTVD}} &= \int_{\mathbf{\Omega}} \left[V_2(\mathbf{x}) - V_1(\mathbf{h}(\mathbf{x}))\right]^2 d\mathbf{x} \\ &= \int_{\mathbf{\Omega}} \left[v_2(\mathbf{x})\frac{I_2(\mathbf{x}) + 1000}{1055} - v_1(\mathbf{h}(\mathbf{x}))\frac{I_1(\mathbf{h}(\mathbf{x})) + 1000}{1055}\right]^2 d\mathbf{x} \end{aligned} \tag{3.3}$$

where Ω denotes the union of two lung regions.

Lung motion is a complicated issue therefore the registration algorithm performs better and gets more physiologically meaningful transformation with enforced constraints on the transformation. Continuum mechanical models such as linear elasticity can be employed to suppress and regularize the transformation together with SSTVD. In this paper, Laplacian operator is used to regularize the displacement fields $\mathbf{x} = (x_1, x_2, x_3)^T$.

This regularization term is formed as [5]

$$C_{\text{LAP}} = \int_{\mathbf{\Omega}} ||\nabla^2 \mathbf{u}(\mathbf{x})||^2 d\mathbf{x}. \tag{3.4}$$

where $\nabla = \left[\frac{\partial}{\partial x_1}, \frac{\partial}{\partial x_2}, \frac{\partial}{\partial x_3}\right]$ and $\nabla^2 = \nabla \cdot \nabla = \left[\frac{\partial^2}{\partial x_1^2} + \frac{\partial^2}{\partial x_2^2} + \frac{\partial^2}{\partial x_3^2}\right]$. With the control

of the regularization operator, it helps smooth transformation avoiding mutations in the final displacement fields $\mathbf{x} = (x_1, x_2, x_3)^T$.

Jacobian calculation and reproducibility measurement After image registration, regional lung function can be assessed by calculating the Jacobian metric [36] from the voxel-by-voxel deformation field. For each small piece of lung tissue, its regional lung function is actually the air volume change per unit time, reflecting the air flow-in (expansion) or flow-out (contraction) degree. Jacobian is a function of partial derivatives of the displacement field reflecting local lung expansion and contraction [36], which can be expressed mathematically as

$$J(\mathbf{h}(\mathbf{x})) = \begin{vmatrix} \frac{\partial h_1(\mathbf{x})}{\partial x_1} & \frac{\partial h_2(\mathbf{x})}{\partial x_1} & \frac{\partial h_3(\mathbf{x})}{\partial x_1} \\ \frac{\partial h_1(\mathbf{x})}{\partial x_2} & \frac{\partial h_2(\mathbf{x})}{\partial x_2} & \frac{\partial h_3(\mathbf{x})}{\partial x_2} \\ \frac{\partial h_1(\mathbf{x})}{\partial x_3} & \frac{\partial h_2(\mathbf{x})}{\partial x_3} & \frac{\partial h_3(\mathbf{x})}{\partial x_3} \end{vmatrix}. \tag{3.5}$$

In a Lagrangian reference frame, if the Jacobian is unity, there is no expansion or contraction at that location; if the Jacobian is greater than one, there is local tissue expansion; if the Jacobian is less than one, there is local tissue contraction. For visualization, the Jacobian map is color-coded and overlaid onto the original CT data. In our study, we always use scan1 0%EX as the baseline reference on which all Jacobian maps are overlaid. With the displacement information from registration between scan2 0%EX and scan1 0%EX (T1), JAC_{T2} was warped onto the coordinate of scan1 0%EX for direct comparison.

Color-coded Jacobian maps from scan1 and scan2 are compared to establish

the level of reproducibility. Jacobian ratio map JAC_{RATIO} was acquired by division between the $T - JAC_{\mathrm{T2}}$ and JAC_{T1} voxel-by-voxel. Mean and standard deviation of JAC_{RATIO} were also calculated on a voxel-by-voxel basis.

3.2.4 Assessment of Image Registration Accuracy and Landmarks Reproducibility

A semi-automatic landmark system is employed for landmark annotation [34]. Approximately 120 vascular bifurcation points anatomically identified landmarks within the lungs were picked for each human subject, and used to evaluate the registration accuracy. The landmarks are uniformly distributed in the left and right lung. The observer correspond anatomic landmark location in an image with the identified landmarks in another image. Each landmark pair manually annotated by the observer was added to a thin-plate-spline to warp the image and predict the location for the next unmatched landmark pair as a reference and convenience for the observer. For assessment of registration accuracy, landmark error is calculated by comparison between the actual landmark position and estimated landmark position deformed registration result.

3.3 Results

3.3.1 Registration Accuracy

Figure 3.2 shows a 3D view of landmarks distribution in patient B at scan1 100%IN. We could see the landmarks also form a uniform distribution in the vertical Z direction. Figure 3.3 shows landmark distances before and after image registration in each of the three pairs. The first two columns are for registration between scan2

0%EX and scan1 0%EX (T0), the middle two columns for registration between scan1 100%IN to scan1 0%EX (T1), and the last two columns for registration between scan2 100%IN to scan2 0%EX (T2). The landmark distances before registration of T1 and T2 are not very consistent, because the different breath effort in two scans causes different scale of lung deformation. For registration T0, the landmark distance before registration is already quite small demonstrating the similarity of 0%EX in two scans. The landmark distances are all reduced to the order of 1 mm, confirming with previous reported registration accuracy of SSTVD registration algorithm described by [4, 5]. In general the landmark distance analysis shows good image registration accuracy and guarantees the following Jacobian reproducibility study.

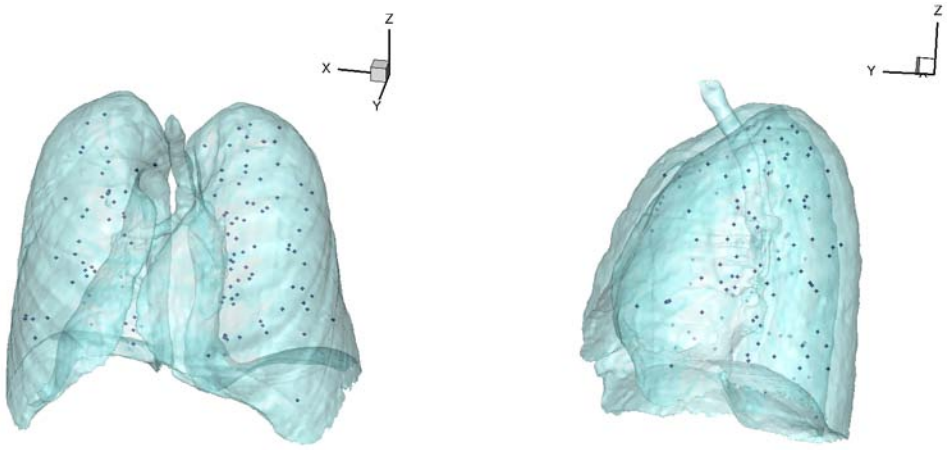

(a) (b)

Figure 3.2: 3D view of the landmarks for patient B in different angles: (a) anterior-posterior and (b) right-left. The dark blue spheres are the automatically defined landmarks.

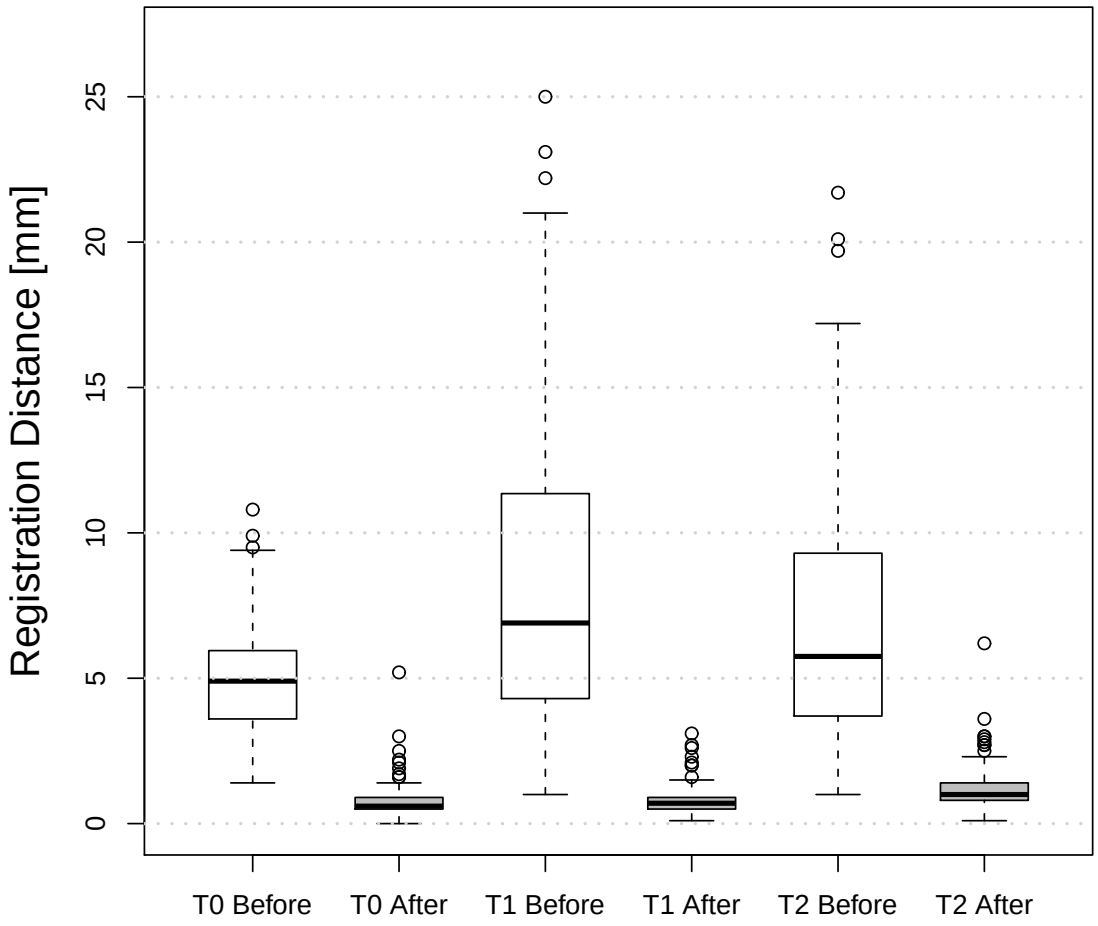

Figure 3.3: Landmarks distances for patient B before and after registration for the three registration pairs involved in this paper. White box represents the landmark distance before image registration, and gray box represents the landmark distance after image registration.

3.3.2 Reproducibility of regional pulmonary function measurement

We are interested in the verification of reproducibility of regional pulmonary function measurement via Jacobian metric in repeat 4DCT scans. Since for human subjects the breathing trace pattern, tidal volume, impact of tumor etc are probably quite different during the 4DCT imaging, we also inspect the Jacobian reproducibility of sheep subjects as the control group for comparison, which were mechanically strictly ventilated and monitored during the experiments.

Figure 3.4 is the panel of sheep A showing the color-coded pulmonary function and JAC_{RATIO} derived from division between JAC_{T1} and $T - JAC_{\mathrm{T2}}$. Scan2 pulmonary function image was mapped to and overlaid on the coordination of scan1 0%EX as described in Section 3.2.1. The first column is the primary CT intensity image of scan1 0%EX, and the second column shows pulmonary function in scan1, while the third column show pulmonary function in scan2. The color bar in the bottom indicates different values of lung expansion. For example, in the second and third columns purple and blue means large lung tissue expansion with Jacobian value larger than 1.15, while red and brown represents lung tissue contraction with Jacobian value less than 1.0. In the coronal view, the pulmonary function of the trachea is about 1.0 almost everywhere with color light brown, indicating no expansion or contraction in trachea. The right-most column is JAC_{RATIO} which shows voxel wise ratio of two repeated pulmonary measurements. Ideally JAC_{RATIO} should be all light brown or dark yellow with Jacobian value 1.0 which means Jacobian values acquired in the two scans are exactly the same voxel to voxel. From this panel, we can see sheep

A shows great pulmonary function reproducibility in spite of minute fluctuations in JAC_{RATIO}. The largest difference is the red region in the upper transverse view in JAC_{RATIO}.

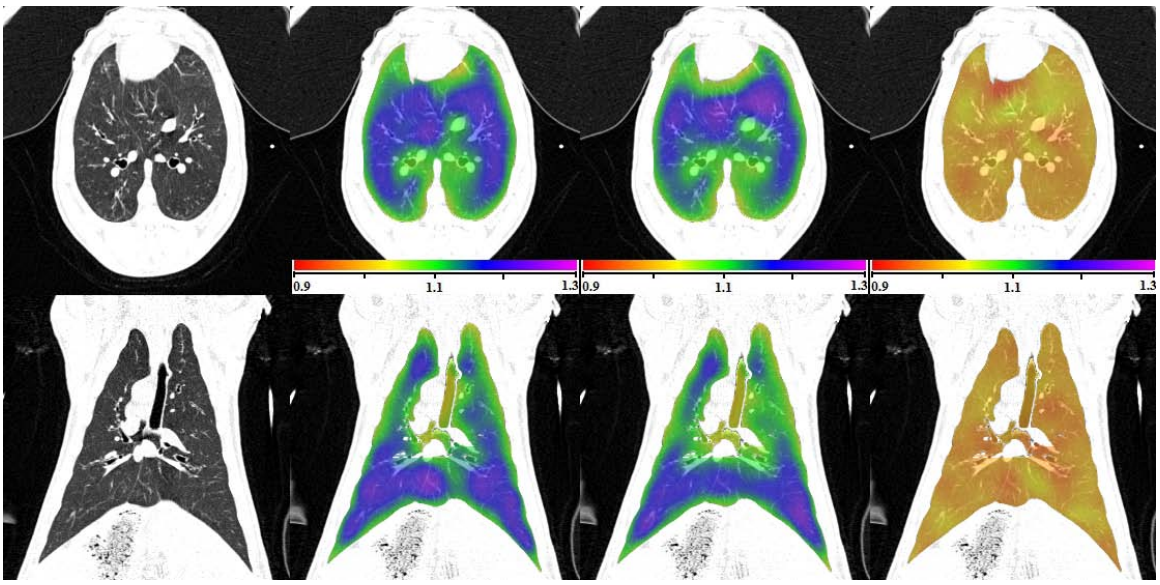

Figure 3.4: Transverse and coronal view of sheep A JAC_{T1}, $T-JAC_{\mathrm{T2}}$ and JAC_{RATIO} by dividing JAC_{T2} with JAC_{T1}.

Table 3.2 is a summary of all three sheep subjects in this study. Lung volume of 0%EX and 100%IN in two scans are listed in the table. The "Diff" column means tidal volume calculated from subtraction of 100%IN lung volume by 0%EX lung volume and "Ratio" column is the number from 100%IN lung volume divided by 0%EX lung volume. The unit of lung volume is in liters (L). The "Jacobian mean" column, "Jacobian std" column and "Jacobian Correlation" column show respectively the statistical mean, standard deviation of JAC_{RATIO}, and the correlation coefficient

of two Jacobian data sets on a voxel-by-voxel basis. All of the statistics are restricted inside the lung tissue area. From Table 3.2, for sheep A as an example, the mean value of JAC_{RATIO} is 0.9989, less than one, which agrees with that tidal volume 0.37 in scan2 is slightly less than that 0.38 in scan1. In other words, the lung in scan2 did not expand as much as in scan1. Mathematically the mean value of JAC_{RATIO} should be equal to the quotient of scan1 lung volume ratio and scan2 lung volume ratio in "Ratio" column. The standard deviation of JAC_{RATIO} is only 0.0139. If the lung is a homogenous mechanical model and the regional pulmonary function in the two scans are of exact the same pattern and distribution independent of degrees of breath effort, the final standard deviation of JAC_{RATIO} should be reduced to 0. So standard deviation is one measurement criteria we employ in this paper to assess the regional pulmonary function reproducibility. The linear correlation coefficient for sheep A is 0.922, measuring the strength of linear relationship between two Jacobian data sets. All of these three sheep subjects show great reproducibility of regional pulmonary function.

Figure 3.5 (a) shows a smooth scatter plot for JAC_{T1} and $T - JAC_{\mathrm{T2}}$ and their respective histograms in the margins. In the center is a smoothed color density representation of the scatter plot of JAC_{T1} and $T - JAC_{\mathrm{T2}}$, obtaining through a kernel density estimate. The five colors (red, yellow, green, purple and white) encode the local densities at each point in the scatter plot, representing distribution density in 5 equal levels from highest to lowest. The top marginal bar plot is the histogram distribution of JAC_{T1}, while the right marginal bar plot is that of $T - JAC_{\mathrm{T2}}$. The

subject	scan	0%EX (:L)	100%IN (:L)	Diff (:L)	Ratio	Jacobian mean	Jacobian std	Jacobian correlation
sheep A	1	2.79	3.14	0.38	1.1376	0.9956	0.0139	0.922
	2	2.87	3.24	0.37	1.1306			
sheep B	1	2.50	2.88	0.38	1.1535	1.1001	0.0226	0.843
	2	2.62	3.01	0.39	1.1513			
sheep C	1	2.80	3.34	0.54	1.1929	0.9996	0.0264	0.887
	2	2.93	3.49	0.56	1.1899			

Table 3.2: Summary of sheep lung volume of 0%EX and 100%IN in both scans, tidal volume, volume ratio 100%IN/0%EX, mean value of JAC_{RATIO} from two scans, standard deviation of JAC_{RATIO}, and the statistical correlation value between JAC_{T1} and $T - JAC_{\mathrm{T2}}$. The unit for lung volume is in liters(L).

reference line y=x in solid, the linear regression line in dash and the corresponding equation of regression line on the upper left corner are shown. Corresponding statistical mean, standard deviation for each scan and correlation coefficient are also added at proper positions. The better the reproducibility, the more concentration of the scatter distribution to the regression line, with a higher correlation coefficient, while in the extreme case of perfect reproducibility, the scatter distribution should shrink to be along the regression line. Figure 3.5 (b) shows on the left a colorful smooth scatter plot of JAC_{RATIO} against geometrical average calculated from Jacobian maps of two scans ($\sqrt{JAC_{\mathrm{T1}}. * T - JAC_{\mathrm{T2}}}$), and on the right the marginal histogram of JAC_{RATIO}. An reference line y=1 in solid is also drawn, with corresponding statistical mean and standard deviation(same as in Table 3.2) also displayed beside the histogram. In fact figure 3.5 (b) reflects the regional reproducibility status of pulmonary function along the span of Jacobian value. The distribution should be closer to y=1 with a higher regional reproducibility. We can see JAC_{RATIO} of sheep A is

restricted between around 0.92 and line 1.07 with a Gaussian distribution, and the most dense red part (gathering most lung voxels) is between 0.98 and 1.02 with only 2% difference.

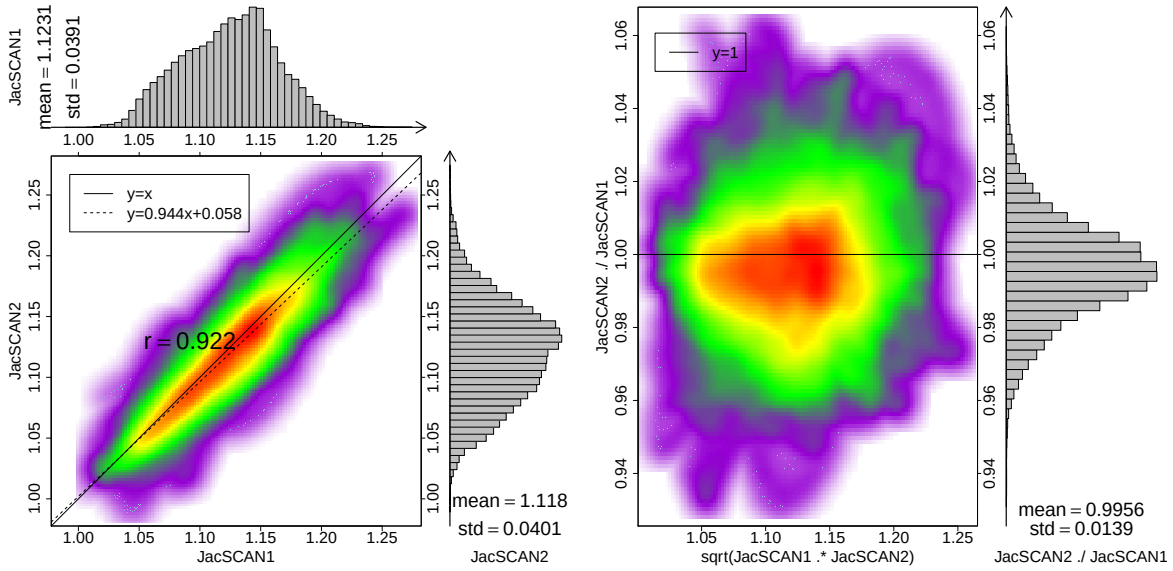

(a) (b)

Figure 3.5: For sheep A, (a) smoothed color density scatter plot and marginal histograms of JAC_{T1} and $T - JAC_{\mathrm{T2}}$; (b) smoothed color density scatter plot of JAC_{RATIO} against geometrical average of two Jacobian maps, and the marginal histogram of JAC_{RATIO}.

Table 3.3 is a summary of all nine human subjects we have. The format of Table 3.3 is similar to Table 3.2 for Sheep subjects showing lung volume, tidal volume, volume quotient, and statistical parameters of JAC_{RATIO}. We can notice that the lung volume and tidal volume in two scans are of larger difference compared to sheep subjects, since sheep are mechanically ventilated. In addition the standard deviation and correlation coefficient are not as good as in sheep subjects. Figure 3.6

is the color-coded panel of regional pulmonary function in two scans and JAC_{RATIO} for patient B. The color scales for the three color maps are all the same. From Table 3.3, the tidal volume in scan2 is only 0.57 L, less than 0.62 L as in scan1, so we could see from the panel the lung in scan2 does not expand as much as scan1. Most of the lung shows high reproducibility while the distinct part appears mainly near the diaphragm. Another obvious nonreproducible region appears at the right lower corner of the left lung, where lung in scan2 expands abnormally more than that in scan1. Regions around the tumor also shows high similar pattern and high reproducibility. According to Table 3.3, patient B is the one with lowest standard deviation 0.0359 and a relatively high Jacobian correlation 0.811 among all the human subjects. Figure 3.8 shows the corresponding smoothed color density scatter plot and respective histograms in the margins for JAC_{T1} and $T - JAC_{\mathrm{T2}}$, for all patients. As we can see in figure 3.8 (b), although there is a difference of the tidal volume in two scans, the scatter plot is still distributed convergently around line y=x. The tidal volume change from scan1 to scan2 can also be found by the intersection angle of the dash regression line and the solid y=x line. Though the scatter distribution does not fit closely to the regression line like the sheep subject, it still shows good repeatability pattern of two Jacobian data sets. Figure 3.9 (a) shows the scatter plot of JAC_{RATIO} against geometrical average Jacobian ($\sqrt{JAC_{\mathrm{T1}}. * T - JAC_{\mathrm{T2}}}$) for patient B. Relative to the reference line y=1, the sparse diffused purple points top and bottom in the figure indicates points in most nonreproducible region, as shown in the color-coded panel.

Figure 3.7 shows the color-coded panel for patient E, which has the worst standard deviation 0.0757 among all the human subjects. For patient E, there is a big difference between the tidal volumes in two scans from 100%IN to 0%EX (see Table 3.3). The tidal volume in scan1 is 0.77 L, while it is 1.23 L in scan2 increasing by 60 percent. In Section 3.3.3, we will try to improve the repeatability of patient E by matching the tidal volume, i.e. looking for a intermediate breathing phase that has a more similar respiratory capacity with scan1 from 0%EX to 100%IN. In Figure 3.8 (e), the scatter distribution is more above line y=x indicating this subject had a larger tidal volume in scan2 than scan1, which could be also demonstrated by looking at the relative shift of the margin histograms. It is also interesting in figure 3.9 (b) that the standard deviation of JAC_{RATIO} varies along the Jacobian value axis, showing for instance higher standard deviation at Jacobian value 1.2 than that at 1.6.

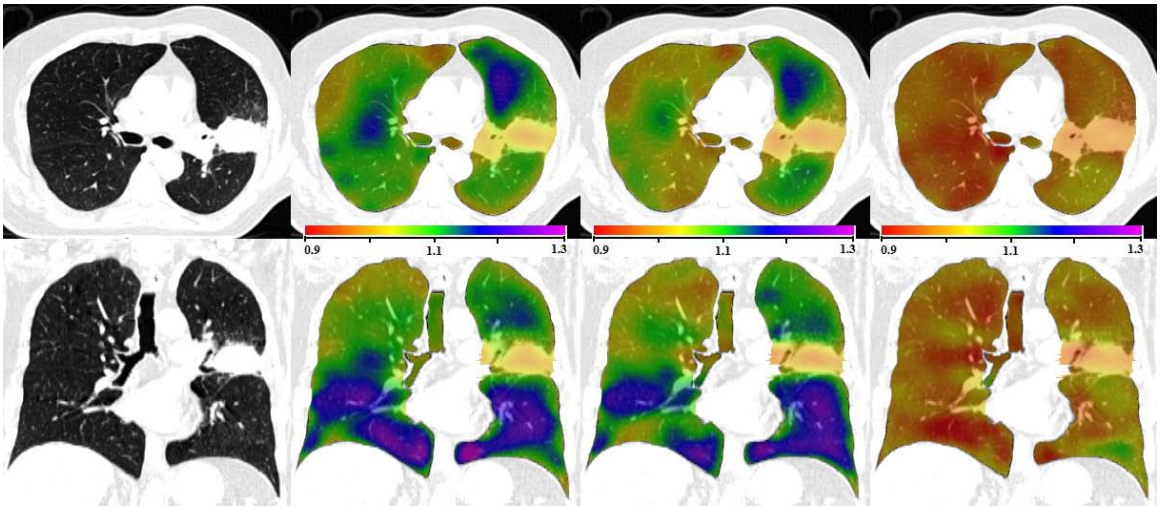

Figure 3.6: Transverse and coronal view of patient B JAC_{T1}, $T - JAC_{\mathrm{T2}}$ and JAC_{RATIO}. The color scales are all 0.9-1.3.

subject	scan	0%EX (:L)	100%IN (:L)	Diff (:L)	Ratio	Jacobian mean	Jacobian std	Jacobian correlation
patient A	1	1.24	1.72	0.48	1.3872	1.0986	0.0565	0.937
	2	1.26	1.94	0.68	1.5401			
patient B	1	5.24	5.86	0.62	1.1181	0.9922	0.0359	0.811
	2	5.34	5.91	0.57	1.1083			
patient C	1	2.90	3.39	0.49	1.1684	1.0254	0.0681	0.860
	2	2.83	3.41	0.58	1.2069			
patient D	1	5.26	5.72	0.46	1.0875	1.0088	0.0515	0.570
	2	5.69	6.37	0.68	1.1198			
patient E	1	3.02	3.79	0.77	1.2575	1.0996	0.0757	0.894
	2	3.12	4.35	1.23	1.3928			
patient F	1	3.65	4.50	0.85	1.2333	0.9513	0.0527	0.772
	2	3.81	4.33	0.52	1.1365			
patient G	1	2.09	2.63	0.54	1.2537	0.9828	0.0635	0.820
	2	2.14	2.61	0.47	1.2211			
patient H	1	3.51	4.09	0.58	1.1663	1.0204	0.0666	0.755
	2	3.54	4.22	0.67	1.1901			
patient I	1	3.95	5.11	1.16	1.2932	1.0223	0.0747	0.850
	2	3.91	5.14	1.23	1.3140			

Table 3.3: Summary of human lung volume of 0%EX and 100%IN in both scans, tidal volume, volume ratio 100%IN/0%EX, mean value of JAC_{RATIO} from two scans, standard deviation of JAC_{RATIO}, and the statistical correlation value between JAC_{T1} and $T - JAC_{\mathrm{T2}}$. The unit for lung volume is in liters(L).

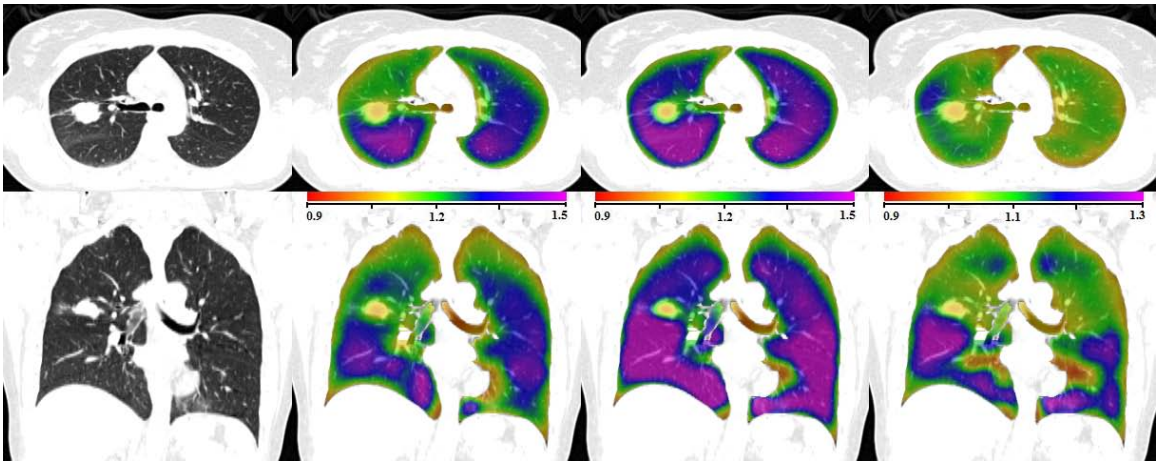

Figure 3.7: Transverse and coronal view of patient E JAC_{T1}, $T - JAC_{\mathrm{T2}}$ and JAC_{RATIO}. Note the color scale for JAC_{T1} and $T - JAC_{\mathrm{T2}}$ is 0.9-1.5, while for JAC_{RATIO}, it is 0.9-1.3.

Figure 3.10, figure 3.11 and figure 3.12 show the reproducibility of ventilation measurement at different Jacobian values (different scale of lung tissue expansion), for sheep A, patient B and patient E respectively. The same tissue which expands at a certain degree in scan1 may expand or contract at a different degree in scan2. To look into the reproducibility at a certain Jacobian value, first we fix a Jacobian value in JAC_{T1}, record the voxel locations, collect the corresponding $T - JAC_{\mathrm{T2}}$ values at the same locations, and make statistics. In practice, to increase the number of samples, we set a bandwidth 0.005 for every fixed JAC_{T1} value. For instance, the fixed value 1.1 in JAC_{T1} is actually a narrow range from 1.095 to 1.105, so any voxel in JAC_{T1} falling in this range are recorded and analyzed. For example in figure 3.10 for sheep A, (a) and (b) shows the conditional histograms of $T - JAC_{\mathrm{T2}}$ at the same locations when JAC_{T1} value is fixed at 1.08 and 1.10. The red vertical line indicates the fixed

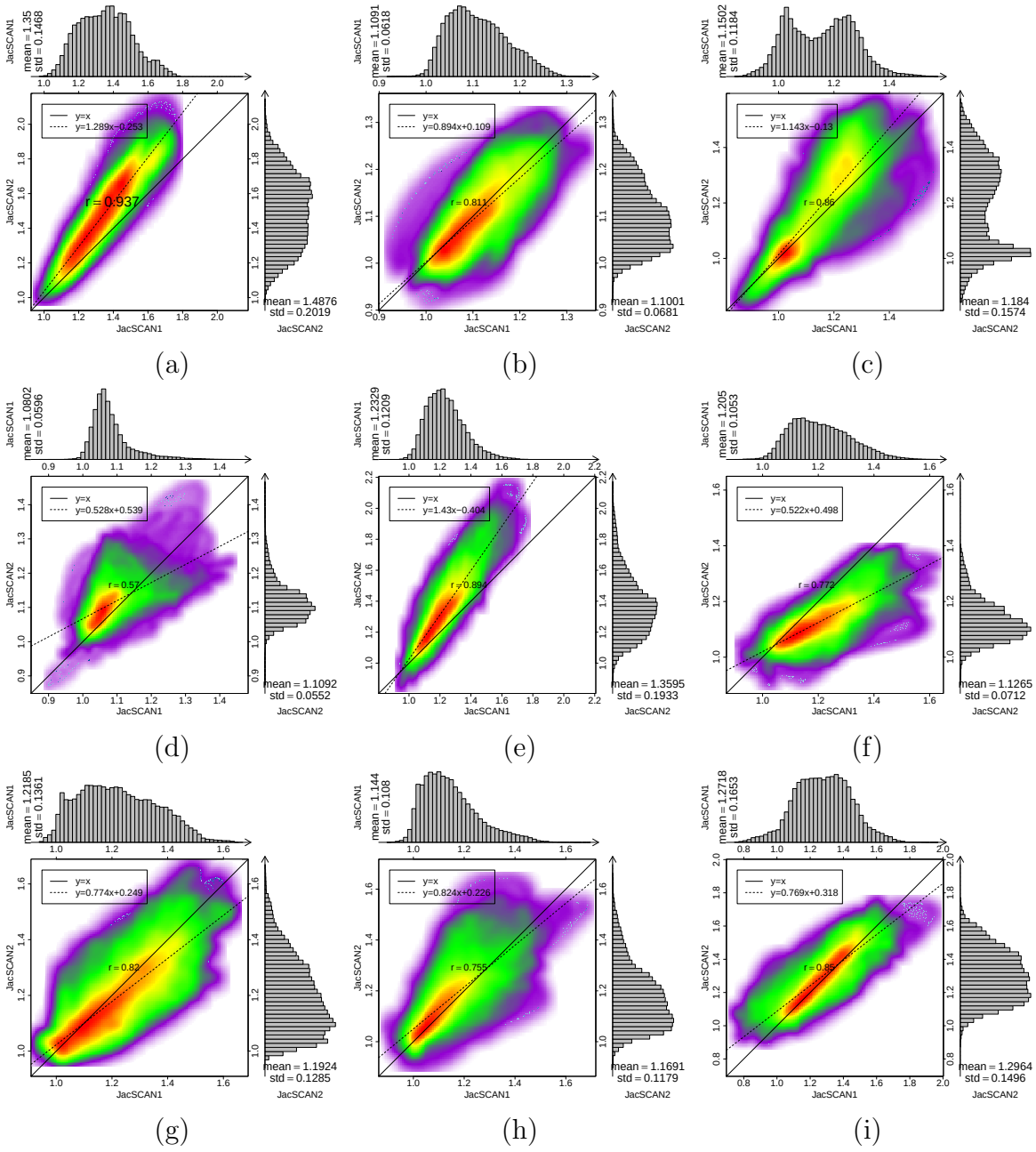

Figure 3.8: Smoothed color density scatter plot and marginal histograms of JAC_{T1} and $T - JAC_{\mathrm{T2}}$ for 9 patients A-I, in the same order (a)-(i).

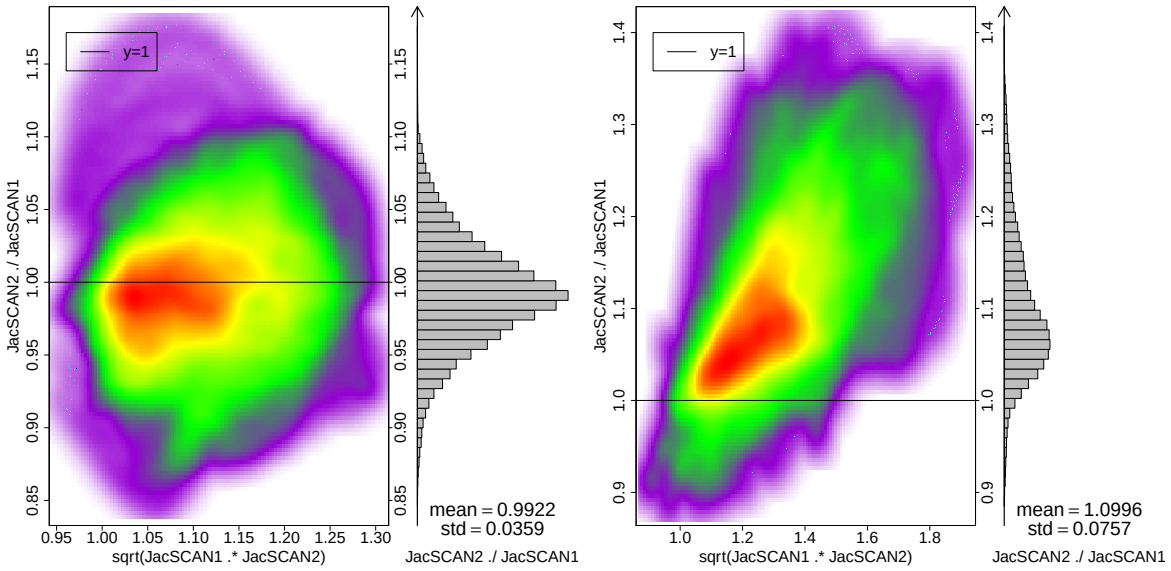

(a) (b)

Figure 3.9: Smoothed color density scatter plot of JAC_{RATIO} against geometrical average of two Jacobian maps (both from 100%IN to 0%EX), and the marginal histogram of JAC_{RATIO}. (a) Patient B; (b) Patient E.

JAC_{T1} value. Corresponding mean and standard deviation of each histogram are displayed on the top right corner. The blue stars in figure 3.10 (c) shows the mean of $T-JAC_{\mathrm{T2}}$ conditional histograms when JAC_{T1} varies from 1.0 to 1.2, and the red line is the reference line y=x. In the case with ideally perfect reproducibility everywhere for all different scales of tissue expansion, the blue stars should overlap with the red reference line. figure 3.10 (d) shows the standard deviation and voxel counts of $T-JAC_{\mathrm{T2}}$ conditional histograms when JAC_{T1} varies from 1.0 to 1.2. The standard deviation here is another parameter to check the regional reproducibility. The voxel counts of Jac2 conditional histograms show the number of statistical events, which reflects the reliability of our statistics. Figure 3.11 is for patient B, and figure 3.12 is

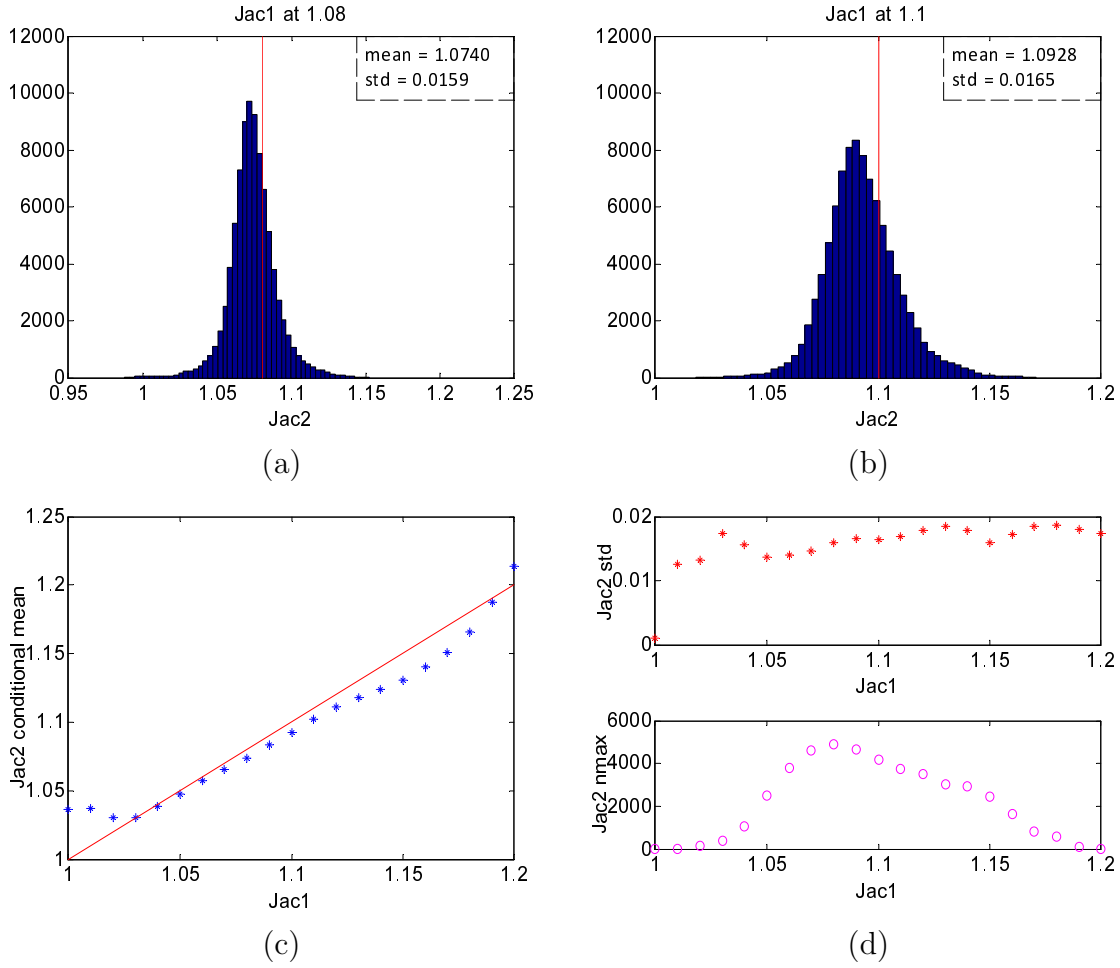

Figure 3.10: For sheep A, $T - JAC_{\mathrm{T2}}$ dispersion distribution at fixed JAC_{T1} value for sheep A. (a) Conditional histograms of $T - JAC_{\mathrm{T2}}$ at the same locations when JAC_{T1} value is fixed at 1.08; (b) Conditional histograms of $T - JAC_{\mathrm{T2}}$ at the same locations when JAC_{T1} value is fixed at 1.10; (c) Mean of $T - JAC_{\mathrm{T2}}$ at the same locations when JAC_{T1} varies from 1.0 to 1.2. The red line is reference line y = x; (d) Standard deviation and voxel counts of $T - JAC_{\mathrm{T2}}$ at the same locations when JAC_{T1} varies from 1.0 to 1.2;

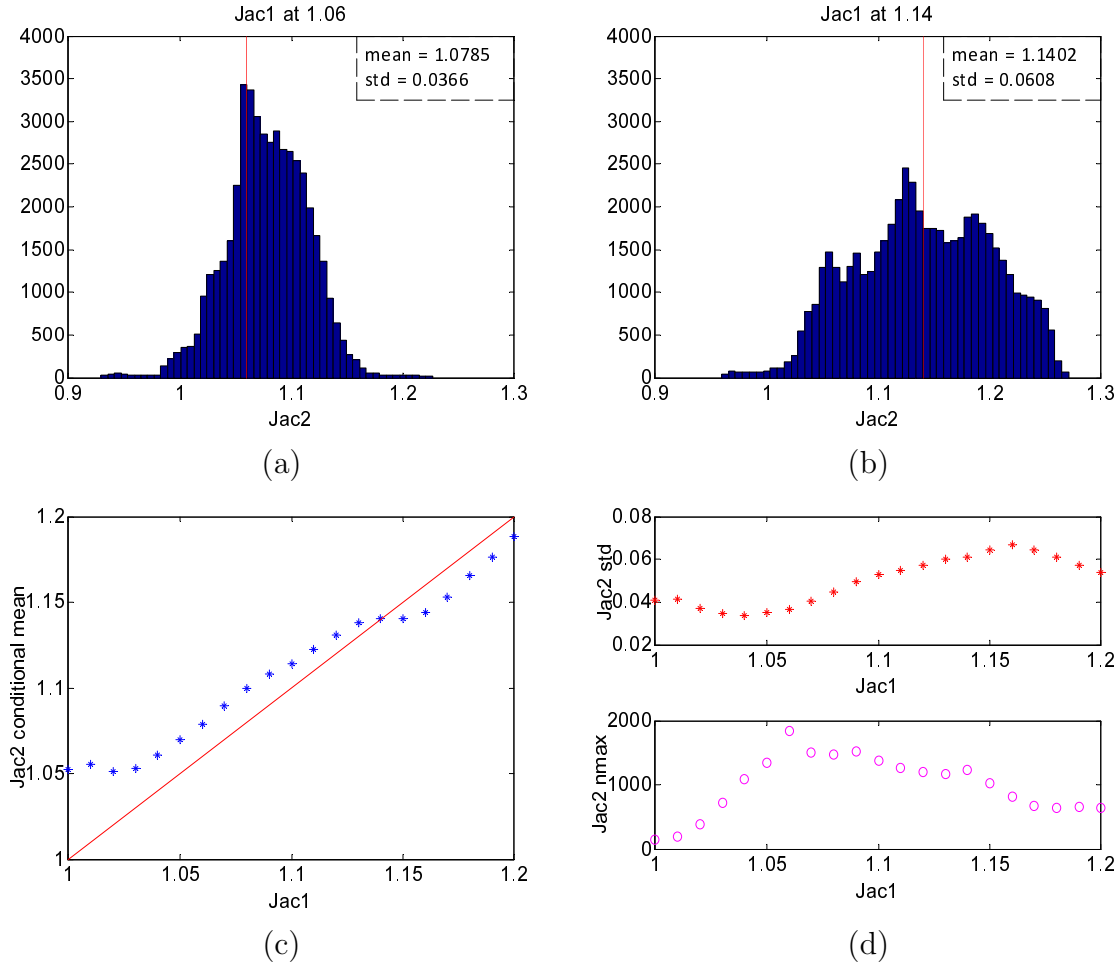

Figure 3.11: $T - JAC_{\mathrm{T2}}$ dispersion distribution at fixed JAC_{T1} value for patient B. (a) Conditional histograms of $T - JAC_{\mathrm{T2}}$ at the same locations when JAC_{T1} value is fixed at 1.06; (b) Conditional histograms of $T - JAC_{\mathrm{T2}}$ at the same locations when JAC_{T1} value is fixed at 1.14; (c) Mean of $T - JAC_{\mathrm{T2}}$ at the same locations when JAC_{T1} varies from 1.0 to 1.2. The red line is reference line y = x; (d) Standard deviation and voxel counts of $T - JAC_{\mathrm{T2}}$ at the same locations when JAC_{T1} varies from 1.0 to 1.2;

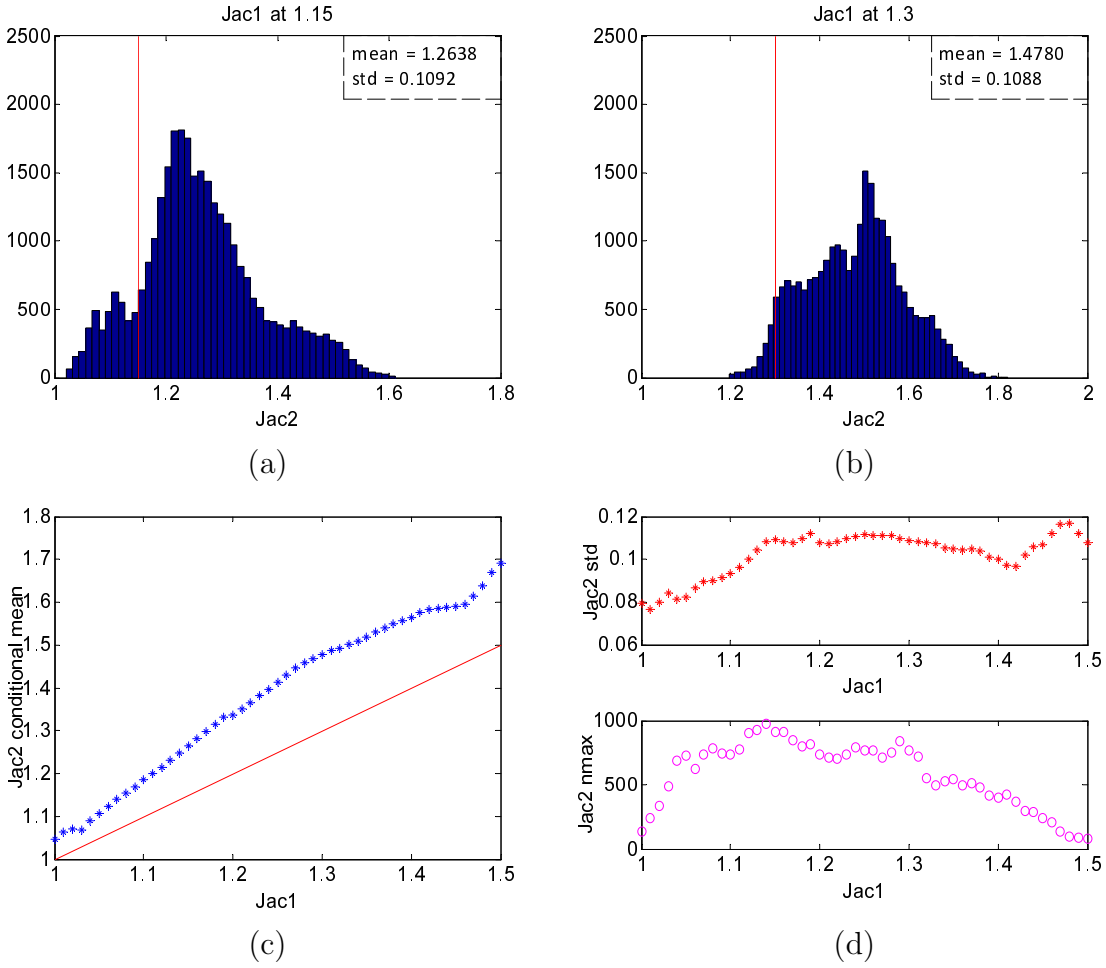

Figure 3.12: $T - JAC_{\mathrm{T2}}$ dispersion distribution at fixed JAC_{T1} value for patient E. (a) Conditional histograms of $T - JAC_{\mathrm{T2}}$ at the same locations when JAC_{T1} value is fixed at 1.08; (b) Conditional histograms of $T - JAC_{\mathrm{T2}}$ at the same locations when JAC_{T1} value is fixed at 1.10; (c) Mean of $T - JAC_{\mathrm{T2}}$ at the same locations when JAC_{T1} varies from 1.0 to 1.5. The red line is reference line y = x; (d) Standard deviation and voxel counts of $T - JAC_{\mathrm{T2}}$ at the same locations when JAC_{T1} varies from 1.0 to 1.5;

for patient E.

3.3.3 Human data reproducibility improvement after lung volume matching

The standard deviation of JAC_{RATIO} represents the reproducibility of pulmonary function measurement. In this section, we are looking into the standard deviation of JAC_{RATIO} for patient E after matching the tidal volume (breath effort) in two scans. Table 3.4 is a summary of lung volume in all breathing phases for patient E, which could be reconstructed in the breath trace curve by calculating the relative respiratory extent to the magnitude of 100%IN breathing phase. As displayed in boldface, Table 3.4 show the result from matching the tidal volume 0.78 L (50%IN to 0%EX) in scan2, the same tidal volume in scan1 from 100%IN to 0%EX. We can see the volume ratio in two scans matches too if we choose 50%IN and 0%EX as the registration pair in scan2. Figure 3.13 is the color-coded panel of patient E after volume matching. It can be observed that compared to Figure 3.7, the second column (scan2) got a more similar pattern like the first column (scan1), besides more green and brown region arises obviously due to decrease of the respiratory volume in scan2. The tissue on the left lung near the diaphragm still differed in regional repeatability. Figure 3.14 (a) shows the scatter distribution encloses line y=x much better and the intersection angle between regression and line y=x becomes smaller after tidal volume matching. The histograms in the margin present a more similar pattern too. In Figure 3.14 (b), the Jacobian ratio scatter plot, changing with different geometrical mean Jacobian values, regresses to line y=1 more closely, and the histogram on the right is more Gaussian-like.

Phases		0%EX	20%IN	40%IN	50%IN	60%IN	70%IN	80%IN	100%IN
scan1	volume	3.02	*3.13*	3.25	N/A	3.41	N/A	*3.57*	3.79
	diff	0	0.11	0.23	N/A	0.39	N/A	0.56	**0.78**
	ratio	1	1.0362	1.0760	N/A	1.1307	N/A	1.1850	1.2600
scan2	volume	*3.12*	3.34	*3.63*	3.90	4.05	4.20	4.36	4.35
	diff	0	0.22	0.51	**0.78**	0.93	1.08	1.24	**1.23**
	ratio	1	1.0714	1.1638	1.2493	1.2975	1.3468	1.3968	1.3928

Table 3.4: Summary of patient E lung volumes in a serial respiratory phases in two 4DCT scans. The unit of lung volume in this table is in liters(L). Since 100%IN means maximum inspiration i.e. end of inspiration, 20%IN, 40%IN, etc. represent step breathing volume of the lung during the process of inspiration. The bold numbers are tidal volumes that are used to make tidal volume matching. The underlined numbers show how to make a head-and-tail volume matching.

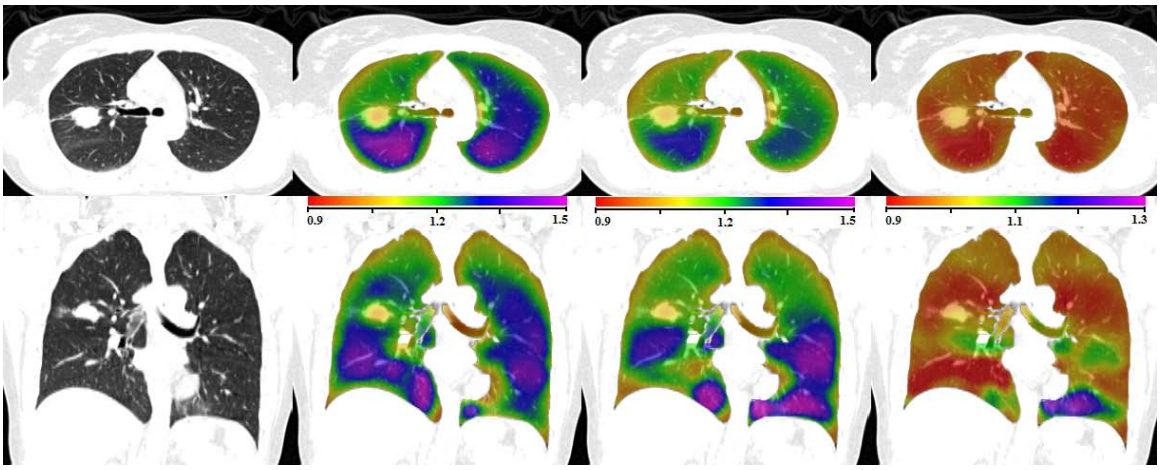

Figure 3.13: Transverse and coronal view of patient E JAC_{T1}, $T - JAC_{\mathrm{T2}}$ and JAC_{RATIO} after lung volume match. JAC_{T1} is got from registration between scan1 100%IN and scan1 0%EX, while $T - JAC_{\mathrm{T2}}$ is got from registration between scan2 50%IN and scan2 0%EX to approach the tidal volume in scan1 from 0%EX to 100%IN. Note the color scale for JAC_{T1} and $T - JAC_{\mathrm{T2}}$ is 0.9-1.5, while for JAC_{RATIO} it is still 0.9-1.3, kept in the same with figure 3.7 the patient E panel before lung volume matching.

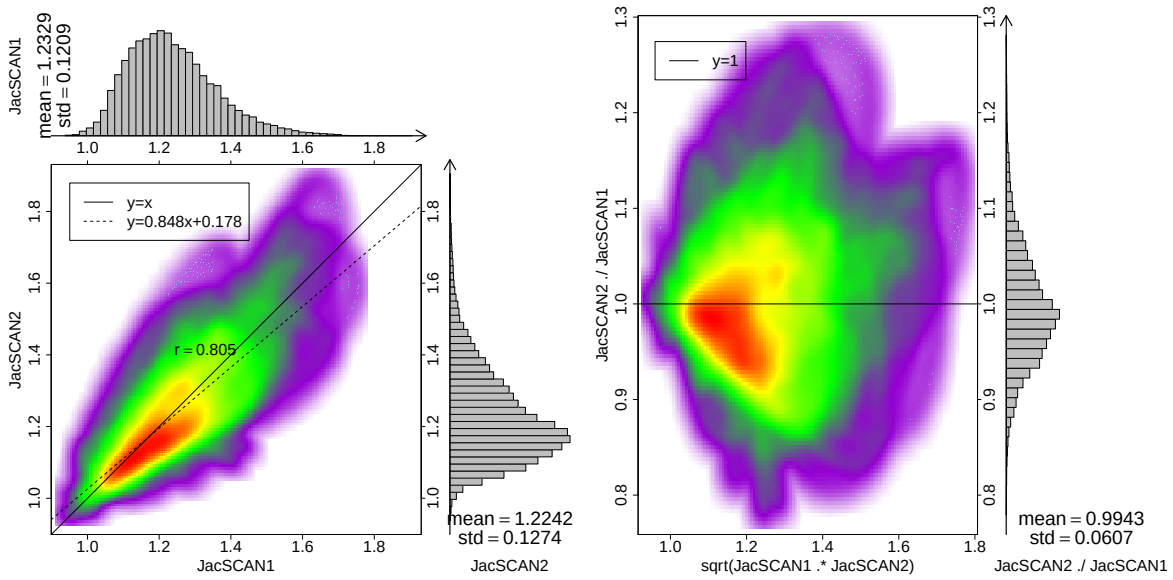

(a) (b)

Figure 3.14: Scatter plot for patient E after volume matching by using 50%IN to 0%EX in scan2. (a) Smoothed color density scatter plot and marginal histograms of JAC_{T1} and $T - JAC_{\mathrm{T2}}$; (b) Smoothed color density scatter plot of JAC_{RATIO} against geometrical average of two Jacobian maps

The above volume matching strategy is to match the tidal volume in two scans. Since globally Jacobian can be treated as the volume ratio of registered lung images, we can also carry out the volume matching by looking for most similar volumes from the inspiration series in two scans, as shown by the italic numbers in table 3.4 and volume curves in figure 3.15. This volume matching is head-and-tail. In scan1, 80%IN was registered to 20%IN, while in scan2 40%IN was registered to 0%EX. Figure 3.16 shows the Jacobian after head-and-tail volume matching. Figure 3.17 (a) shows the smoothed color scatter plot and figure 3.17 (b) shows the scatter plot between Jacobian geometrical average and Jacobian ratio.

Table 3.5 is a summary of mean and standard deviation of JAC_{RATIO} before

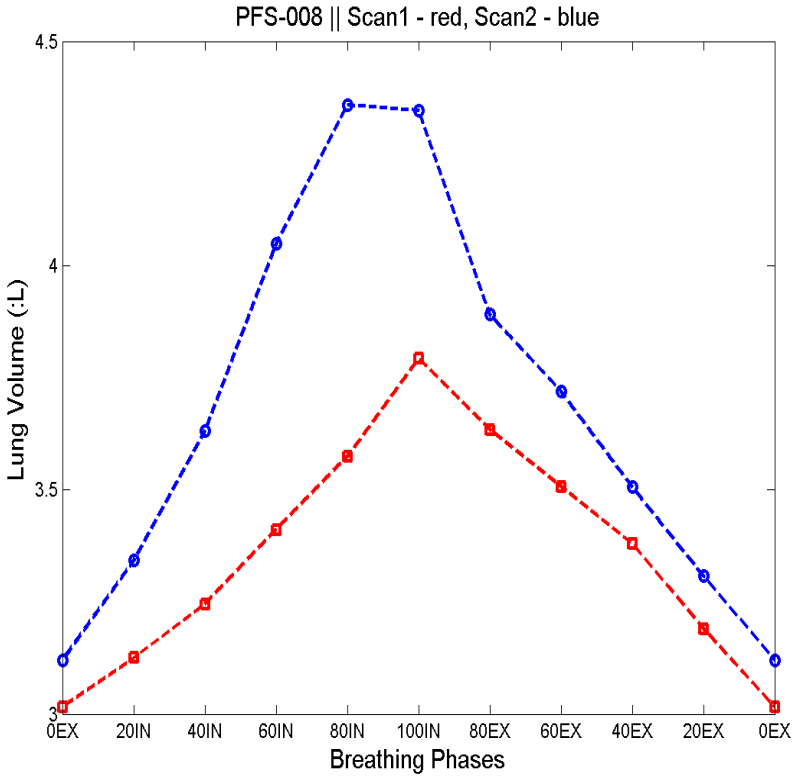

Figure 3.15: Illustration of volume matching for Patient E.

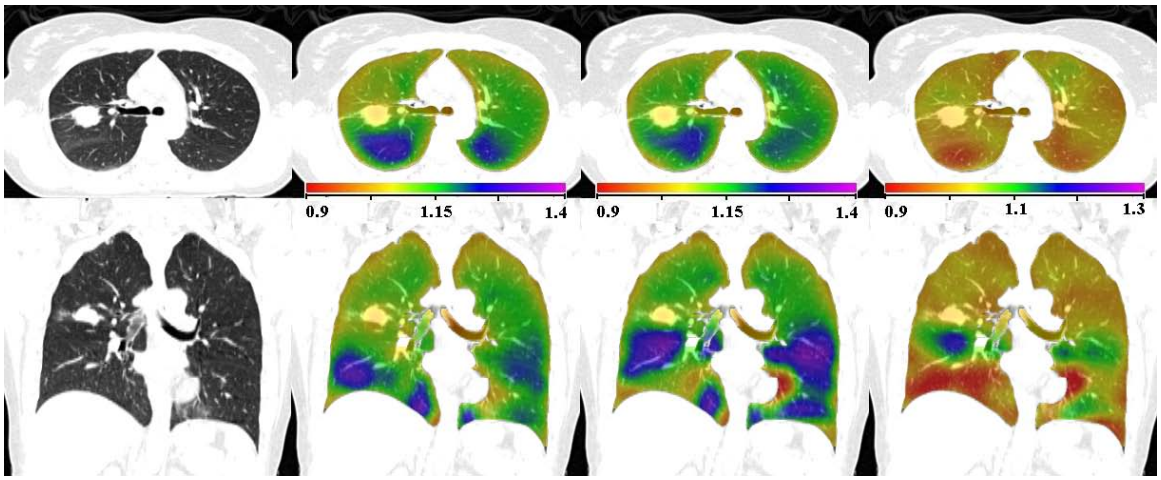

Figure 3.16: Transverse and coronal view of patient E JAC_{T1}, $T - JAC_{\mathrm{T2}}$ and JAC_{RATIO} after head-and-tail volume matching. In scan1, 80%IN was registered to 20%IN. In scan2, 40%IN was registered to 0%EX.

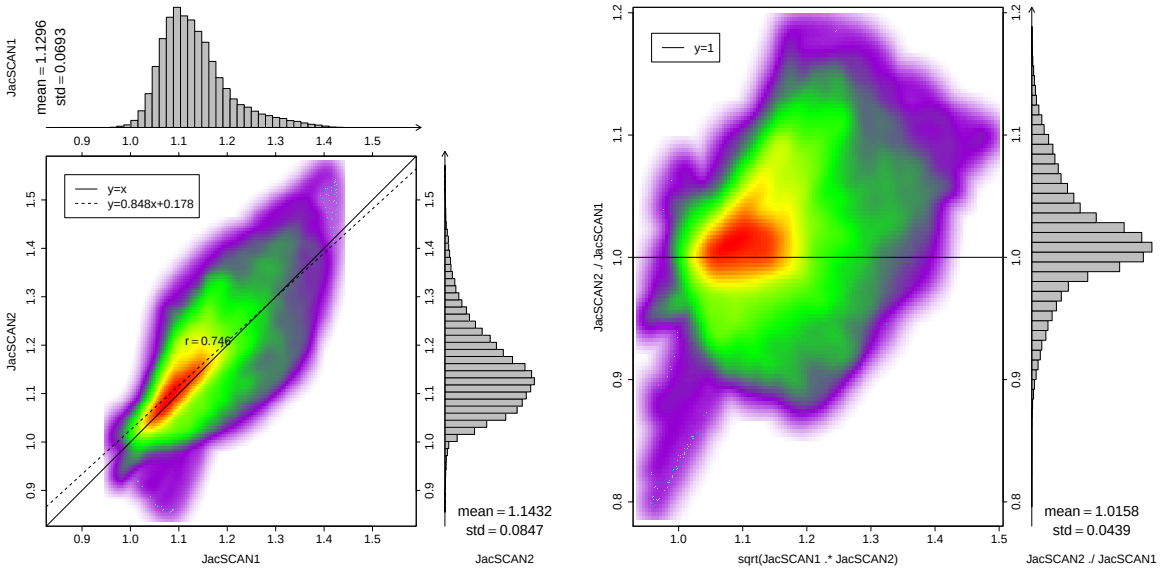

(a) (b)

Figure 3.17: Scatter plot for patient E after head-and-tail volume matching. (a) Smoothed color density scatter plot and marginal histograms of JAC_{T1} and $T - JAC_{\mathrm{T2}}$; (b) Smoothed color density scatter plot of JAC_{RATIO} against geometrical average of two Jacobian maps

Patient E JacRatio	Original	Tidal volume matching	Head&tail volume matching
mean	1.0996	0.9943	1.0158
standard deviation	0.0757	0.0607	0.0434
coefficient of variation	6.8843	6.1048	4.2725

Table 3.5: Summary of volume matching improvement for patient E. Coefficient of Variation (CV) is introduced.

and after two volume matching methods. Since the global volume ratio of these three pairs is different, and in general standard deviation is increasing withe sample mean, we introduce the coefficient of variation (CV) which is defined as the ratio of standard deviation to the mean, multiplied by 100. From the table we can find both volume matching methods improves the reproducibility, and the head-and-tail method performs better.

3.3.4 Normalization of Jacobian in different breath effort

Due to the breath effort difference and lung expansion heterogeneity in different 4DCT scans, normalization of pulmonary function is necessary before comparison of reproducibility. The most straightforward approach is to treat the whole lung as a homogeneously expanding organ, i.e. there is a linear relationship between global volume change and pulmonary function at each voxel location. Zhang [54] et al. proposed a more complicated normalization method to normalize each SPECT scan to the sum of SPECT values of the regions received less than 5 Gy total dose, a dose range in which it is assumed that there is no RT induced perfusion changes. In this section, we will show the high correlation between global volume change and average of whole lung Jacobian, and the application of homogenous Jacobian normalization. Figure 3.18 shows how to normalize Jacobian with different air volume of breath effort(tidal volume). The red marks indicate sheep subjects and the rest indicate patients. The linear regression line of all scatter points is drawn with its equation and correlation coefficient R^2 displayed. Figure 3.18 (a) and (b) show the high correlation between mean of Jacobian map and global lung volume ratio in 2

scans. Figure 3.18 (c) is the scatter plot of mean of JAC_{T1} and $T - JAC_{\mathrm{T2}}$ before volume ratio normalization;. Figure 3.18 (d) shows the result of normalization. As shown in equation 3.6, each Jacobian value in $T - JAC_{\mathrm{T2}}$ was normalized to JAC_{T1} according to the volume ratio information in 2 scans. The scatter plot of mean of normalized $T - JAC_{\mathrm{T2}}$ and mean of JAC_{T1} is plotted in Figure 3.18 (d).

$$\mathrm{NormJac2} = \mathrm{Jac2} \times \frac{(\frac{100\%IN\ volume}{0\%EX\ volume})_{scan1}}{(\frac{100\%IN\ volume}{0\%EX\ volume})_{scan2}} \tag{3.6}$$

3.4 Conclusion and Discussion

In this study we compared Jacobian images generated from two repeat 4DCT data sets prior to radiation therapy, demonstrated regional lung pulmonary function could be reproducibly measured using 4DCT in human subjects and these measurements are consistent with lung spirometry. We also studied the reproducibility of 4DCT scans acquired from sheep which were mechanically ventilated. The ventilation images were generated by calculating the Jacobian metric from the displacement fields of registration between end inspiration phase and end expiration phase with SSTVD plus Laplacian Regularization Constraint registration algorithm. Additionally we explored the feasibility to enhance the measurement reproducibility by matching the tidal volume in repeat scans, and preliminarily discussed how to normalize Jacobian in different breath effort with global lung volume ratio.

The animal subjects which we used as the control group show excellent ventilation measurement reproducibility. From the color-coded Jacobian maps in Figure 3.4,

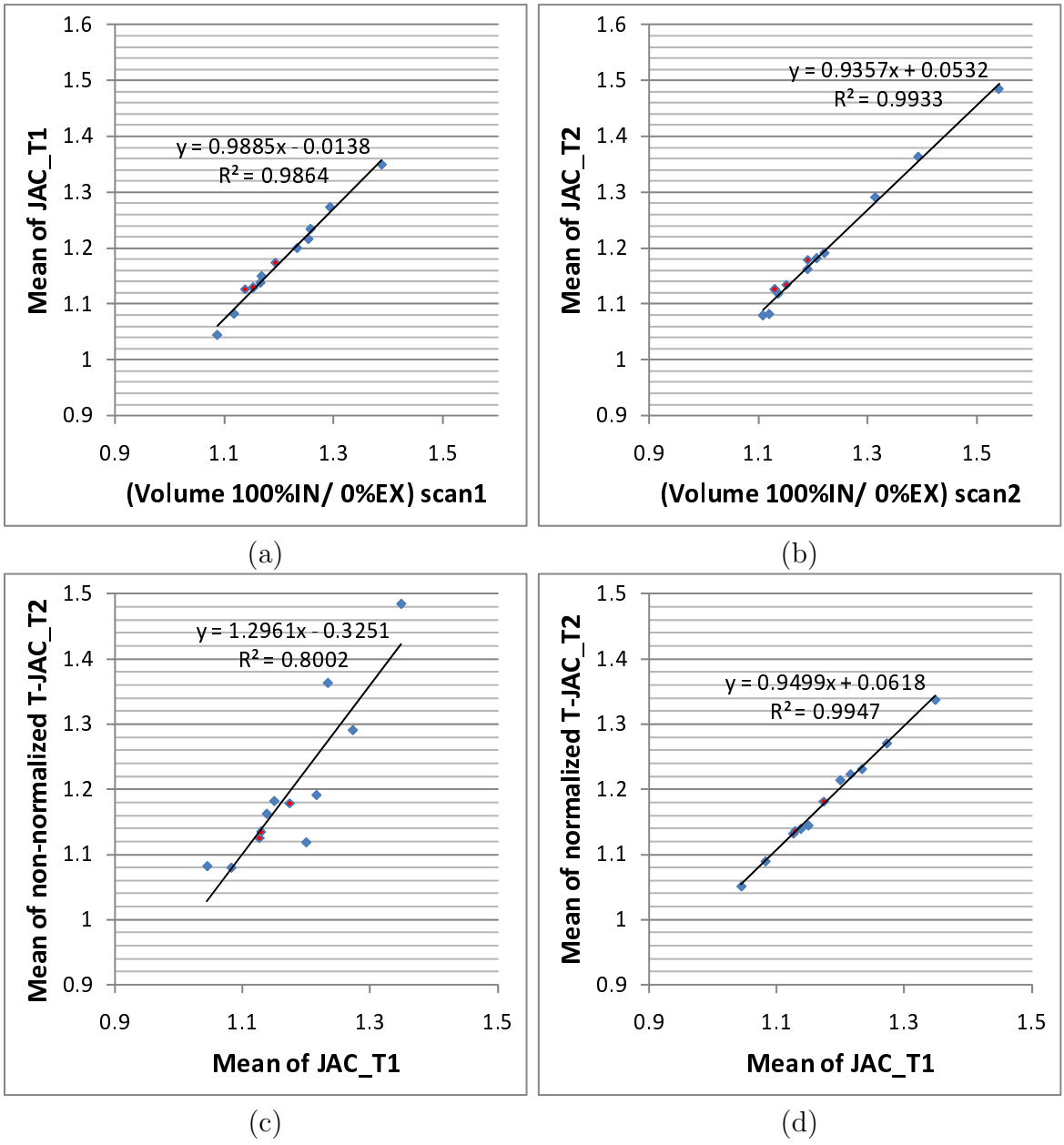

Figure 3.18: Normalize Jacobian in different breath effort across scans. (a) Scatter plot of mean of JAC_{T1} and corresponding global lung volume ratio between 100%IN and 0%EX, for all subjects involved in this paper; (b) Scatter plot of mean of $T - JAC_{\mathrm{T2}}$ and corresponding global lung volume ratio for all subjects; (c) Scatter plot of mean of JAC_{T1} and $T - JAC_{\mathrm{T2}}$ before volume ratio normalization; (d) Scatter plot of mean of JAC_{T1} and normalized $T - JAC_{\mathrm{T2}}$ using volume ratio normalization; The red marks are animal subjects.

we can see that the first two columns have a consistent distribution pattern. In Figure 3.5 (a), the histograms of scan1 and scan2 are similar. The smoothed color density scatter points distribute along the green regression line closely, which means small deviation from scan1 to scan2. In addition, the green regression line is almost parallel to the red line y=x, which reflects the small tidal volume difference in 2 scans. The histograms and standard deviation in figure 3.5 (b) and figure 3.10 show good reproducibility of lung tissue at different level of ventilation. One obvious characteristic feature for the animal data is the images were acquired from anesthetized and mechanically breathed sheep. The excellent reproducibility of regional ventilation measurement in animal data demonstrates the importance of breath control in 4DCT imaging.

In this paper, we also show the color panels and scatter plots of patient B (the best reproducibility) and patient E (the worst reproducibility). The human data appears not so reproducible as the animal data. The standard deviation of JAC_{RATIO} for human subjects is on the order of 3.6 percent to 7.6 percent (on average 5.8 percent), while that for animal subjects is less than 2.6 percent (on average 2.1 percent). The scatter plot distribution is also more biased against the regression line and y=x line. The deteriorated reproducibility in human subjects is understandable because regional deformation of human lung tissue is a very complex process during respiratory without mechanically ventilation as we did on sheep subjects. The reproducibility of ventilation measurement are affected by many factors.

During the 4DCT imaging of human subjects, patients breathed according

to music cue which has rhythmic ups and downs in tones. In the first place, the end of expiration phase and the end of inspiration phase of breath could not be strictly controlled in each independent 4DCT scan. After the imaging interval (about 30 minutes) in our coffee break scan plan, it is hard for patients to remember and reproduce exactly how they breathed previously in scan1. In table 3.3, we can find some subjects who have distinct lung volumes of 0%EX and 100%IN in 2 scans. patient D is the most typical, for which the finishing line of scan1 becomes almost the baseline of scan2. Regional lung ventilation pattern changes at different breath effort, which impacts the measurement reproducibility. Again the tidal volume could not be controlled exactly the same in 2 scans. From figure 3.7, we can see that although the pattern is similar, most lung tissue in scan2 expands more than in scan1, due to the larger tidal volume in scan2. Second, breathing patterns also affect the ventilation measurement reproducibility. Patients may make thoracic breathing in scan1 and switch to abdominal breathing in scan2, or combine into a bi-mode differently in 2 scans. As shown in figure 3.8 (c), patient C is one typical subject with bi-mode breath in both scans. In figure 3.8 (e) we can see the obvious difference of breathing pattern form the histograms of 2 scans. Third, the patients in this paper were all undergoing radiation therapy for lung tumor radiation. As lung tissue compliance and resistance changes due to disease or injury, so does the breathing pattern. When a person suffers from lung cancer for instance, the tumor may block some part of the lung and interfering with the flow of air. So it becomes more difficult for these patients to breath in a same pattern in 2 scans.

Among the factors impacting reproducibility, breathing volume matching is one approach easy to implement by matching the tidal volumes in 2 scans. As what we did for for patient E in Section 3.3.3, we proposed two volume matching methods. As shown in table 3.4, we can match the tidal volume or match the head-and-tail volumes in two scans. After both volume matching methods, the scatter plot goes more closely along the regression line and y=x line, Jacobian histograms appears in a more similar pattern in 2 scans, and JAC_{RATIO} histogram is more Gaussian-like, as shown in figure 3.13, 3.14, 3.16 and 3.17. The coefficient of variation (CV) of JAC_{RATIO} reduces by 0.8 percent after tidal volume matching, and 2.6 percent after head-and-tail volume matching indicating bettter improvement of reproducibility.

Another approach to reduce the affect of breathing effort to reproducibility is to normalize the Jacobian in different volume change. In figure 3.18 (a) and (b), we can see the extreme high correlation of mean of Jacobian value and the global volume ratio in both 2 scans, which inspires us to make use of the volume ratios to normalize Jacobian. As shown in equation 3.6, each voxel in $T - JAC_{\mathrm{T2}}$ were multiplied with a parameter which is the ratio of lung volume ratio from 0%EX to 100%IN in 2 scans. Compared with figure 3.3.4 (c) which shows mean value of $T - JAC_{\mathrm{T2}}$ and JAC_{T1} without normalization, the mean normalized $T - JAC_{\mathrm{T2}}$ correlates very well with JAC_{T1} in figure 3.18 (d). The advantage of this method is that whenever we get a third 4DCT scan of the same patient after RT, we can check the reproducibility or lung function change before and after RT [12] using Jacobian normalization, without considering the variant tidal volume in different 4DCT scans. Jacobian normalization

in euqation 3.6 provides a way to offset the influence of breathing effort difference in lung 4DCT scans.

The purpose of study on regional lung ventilation reproducibility is to demonstrate the pulmonary function can be reproducibly measured using 4DCT and image registration, so that the measured lung function change before and after RT reflects real pulmonary function change rather than measurement error in the process of image acquisition and processing. To improve the reproducibility, firstly we need more precise breathing control during 4DCT. Secondly patients should be trained more and better on breathing and following to the music cue in 4DCT. The coffee break time should also be studied to establish a more reasonable scanning plan. Better normalization method could also help avoid the influence of different breathing effort.

Although not so perfect as the animal data, the reproducibility results of human subjects in this paper is convincing and useful. It is our expectation that reproducibility of human subjects is worse than animal subjects due to lack of strict breathing control. Similar pulmonary function distribution can be directly seen from color coded Jacobian map, and the standard deviation of JAC_{RATIO} is on the order of 0.036-0.076, most of which are around 0.05. The reproducibility of different Jacobian values was analyzed in conditional histograms, demonstrating that the whole lung standard deviation of JAC_{RATIO} is sound with small fluctuation of regional standard deviation shown in (figure 3.10, figure 3.11 and figure 3.12).

In conclusion, we have described a method to study regional reproducibility of pulmonary function measurement using 4DCT imaging and image registration before

radiation therapy. This paper demonstrates the significance of registration-based measurement of lung function change before and after radiation therapy, and supports the study on the relationship between radiation dose distribution and pulmonary function change.

CHAPTER 4
METRICS FOR REPRODUCIBILITY ASSESSMENT ON 4DCT-BASED PULMONARY FUNCTION

4.1 Introduction

Regional pulmonary function is the term used to characterize the volume fraction of fresh gas per unit time that enters or exits the lung at the acinar (gas exchange) level. Regional pulmonary function can reflect alterations in airways (physiological or pathological), parenchymal mechanics, muscles of respiration, body posture effects and inhaled gas properties. Four-dimensional computed tomography (4DCT) and image registration based technique has been previously proposed to measure regional ventilation and track radiation induced pulmonary function change in the normal lung tissue in mice and human subjects [17, 6, 11]. Patients goes through a 4DCT scan with proper respiratory control and gating prior and post to RT. After the deformable 3D image registration between end of inspiration and end of expiration, we obtain transformative voxel-by-voxel displacement field from which we can calculate regional pulmonary function [36].

However, the measured regional pulmonary function change could be affected by many uncertainties. The baseline volume and tidal volume in the respiratory cycles of two scans may vary much, causing different magnitude and pattern of expansion and contraction of lung tissue. The various breathing patterns may also be a problem, especially for patients with seriously damaged lungs who cannot control their breath

well. There may be inconformity of the imaging process in the two scans, for example the Hounsfield Units (HU) may be different. Image processing algorithm might also induce influences on the reproducibility. Therefore in order to validate how much the measured function change is affected by uncertain factors except the inducement of radiation itself, we need to establish the measurement reproducibility study first.

In this chapter, we investigate the pulmonary function measurement reproducibility in repeated 4DCT scans prior to RT. We introduce four methods to quantitatively and regionally measure reproducibility. They all show good reproducible pulmonary function for our best human subjects from registration-based calculation in Chapter 3. Registration accuracy is computed by lung landmark distances before and after registration. A made shift of scan2 Jacobian was tested on all of the four metrics to assess of the sensitivity to spatial misalignment.

4.2 Materials and Methods

4.2.1 Method Overview

Figure 4.1 shows a block diagram of the entire process. For each 4DCT, 100%IN (end inspiration) is registered to 0%EX (end inspiration) using non-linear 3D image registration to assess local pulmonary function (PF) via the Jacobian determinant. 4DCT scan2 0%EX image is also registered onto the coordinate system of scan1 0%EX image, so that JAC_{T2} is warped by transform T0 to $T - JAC_{\mathrm{T2}}$. JAC_{RATIO} is calculated for reproducibility analysis. Mean and standard deviation of JAC_{RATIO} are computed as reproducibility parameters. Gamma comparison [29] applied to JAC_{T1} and $T - JAC_{\mathrm{T2}}$ is a method which takes into consideration the spatial

shift and steep Jacobian distributions. Registration displacement fields are also compared for reproducibility after displacement of scan2 is warped to our coordinate, in two metrics - area of vector parallelogram and magnitude of vector difference. Due to limit of space, we use one subject for the explanation across our four reproducibility metrics, and at the end correlations of the four methods on all nine human subjects are compared.

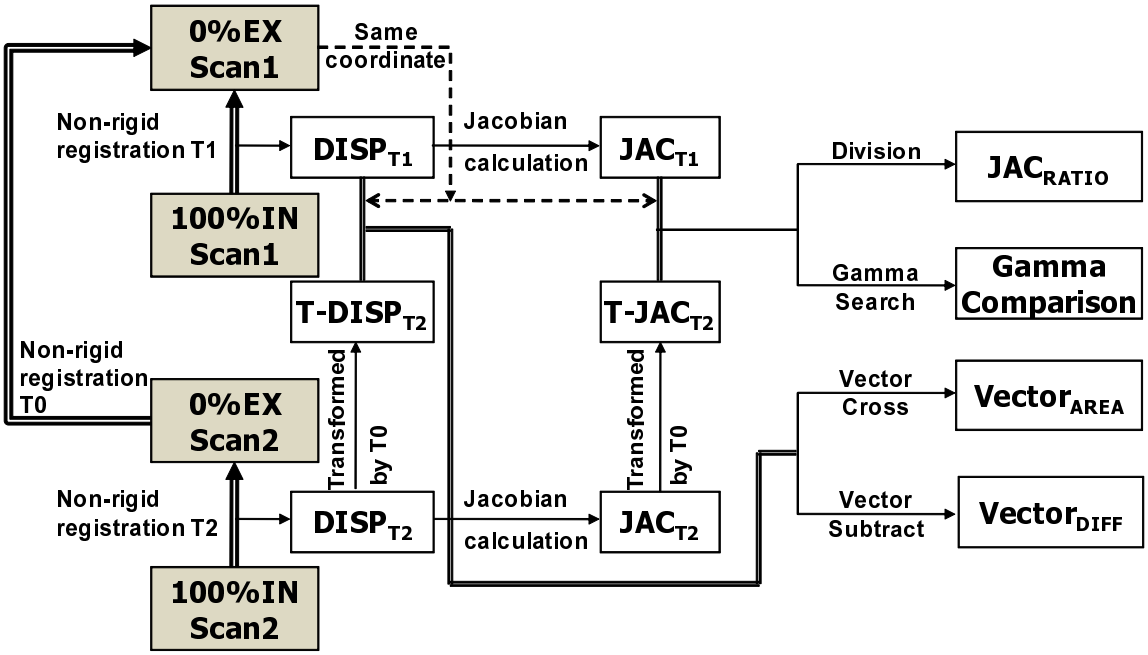

Figure 4.1: Figure shows repeated 4DCT prior to RT (scan1, and scan2) that are analyzed during the processing. Shaded boxes indicate 4DCT image data; white boxes indicated derived or calculated data; thick arrows indicate image registration transformations being calculated; thinner solid lines indicate other operations. All the derived pulmonary function analysis and displacement analysis are based on the scan1 0%EX coordinate.

4.2.2 Data Acquisition

All human data sets were gathered under a protocol approved by the University of Iowa IRB. 4DCT data from nine patients with lung tumors treated in the Department of Radiation Oncology at the University of Iowa Hospitals and Clinics was used for this study. The patients took two 4DCT imaging prior to RT with interval of around 30 minutes(called "coffee break scans"). Musical cues were used to pace respiration during imaging, a technique developed at our institution and shown to have high success and compliance [44]. The patient identifier was removed from the image data. 4DCT images from three anesthetized and mechanically ventilated sheep are also used for analysis. The in-plane pixel spacing of images is approximately 0.97 mm $\times$ 0.97 mm, with slab thickness 2mm.

4.2.3 Image Registration and Regional Lung Expansion

The tissue volume preserving nonrigid registration algorithm, combined with cubic b-spline transformation model and Laplacian Regularization Constraints (LAP), is used to match the lung structure across the respiratory circle, which provides a voxel-by-voxel displacement field between the two images being matched. This algorithm minimizes the sum of squared tissue difference (SSTVD) while at the same time regularizing LAP constraints as shown in Equation 4.1. This method has been shown to be effective at registering lung CT images with high accuracy [5].

$$C_{\mathrm{TOTAL}} = C_{\mathrm{SSTVD}} + \rho C_{\mathrm{LAP}}, \tag{4.1}$$

where C_{SSTVD} is the SSTVD cost, C_{LAP} is the Laplacian regularization constraint, and ρ is a weighting parameter.

In our registration algorithm, SSTVD serves as the intensity similarity criterion because it compensates the change in CT intensity as air inhaled or exhaled in the respiratory process. Therefore it is especially useful when it comes to the registration of images acquired at different air pressure levels. The SSTVD cost function assumes Hounsfield Units (HU) of lung CT images is a function of tissue and air content. The factual tissue volume V($\mathbf{x}$) at voxel coordinate $\mathbf{x}$ can be estimated as

$$V(\mathbf{x}) = v(\mathbf{x})\frac{HU(\mathbf{x}) - HU_{air}}{HU_{tissue} - HU_{air}}, \tag{4.2}$$

Where v($\mathbf{x}$) is the total volume of voxel $\mathbf{x}$. HUair and HUtissue refer to the intensity of air and tissue respectively. We assume air intensity is -1000 and tissue intensity is 55. Then the intensity similarity metric becomes as

$$\begin{aligned} C_{\mathrm{SSTVD}} &= \int_{\mathbf{\Omega}} \left[V_2(\mathbf{x}) - V_1(\mathbf{h}(\mathbf{x}))\right]^2 d\mathbf{x} \\ &= \int_{\mathbf{\Omega}} \left[v_2(\mathbf{x})\frac{I_2(\mathbf{x}) + 1000}{1055} - v_1(\mathbf{h}(\mathbf{x}))\frac{I_1(\mathbf{h}(\mathbf{x})) + 1000}{1055}\right]^2 d\mathbf{x} \end{aligned} \tag{4.3}$$

where Ω denotes the union of two lung regions.

After image registration, the vector transformation function $\vec{h}(x, y, z)$ that maps template image to target image is used to calculate the local lung expansion

and contraction using the Jacobian determinant $J(x, y, z)$ defined as [36]:

$$J(\vec{h}(x,y,z)) = \begin{vmatrix} \frac{\partial h_1(x,y,z)}{\partial x_1} & \frac{\partial h_2(x,y,z)}{\partial x_1} & \frac{\partial h_3(x,y,z)}{\partial x_1} \\ \frac{\partial h_1(x,y,z)}{\partial x_2} & \frac{\partial h_2(x,y,z)}{\partial x_2} & \frac{\partial h_3(x,y,z)}{\partial x_2} \\ \frac{\partial h_1(x,y,z)}{\partial x_3} & \frac{\partial h_2(x,y,z)}{\partial x_3} & \frac{\partial h_3(x,y,z)}{\partial x_3} \end{vmatrix}. \tag{4.4}$$

where $h_1(x, y, z)$ is the x component of $\vec{h}(x, y, z)$, $h_2(x, y, z)$ is the y component of $\vec{h}(x, y, z)$, and $h_3(x, y, z)$ is the z component of $\vec{h}(x, y, z)$. In the Eulerian coordinate, if the Jacobian is greater than one, there is local tissue expansion; if the Jacobian is less than one, there is local tissue contraction. In our study, we registered the maximum inhalation image to the maximum exhalation image for the calculation of local lung expansion and contraction as a measurement of regional pulmonary function. For visualization, the Jacobian map is color-coded and overlaid onto the original CT data.

4.2.4 Reproducibility Metrics

Displacement Vector Area and Magnitude of Vector Difference As shown in equation 4.4, the Jacobian determinant is directly related to vector motion information in registration displacement field. Comparison between two displacement fields should tell us reproducibility information of tissue expansion in two scans. Figure 4.1 shows the operations on two displacement fields. On the coordinate of scan1 0%EX, every voxel has a motion vector $\overrightarrow{v_1}$ in $DISP_{\mathrm{T1}}$ and $\overrightarrow{v_2}$ in $DISP_{\mathrm{T2}}$. For each voxel, the area of parallelogram formatted by $\overrightarrow{v_1}$ and $\overrightarrow{v_2}$ is computed representing regional

tissue motion reproducibility.

$$\text{vectorarea} = |\overrightarrow{v_1} \times \overrightarrow{v_2}| \tag{4.5}$$

Averaged vector area over all lung voxels can be used as a global reproducibility parameter. Besides the vector area, we can also compute the magnitude of vector difference ($|\overrightarrow{v_1}\text{-}\overrightarrow{v_2}|$) for each voxel. Averaged magnitude of vector difference is also computed.

Jacobian Ratio Map The most straightforward method to compare JAC_{T1} and $T-JAC_{\text{T2}}$ is by dividing these two maps voxel-by-voxel to get a ratio map JAC_{RATIO}. Since Jacobian is nonlinear and exponential we use ratio map instead of difference map. Suppose the pulmonary function measurement has perfect reproducibility, in that way JAC_{RATIO} should have 1.0 everywhere with standard deviation 0. However, due to baseline shift and tidal volume difference in two scans, the mean of JAC_{RATIO} is always larger or less than 1.0. The heterogeneity of tissue expansion also induces a nonzero standard deviation, which is an important parameter in our reproducibility study.

Gamma Comparison Although Jacobian ratio map makes it clear by how much the two Jacobian distributions disagree on a voxel-by-voxel level, there are practical limitations to this method. The two Jacobian may not be precisely aligned. One of them is measured in the first 4DCT, and in the second 4DCT there is a spatial error

tolerance on the ability to position the patient, image readout, and image registration error. If there is a spatial disalignment in the two measurement, the Jacobian ratio value that lies within steep Jacobian gradients will be artificially enhanced by the spatial shift of the two pulmonary distributions. Gamma dose evaluation tool is used in quantitative comparison of dose distributions to assure high quality RT dose delivery [29]. In this paper we introduce a similar γ equation for Jacobian distribution comparison:

$$\gamma(\overrightarrow{r_2}, \overrightarrow{r_1}) = \min_{\overrightarrow{r_2}} \{\Gamma(\overrightarrow{r_2}, \overrightarrow{r_1})\} = \min_{\overrightarrow{r_2}} \{\sqrt{(\frac{\overrightarrow{r_2} - \overrightarrow{r_1}}{\Delta d_0})^2 + (\frac{\hat{J}_2(\overrightarrow{r_2}) - J_1(\overrightarrow{r_1})}{\Delta J_0})^2}\} \tag{4.6}$$

where

$$\hat{J}_2 = J_2 \times \frac{(\frac{100\%IN\ \ volume}{0\%EX\ \ volume})_{scan1}}{(\frac{100\%IN\ \ volume}{0\%EX\ \ volume})_{scan2}} \tag{4.7}$$

J_2 is normalized to the effort scale of J_1 by equation 4.7 before gamma search comparison. The Jacobian normalization is to compensate large volume mismatch. $\overrightarrow{r_1}$ and $\overrightarrow{r_2}$ are the vector positions of JAC_{T1} and $T - JAC_{\mathrm{T2}}$ points respectively. $J_1(\overrightarrow{r_1})$ and $J_2(\overrightarrow{r_2})$ are Jacobian values in two scans. Δd_0 is our criteria for spatial offset tolerance and ΔJ_0 is the Jacobian difference criteria. In this paper we use $\Delta d_0 = 4mm$ and $\Delta J_0 = 5\%$. For any given point in JAC_{T1} there are as many Γ as there are evaluated points in the search space in $T - JAC_{\mathrm{T2}}$. The minimum value of Γ is the value of γ. In our algorithm, the intensity difference criterion ΔJ_0 is dynamic determined. $\Delta J_0 = 5\%$ means for each voxel, the criterion is 5 percent of Jacobian in that voxel. By dynamic ΔJ_0 we make allowance for different expansion rate.

The angle in equation 4.8 can be used to determine if the γ function between the two Jacobian distribution is due to the Jacobian difference or voxel location or intermediate reason.

$$\theta = \arctan\left(\frac{|\frac{\hat{J}_2(\vec{r_2}) - J_1(\vec{r_1})}{\Delta J_0}|}{|\frac{\vec{r_2} - \vec{r_1}}{\Delta d_0}|}\right) \tag{4.8}$$

The γ function is the minimum distance between two Jacobian distributions. Figure 4.2 shows that the distance takes into consideration not only spatial distance, but also Jacobian values. The passing and failing threshold of γ test is $\gamma = 1$. The voxel with $\gamma < 1$ passes implying that the voxel can find a voxel in the other distribution with less than 5% Jacobian difference within distance of 4mm. The pass region percent rate is computed by counting all passed voxel divided by total lung voxel number. To compare the four reproducibility metrics, we deliberately shifted down the scan2 Jacobian map by 10 mm in the z direction towards the diaphragm. Metrics color maps and histograms were compared before and after the shift test.

4.3 Results

4.3.1 Registration Accuracy

Approximately 120 automatic identified landmarks within the lungs are used to compute the registration accuracy. The landmarks are uniformly distributed in the lung regions. Figure 4.3 shows registration accuracy assessment of one subject with landmark points distribution and landmark distances before and after image registration in registration T0, T1 and T2 4.2.1. And for all subjects the landmark distance after registration are all reduced to the order of less than 1.0 mm, confirming with

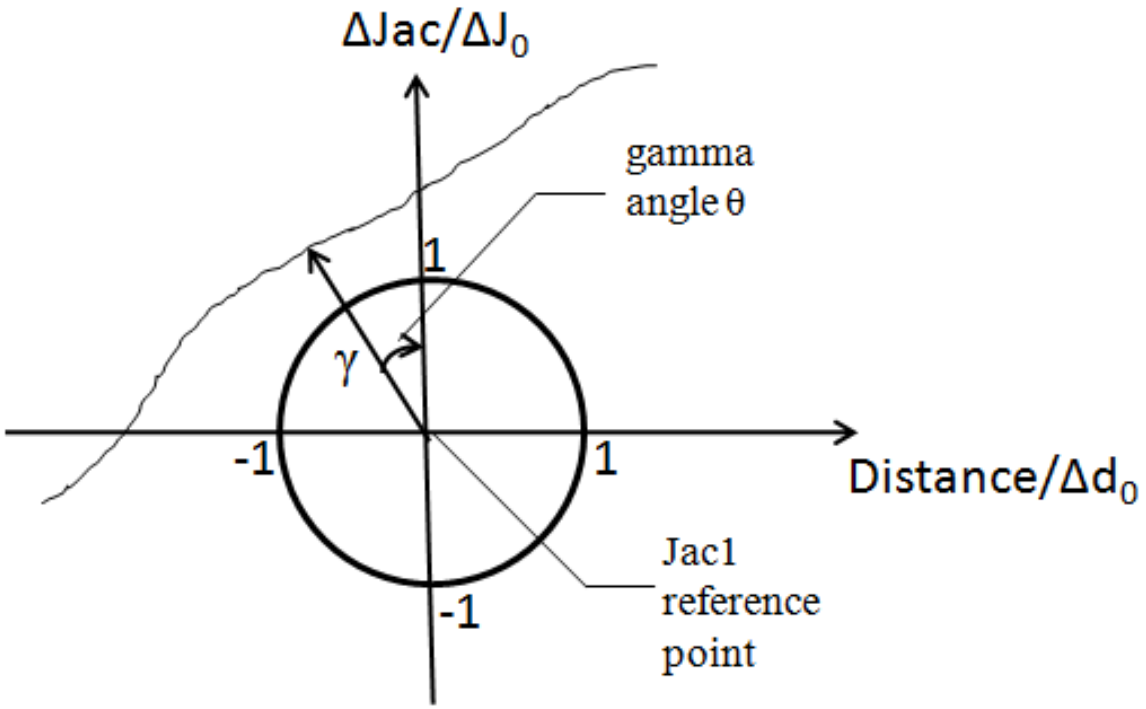

Figure 4.2: Gamma comparison gives consideration to both spatial difference and Jacobian difference.

previous reported registration accuracy of SSTVD registration algorithm [5]. The landmark distance analysis shows good image registration accuracy and guarantees the further regional lung function study.

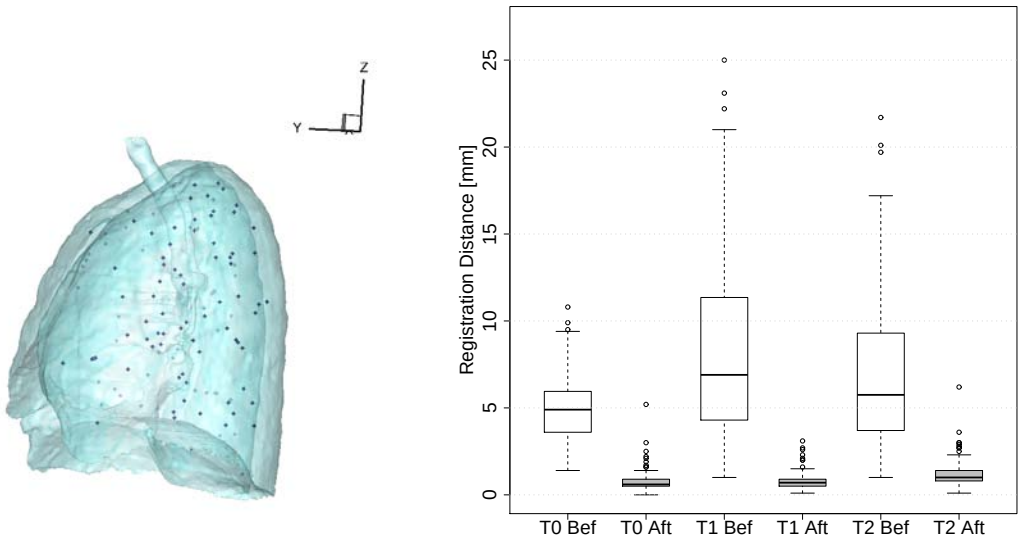

(a) (b)

Figure 4.3: Registration accuracy. (a) Landmark points distribution in sagittal view; (b)Lung landmark distance before and after registration in registration T0, T1 and T2.

4.3.2 Reproducibility

Table 4.1 is a summary of global lung volumes in extreme breathing phases, tidal volume, volume ratio and statistical information of JAC_{RATIO}. Figure 4.4 is the color-coded panel of regional pulmonary function in two scans and JAC_{RATIO} for one patient. The color scales for the three color maps are all the same. From Table 4.1, the tidal volume in scan2 is only 0.57 L, less than 0.62 L as in scan1, so we could

see from the panel the lung in scan2 does not expand as much as scan1. Most of the lung shows high reproducibility while the distinct part appears mainly near the diaphragm. Another obvious nonreproducible region appears at the right lower corner of the left lung, where lung in scan2 expands abnormally more than that in scan1. Regions around the tumor also shows high similar pattern and high reproducibility.

subject	scan	0%EX (:L)	100%IN (:L)	Diff (:L)	Volume Ratio	Jacobian mean	Jacobian std
PFS-002	1	5.24	5.86	0.62	1.1181	0.9922	0.0359
	2	5.34	5.91	0.57	1.1083		

Table 4.1: Summary of lung volume of 0%EX and 100%IN in both scans, tidal volume, volume ratio 100%IN/0%EX, mean value of JAC_{RATIO} from two scans, standard deviation of JAC_{RATIO}, and the statistical correlation value between JAC_{T1} and $T - JAC_{\mathrm{T2}}$, for one specific subject. The unit for lung volume is in liters(L).

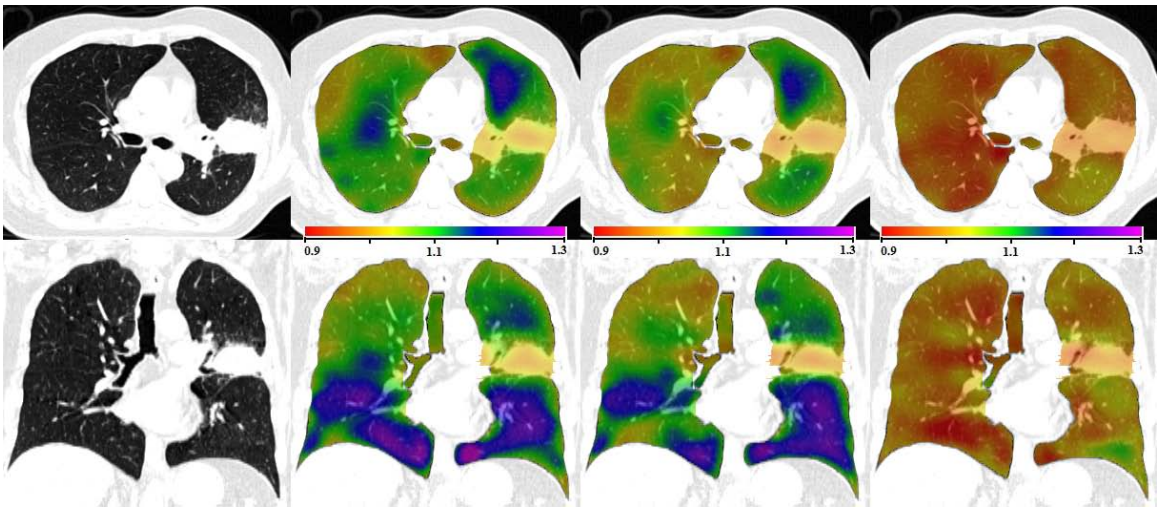

Figure 4.4: Transverse and coronal view of JAC_{T1}, $T - JAC_{\mathrm{T2}}$ and JAC_{RATIO} by dividing JAC_{T2} with JAC_{T1}.

Figure 4.5 (a) shows the color-coded map of displacement field vector area (left) and magnitude of displacement field vector subtract (right). Both vector area and vector subtract magnitude show worse reproducibility near the diaphragm. Figure 4.5 (b) shows the color map of gamma value (left) and gamma angle (right) in gamma comparison metric. Figure 4.6 shows the shifted $T - JAC_{\mathrm{T2}}$ and shifted JAC_{RATIO} towards the diaphragm. Figure 4.7 proposes the color maps of vector area, vector difference and gamma value after the shift test. Figure 4.8 shows the histograms of the four metrics we used, before and after the shift test. All of the histograms are computed inside the lung mask - only considering lung voxels. The blue curve is the histogram before shift test, and the red curve is the histogram after the shift test. Quantitative parameters of each metric were also displayed on the corner of figures. The vertical blue line in Figure 4.8 (d) is the pass criterion of gamma comparison.

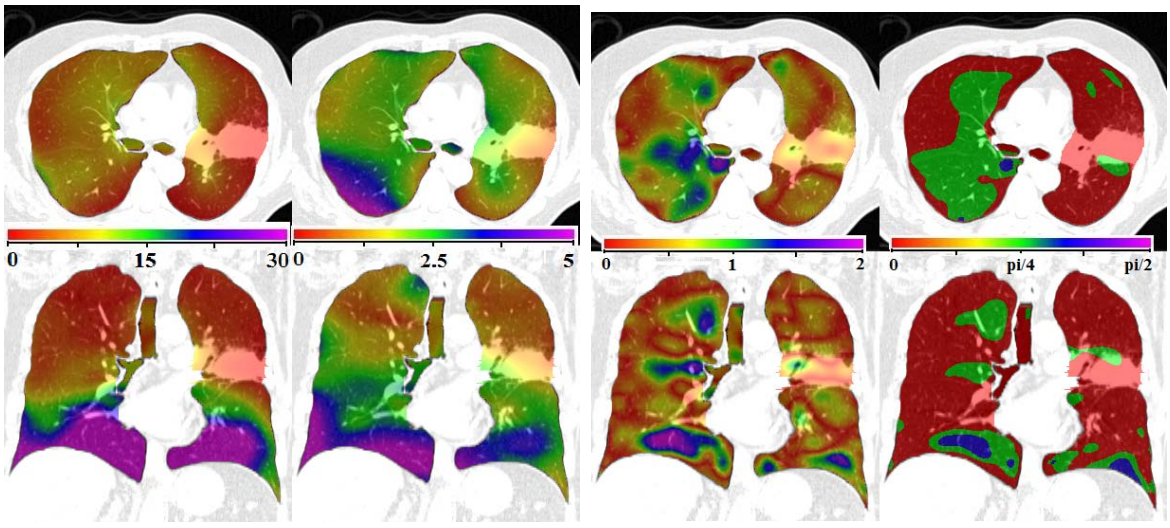

(a) (b)

Figure 4.5: Reproducibility metric color maps. (a) Color coded vector area (left) and vector subtract (right); (b)Color coded gamma value (left) and gamma angle (right).

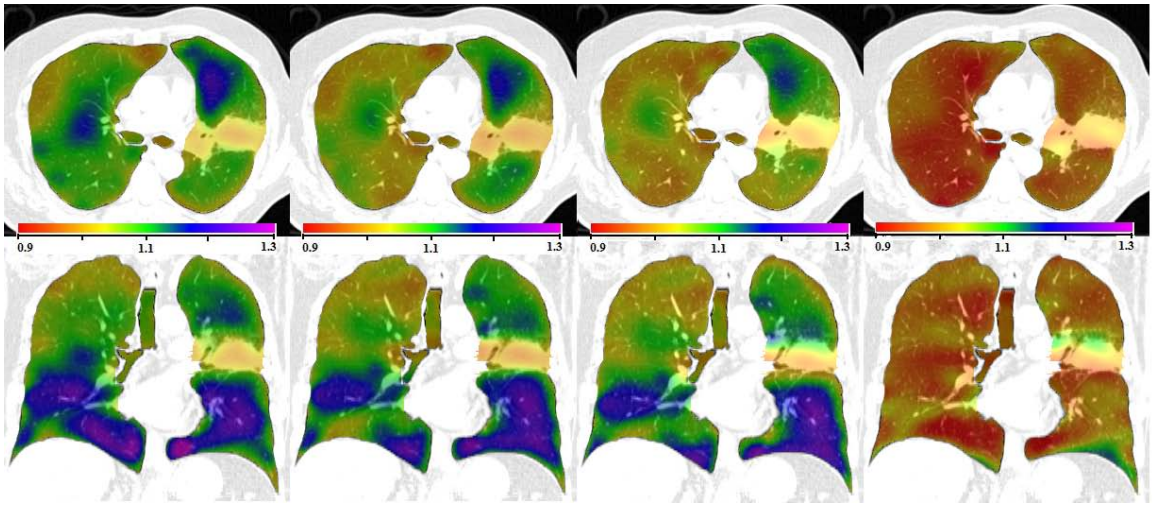

Figure 4.6: Transverse and coronal view of the shift test. From left to right they are JAC_{T1}, $T - JAC_{\mathrm{T2}}$ before shift, $T - JAC_{\mathrm{T2}}$ after shift and JAC_{RATIO} by after shift.

4.4 Discussion

We propose four kinds of metric to quantify the reproducibility of 4DCT-based pulmonary function measurement using image registration. The color map of the four metrics on one same subject were compared and the histograms of four metrics before and after the shift test were also analyzed. Compared to the other three metrics, the gamma method has the advantage of tolerating the spatial misalignment coming from imaging and image registration error.

The most straightforward metric is the simple voxel-to-voxel Jacobian ratio map from two prior-RT scans. We can directly observe from the Jacobian ratio map which regions are reproducible or not. But due to breath effort difference and uncertainties from spatial shift, the voxel-by-voxel Jacobian ratio map may not be accurate and cannot reflect actual pulmonary function reproducibility. If we compare

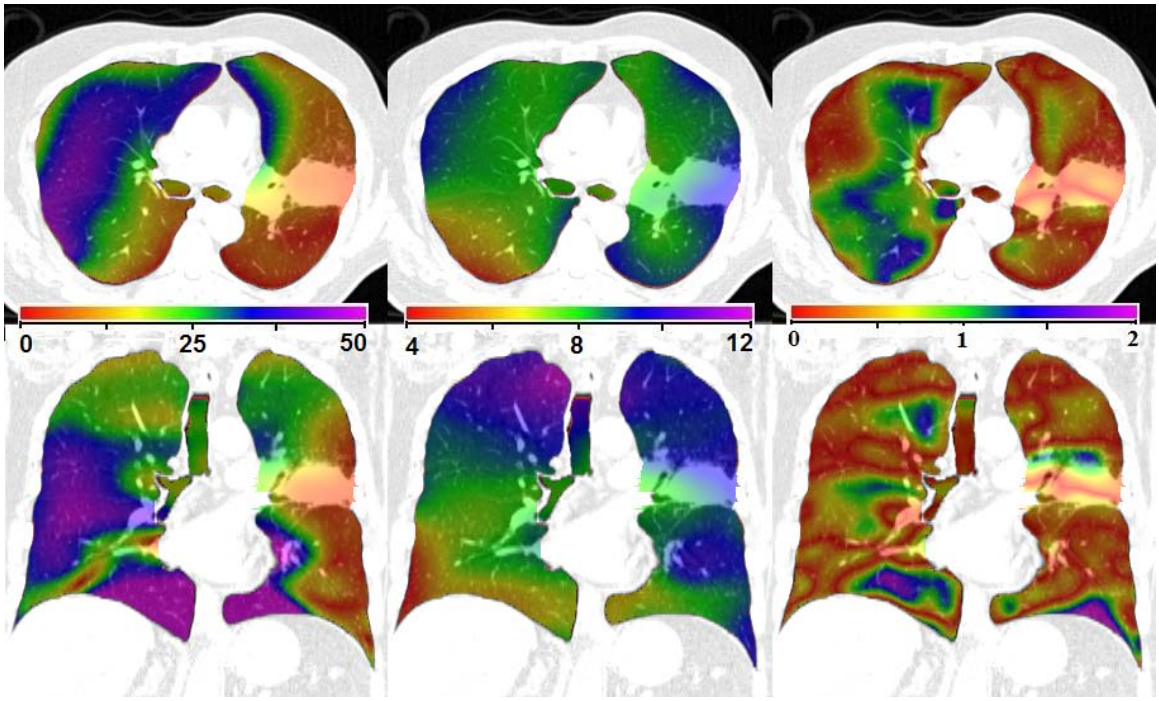

Figure 4.7: Reproducibility metric color maps after shift test. From left to right they are vector area, vector difference, and gamma value, after shift test.

figure 4.4 (d) and figure 4.6 (d), we can notice the obvious shift and deteriorated reproducibility especially near the regions with high gradient ventilation. Figure 4.8 (a) shows the degradation of convergence, in which the standard deviation increases from 3.59 percent to 4.35 percent, around 22% change.

The Jacobian map is directly computed from displacement field after image registration. The reproducibility of displacement field in two scans should interconnect with Jacobian reproducibility in two scans. By looking into the vector area and magnitude of vector difference, we convert the voxel motion inhomogeneity to a quantified value at each location, based on the assumption that each voxel should move in the same direction with same magnitude in the perfect case of reproducibil-

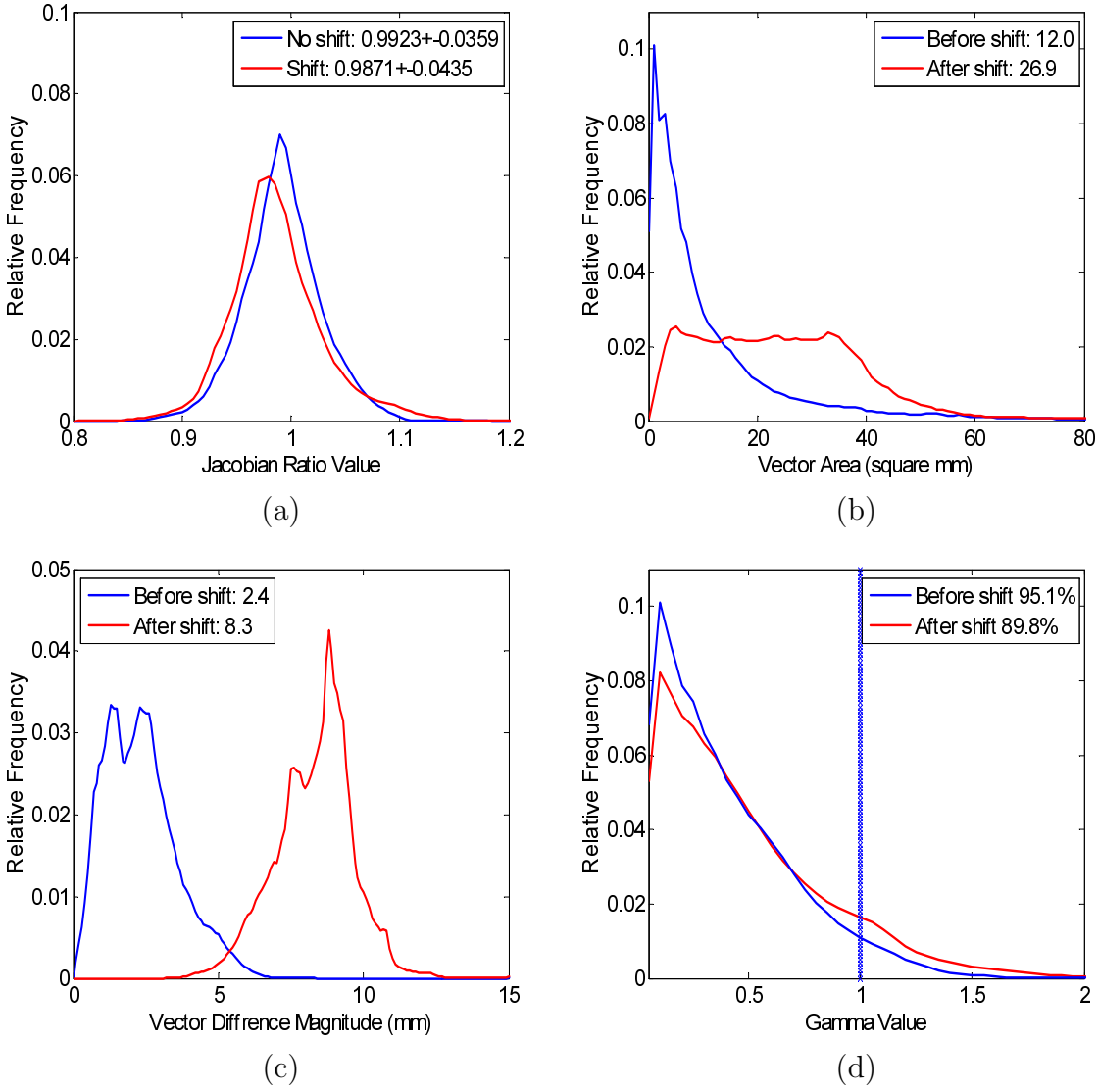

Figure 4.8: Histograms of four reproducibility metrics before and after shift test. (a) Jacobian ratio map JAC_{RATIO}; (b) Displacement field vector area; (c) Displacement field vector difference; (d) Gamma comparison values between JAC_{T1} and $T-JAC_{\mathrm{T2}}$;

ity. The larger the vector area and vector difference magnitude are, the worse the reproducibility. Figure 4.5 (a) shows that tissue near the bottom of lung is less reproducible, in consistent with jacobian ratio map. The gradient of vector area is larger than that of vector difference magnitude because vector area is more related to the magnitude of two vectors themselves. The ventilation distribution in the lung from top to bottom has been proved that ventilation near the bottom is larger. Therefore the vector magnitude is larger. Suppose with the same vector difference, the vector area is more sensitive to the nonreproducibility than the vector difference magnitude. The vector-related metrics are most affected by the spatial disalignment. From figure 4.7 and figure 4.8 (b) and (c), obvious increase of vector area and vector difference were noticed after the shift test on purpose.

The essence of gamma comparison method is a balance between distance-to-agreement (DTA) and Jacobian value tolerance. Since there are many uncertainties i.e. in image acquisition, CT reconstruction and image registration, the Jacobian map probably mismatch precisely voxel to voxel at some locations. Moreover, in practice voxel-by-voxel Jacobian is not necessary and probably meaningless most of the time, since there are no other clinical measurement to verify Jacobian in such detail. For example, the radiation dose map was compared to Jacobian ratio map before and after radiation therapy [11]. But the resolution of dose map is only 4 mm $\times$ 4 mm $\times$ 4 mm, while the Jacobian map is on the scale of 1 mm resolution. Therefore for each voxel in Jacobian scan1, as long as it can find a intensity-similar voxel in Jacobian scan2 at a acceptable distance, then we would say this is a "pass" voxel. That is

why we used 4 mm as the distance criterion in our gamma comparison method. The pass region percent of the whole lung can be used as a quantitative parameter of reproducibility, like the standard deviation of Jacobian ratio map. The gamma color map in figure 4.5 (b) on the left shows regional gamma distribution. Purple and blue voxels with gamma value larger than 1.0 imply that these voxels cannot find a corresponding voxel in the other Jacobian distribution within predefined distance tolerance and Jacobian tolerance. From the angle map on the right, we can find that most failed voxels are related to a large gamma angle which means the voxel finally find a voxel far away from the location, i.e. the distance factor is dominant. After the shift test, the gamma map in figure 4.7 has less changes than the Jacobian ratio map. Also the histograms in figure 4.8 (d) show that the pass% changes from 95.1 to 89.8, around 5.5% percent change. Gamma method tries to find similar Jacobian values in the neighborhood locations, and marks it as pass voxel as long as the distance to agreement (DTA) can tolerate the spatial misalignment. The gamma method is more appropriate for ventilation comparison.

In conclusion, in this chapter we proposed four metrics to assess reproducibility level of pulmonary function map in lung 4DCT. The four metrics all present good reproducibility of given subject with different emphasis. Vector area and magnitude of vector subtract tell more about the registration displacement field reproducibility. The Jacobian ratio map is the most straightforward and simple method to compare two ventilation maps. The gamma comparison method can tolerate the spatial shift in different scans and compensate the mutations in Jacobian map. In the shift test, the

vector-based metrics are most sensitive, and Jacobian ratio map is also considerably affected by the shift, while the gamma method has the smallest changes.

CHAPTER 5
SUMMARY AND CONCLUSIONS

This chapter is a summary of the thesis, with future work proposal.

5.1 Summary of Results

In this thesis, we studied regional pulmonary function measurement method and analysis of pulmonary function on both animals and human. Reproducibility of regional pulmonary function in 4DCT is established and four reproducibility metrics are proposed.

5.1.1 Dynamic Lung Ventilation Analysis of 4DCT Using Image Registration

The use of multiple respiratory phase images from 4DCT allows instantaneous ventilation maps to be produced and the maximum ventilation phase to be identified regionally. We have described a new scheme for measuring instantaneous ventilation at each phase within respiratory cycle from a regularized tissue volume and vesselness preserving image registration of 4DCT phase images. $t_{MIV}(\mathbf{x})$ and $t_{MEV}(\mathbf{x})$ are used to represent the phase when a local region reaches its highest inspiring ventilation and highest expiring ventilation separately. The maximum ventilation is verified by a significance check. The ventilation variation is quantified using the distribution of volume ratio of voxels that reach to $\dot{V}_{max}(\mathbf{x}, t_i)$ at different phase. 39% of the total lung volume reaches maximum ventilation at T_1 to T_2 during inspiration and

the 75% of the total lung volume reaches max ventilation at T_4 to T_5 during expiration. About 200 anatomical landmarks are identified and annotated to evaluate the registration accuracy. The average landmark error is on the order of 1 mm after registration. The distribution of phases at which regions reaches highest ventilation is more homogeneous at expiration than the inspiration. This is consistent with our expectation and global mouth pressure measurement since during tidal breathing, the lung usually releases most of the expired gas within the short time period at the beginning of the expiration while in inspiration it typically takes more time to reach to its tidal volume. From 75%EX to 100%IN, the dorsal lung exhales more than ventral part. The interesting symmetric curves from 75%EX to 100%IN and from 100%IN to 0%IN indicates the active regions are almost the same in the inspiration and the first expiratory phase. Basically larger standard deviation corresponds to lower mean value, showing that lung tissue undergoing more ventilation would have larger lung function variance. At both ROIs near the diaphragm and near the middle lung, the results show the dorsal lung tissue is more active than the ventral. If we compare the ventral-dorsal distribution near the diaphragm and near the middle, the middle lung tissue looks more monotonous than lung tissue near the diaphragm.

5.1.2 Reproducibility of 4DCT Pulmonary Function Measurement Using Image Registration

We described a method to study regional reproducibility of pulmonary function measurement using 4DCT imaging and image registration before radiation therapy, and discussed approaches such as volume matching to improve reproducibility.

Homogeneous Jacobian normalization based on lung volume ratio is presented to compensate various breath effort in 4DCT scan. We demonstrates the significance of registration-based measurement of lung function change before and after radiation therapy, and supports the study on the relationship between radiation dose distribution and pulmonary function change. The excellent reproducibility of regional ventilation measurement in animal data demonstrates the importance of breath control in 4DCT imaging. The human data appears not so reproducible as the animal data. The standard deviation of JAC_{RATIO} for human subjects is on the order of 3.6 percent to 7.6 percent (on average 5.8 percent), while that for animal subjects is less than 2.6 percent (on average 2.1 percent). The scatter plot distribution is also more biased against the regression line and y=x line. The deteriorated reproducibility in human subjects is understandable because regional deformation of human lung tissue is a very complex process during respiratory without mechanically ventilation as we did on sheep subjects. The reproducibility of ventilation measurement are affected by many factors, like breath effort control, breathing patterns difference and radiation-induced tissue change. We can match the tidal volume or match the head-and-tail volumes in two scans. After both volume matching methods, the scatter plot goes more closely along the regression line and y=x line, Jacobian histograms appears in a more similar pattern in 2 scans, and JAC_{RATIO} histogram is more Gaussian-like. The coefficient of variation (CV) of JAC_{RATIO} reduces by 0.8 percent after tidal volume matching, and 2.6 percent after head-and-tail volume matching indicating bettter improvement of reproducibility. Another approach to reduce the affect of breathing

effort to reproducibility is to normalize the Jacobian in different volume change. The advantage of this method is that whenever we get a third 4DCT scan of the same patient after RT, we can check the reproducibility or lung function change before and after RT using Jacobian normalization, without considering the variant tidal volume in different 4DCT scans. Jacobian normalization in provides a way to offset the influence of breathing effort difference in lung 4DCT scans.

5.1.3 Metrics for Reproducibility Assessment On 4DCT-based Pulmonary Function

We proposed four metrics to assess reproducibility level of pulmonary function map in lung 4DCT. Besides simple voxel-to-voxel Jacobian ratio map, displacement field reproducibility metric and a novel gamma comparison method is introduced for combination of distance factor and intensity difference. The four metrics all present reproducibility of given subject besides nuance in distribution pattern. The most straightforward metric is the simple voxel-to-voxel Jacobian ratio map from two prior-RT scans. We can directly observe from the Jacobian ratio map which regions are reproducible or not. But due to breath effort difference and uncertainties from spatial shift, the voxel-by-voxel Jacobian ratio map may not be accurate and cannot reflect actual pulmonary function reproducibility. By looking into the vector area and magnitude of vector difference, we convert the voxel motion inhomogeneity to a quantified value at each location, based on the assumption that each voxel should move in the same direction with same magnitude in the perfect case of reproducibility. The larger the vector area and vector difference magnitude are, the worse the reproducibility.

The vector-related metrics are most affected by the spatial disalignment. Obvious increase of vector area and vector difference were noticed in the histograms after the made shift test. The essence of gamma comparison method is a balance between distance-to-agreement (DTA) and Jacobian value tolerance. Therefore for each voxel in Jacobian scan1, as long as it can find a intensity-similar voxel in Jacobian scan2 at a acceptable distance, then we would say this is a "pass" voxel. After the shift test, the gamma map has less changes than the Jacobian ratio map. Also the histograms in show that the pass% changes from 95.1 to 89.8, around 5.5% percent change, less than Jacobian ratio map change.

In the future work, first our image registration algorithm still needs to be improved in registration accuracy and speed. Regional pulmonary function change before and after radiation therapy will be launched based on our reproducibility research. Construction of a 4D lung statistic model based on time-varying multiple respiratory phases registration could be another interesting topic to be studied with.

REFERENCES

[1] Anaethesia, FRCA. http://www.frca.co.uk/ (accessed June 14, 2010).

[2] R. H. Byrd, P. Lu, J. Nocedal, and C. Zhu. A limited memory algorithm for bound constrained optimization. *SIAM J. Sci. Comput.*, 16(5):1190–1208, 1995.

[3] Kunlin Cao, Gary E. Christensen, Kai Ding, and Joseph M. Reinhardt. Intensity-and-Landmark-Driven, Inverse Consistent, B-Spline Registration and Analysis for Lung Imagery. In *Second International Workshop on Pulmonary Image Analysis*, 2009.

[4] Kunlin Cao, Kai Ding, Gary E. Christensen, and Joseph M. Reinhardt. Tissue volume and vesselness measure preserving nonrigid registration of lung CT images. In *In Fischer, B., Dawant, B., Lorenz, C., eds.: Biomedical Image Registration, Lubeck*, 2010.

[5] Kunlin Cao, Kaifang Du, Kai Ding, Joseph M. Reinhardt, and Gary E. Christensen. Regularized nonrigid registration of lung CT images by preserving tissue volume and vesselness measure. In *2010 MICCAI workshop*, 2010.

[6] Richard Castillo, Edward Castillo, Josue Martinez, and Thomas Guerrero. Ventilation from four-dimensional computed tomography: Density versus Jacobian methods. *Physics in Medicine and Biology*, 55(16):4661–4685, 2010.

[7] Yongchoel Choi and Seungyong Lee. Injectivity conditions of 2D and 3D uniform cubic b-spline functions. *Graphical Models*, 62(6):411–427, 2000.

[8] Deokiee Chon, Brett A. Simon, Kenneth C. Beck, Hidenori Shikata, Osama I. Saba, Chulho Won, and Eric A. Hoffman. Differences in regional wash-in and wash-out time constants for xenon-CT ventilation studies. *Respiratory Physiology & Neurobiology*, 148(1-2):65 – 83, 2005.

[9] Gary E. Christensen, J. H. Song, W. Lu, I. El Naqa, and D. A. Low. Tracking lung tissue motion and expansion/compression with inverse consistent image registration and spirometry. *Med Physics*, 34(6):2155–2165, June 2007.

[10] W R Crum and T Hartkens. Non-rigid image registration: Theory and practice. *British Journal of Radiology*, 77:140–153, 2004.

[11] Kai Ding, John E. Bayouth, John M. Buatti, Gary E. Christensen, and Joseph M. Reinhardt. 4DCT-based measurement of changes in pulmonary function following a course of radiation therapy. *Med. Phys.*, 37(3):1261–1273, 2010.

[12] Kai Ding, Kunlin Cao, Gary E. Christensen, Eric A. Hoffman, and Joseph M. Reinhardt. Registration-based regional lung mechanical analysis: Retrospectively reconstructed dynamic imaging versus static breath-hold image acquisition. volume 7262, page 72620D. SPIE, 2009.

[13] Dennis E. Doherty. A review of the role of FEV1 in the COPD paradigm. *COPD: Journal of Chronic Obstructive Pulmonary Disease*, 5:310–318, 2008.

[14] Alejandro F. Frangi, Wiro J. Niessen, Koen L. Vincken, and Max A. Viergever. Multiscale vessel enhancement filtering. In *MICCAI*, volume 1496, pages 130–137, 1998.

[15] Matthew K. Fuld, R. Blaine Easley, Osama I. Saba, Deokiee Chon, Joseph M. Reinhardt, Eric A. Hoffman, and Brett A. Simon. CT-measured regional specific volume change reflects regional ventilation in supine sheep. *J Appl Physiol*, 104(4):1177–1184, 2008.

[16] Vladlena Gorbunova, Pechin Lo, Haseem Ashraf, Asger Dirksen, Mads Nielsen, and Marleen de Bruijne. Weight preserving image registration for monitoring disease progression in lung CT. In *MICCAI*, volume 5242, pages 863–870, 2008.

[17] Thomas Guerrero, Richard Castillo, Josue Noyola-Martinez, Mylin Torres, Xinhui Zhou, Rudy Guerra, Dianna Cody, Ritsuko Komaki, and Elizabeth Travis. Reduction of pulmonary compliance found with high-resolution computed tomography in irradiated mice. *International Journal of Radiation Oncology*Biology*Physics*, 67(3):879 – 887, 2007.

[18] Thomas Guerrero, Kevin Sanders, Edward Castillo, Yin Zhang, L. Bidaut, and T. Pan R. Komaki. Dynamic ventilation imaging from four-dimensional computed tomography. *Phys Med Biol.*, 51(4):777–791, Feb. 21 2006.

[19] Thomas Guerrero, Kevin Sanders, Josue Noyola-Martinez, Edward Castillo, Yin Zhang, Richard Tapia, Rudy Guerra, Yerko Borghero, and Ritsuko Komaki. Quantification of regional ventilation from treatment planning CT. *International Journal of Radiation Oncology*Biology*Physics*, 62(3):630 – 634, 2005.

[20] Dongfeng Han, John E. Bayouth, Sudershan Bhatia, Milan Sonka, and Xiaodong Wu. Motion artifact reduction in 4D helical CT: Graph-based structure alignment. In *MICCAI Workshop on Medical Computer Vision 2010*, 2010.

[21] R. Scott Harris and Daniel P. Schuster. Visualizing lung function with positron emission tomography. *J Appl Physiol*, 102(1):448–458, 2007.

[22] E. A. Hoffman and E. L. Ritman. Effect of body orientation on regional lung expansion in dog and sloth. *J Appl Physiol*, 59(2):481–491, 1985.

[23] E.A. Hoffman, T. Behrenbeck, P.A. Chevalier, and E.H. Wood. Estimation of pleural surface expansile forces in intact dogs. *Journal of Applied Physiology*, 55(3):935–948, 1983.

[24] Eric A. Hoffman, Rui Jiang, Heather Baumhauer, Michael A. Brooks, J. Jeffrey Carr, Robert Detrano, Joseph Reinhardt, Josanna Rodriguez, Karen Stukovsky, Nathan D. Wong, and R. Graham Barr. Reproducibility and validity of lung density measures from cardiac CT scans–the multi-ethnic study of atherosclerosis MESA lung study1. *Academic Radiology*, 16(6):689 – 699, 2009.

[25] Eric A. Hoffman, Joseph M. Reinhardt, Milan Sonka, Brett A. Simon, Junfeng Guo, Osama Saba, Deokiee Chon, Shaher Samrah, Hidenori Shikata, Juerg Tschirren, Kalman Palagyi, Kenneth C. Beck, and Geoffrey McLennan. Characterization of the interstitial lung diseases via density-based and texture-based analysis of computed tomography images of lung structure and function. *Academic Radiology*, 10(10):1104 – 1118, 2003.

[26] Eric A. Hoffman and Edwin van Beek. Hyperpolarized media MR imaging - expanding the boundaries? *Academic Radiology*, 13(8):929–931, 2006.

[27] R. D. Hubmayr, Walter Bosch, P.A. Chevalier, J. R. Rodarte, and L. Olson. Topographical distribution of regional lung volume in anesthetized dogs. *Journal of Applied Physiology*, 54(4):1048–1056, 1983.

[28] Luis Ibanez, William Schroeder, Lydia Ng, and Josh Cates. *The ITK Software Guide*. Kitware, Inc, 2005.

[29] Daniel A. Low and James F. Dempsey. Evaluation of the gamma dose distribution comparison method. *Medical Physics*, 30:2455–2464, 2003.

[30] Catherine Marcucci, Daniel Nyhan, and Brett A. Simon. Distribution of pulmonary ventilation using Xe-enhanced computed tomography in prone and supine dogs. *J Appl Physiol*, 90(2):421–430, 2001.

[31] Sarah M. McGuire, Sumin Zhou, Lawrence B. Marks, Mark Dewhirst, Fang-Fang Yin, and Shiva K. Das. A methodology for using SPECT to reduce intensity-modulated radiation therapy (IMRT) dose to functioning lung. *International Journal of Radiation Oncology*Biology*Physics*, 66(5):1543 – 1552, 2006.

[32] Vivek Mehta. Radiation pneumonitis and pulmonary fibrosis in non-small-cell lung cancer: Pulmonary function, prediction, and prevention. *International Journal of Radiation Oncology*Biology*Physics*, 63(1):5 – 24, 2005.

[33] Harald E. Moller, X. Josette Chen, Brian Saam, Klaus D. Hagspiel, G. Allan Johnson, Talissa A. Altes, Eduard E. de Lange, and Hans-Ulrich Kauczor. MRI of the lungs using hyperpolarized noble gases. *Magnetic Resonance in Medicine*, 47(6):1029–1051, 2002.

[34] K. Murphy, B. van Ginneken, J.P.W. Pluim, S. Klein, and M. Staring. Semi-automatic reference standard construction for quantitative evaluation of lung CT registration. In *Proc. of International Conference on Medical Image Computing and Computer-Assisted Intervention 2008*, volume 5242, pages 1006–1013, 2008.

[35] P.C. Pratt. *Emphysema and chronic airways disease*, pages 654–659. Springer-Verlag, 1998. edited by D. Dail and S. Hammar.

[36] Joseph M. Reinhardt, Kai Ding, Kunlin Cao, Gary E. Christensen, Eric A. Hoffman, and Shalmali V. Bodas. Registration-based estimates of local lung tissue expansion compared to xenon CT measures of specific ventilation. *Medical Image Analysis*, 12(6):752 – 763, 2008. Special issue on information processing in medical imaging 2007.

[37] H.T. Robertson, R.W. Glenny, D. Stanford, L.M. Mclnnes, D.L. Luchtel, and D. Covert. High-resolution maps of regional ventilation utilizing inhaled fluorescent microspheres. *Journal of Applied Physiology*, 82(3):943–953, 1997.

[38] D. Rueckert, L.I. Sonoda, C. Hayes, D.L.G. Hill, M.O. Leach, and D.J. Hawkes. Nonrigid registration using free-form deformations: application to breast mr images. *Medical Imaging, IEEE Transactions on*, 18(8):712 –721, aug. 1999.

[39] Linda Sarna, Lorraine Evangelista, Donald Tashkin, Geraldine Padilla, Carmack Holmes, Mary Lynn Brecht, and Fred Grannis. Impact of respiratory symptoms and pulmonary function on quality of life of long-term survivors of non-small cell lung cancer. *Chest*, 125:439–445, 2004.

[40] D. P. Schuster. Positron emission tomography: Theory and its application to the study of lung disease. *Am. Rev. Respir. Dis.*, 139:818–40, 1989.

[41] J. K. Tajik, D. Chon, C.-H. Won, B. Q. Tran, and E. A. Hoffman. Subsecond multisection CT of regional pulmonary ventilation. *Academic Radiology*, 9:130–146, 2002.

[42] Edwin J.R. van Beek, Jim M. Wild, Hans-Ulrich Kauczor, Wolfgang Schreiber, John P. Mugler III, and Eduard E. de Lange. Functional MRI of the lung using hyperpolarized 3-helium gas. *Journal Of Magnetic Resonance Imaging*, 20(4):550–554, 2004.

[43] Jose G. Venegas, Tilo Winkler, Guido Musch, Marcos F. Vidal Melo, Dominick Layfield, Nora Tgavalekos, Alan J. Fischman, Ronald J. Callahan, Giacomo Bellani, and R. Scott Harris. Self-organized patchiness in asthma as a prelude to catastrophic shifts. *Nature*, 7034(2-3):777–782, 2005.

[44] T.J. Waldron, J.E. Bayouth, S. Bhatia, and J.M. Buatti. Use of music-based breathing training to stabilize breathing motion in respiration correlated imaging and radiation delivery. *International Journal of Radiation Oncology*Biology*Physics*, 72(1, Supplement 1):S659 – S659, 2008.

[45] T.J. Wellman, T. Winkler, E.L.V. Costa, G. Musch, R. S. Harris, J. G. Venegas, and M. F. V. Melo. Measurement of regional specific lung volume change using respiratory-gated PET of inhaled 13N-nitrogen. *J. Nucl. Med.*, 51:646–53, 2010.

[46] J.M. Wild, M. N. J. Paley, L. Kasuboski, A. Swift, S. Fichele, N. Woodhouse, P.D. Griffiths, and E. J. R van Beek. Dynamic radial projection mri of inhaled hyperpolarized 3he gas. magnetic resonance in medicine. *official journal of the Society of Magnetic Resonance in Medicine / Society of Magnetic Resonance in Medicine*, 49(6):991–997, 2003.

[47] N. Woodhouse, J.M. Wild, M. N.J. Paley, S. Fichele, Z. Said, A.J. Swift, and E. J. R van Beek. Combined helium-3/proton magnetic resonance imaging measurement of ventilated lung volumes in smokers compared to never-smokers. *Journal of magnetic resonance imaging*, 21(4):365–369, 2005.

[48] Tokihiro Yamamoto, Sven Kabus, Tobias Klinder, Cristian Lorenz, Jens von Berg, Thomas Blaffert, Billy W Loo Jr, and Paul J. Keall. Investigation of four-dimensional computed tomography-based pulmonary ventilation imaging in patients with emphysematous lung regions. *Physics in Medicine and Biology*, 56:2279–2298, 2011.

[49] Tokihiro Yamamoto, Sven Kabus, Jens von Berg, Cristian Lorenz, and Paul J. Keall. Impact of four-dimensional computed tomography pulmonary ventilation imaging-based functional avoidance for lung cancer radiotherapy. *Int. J. Radiation Oncology Biol. Phys.*, 2:1–10, 2010.

[50] Brian P. Yaremko, Thomas M. Guerrero, Josue Noyola-Martinez, Rudy Guerra, David G. Lege, Linda T. Nguyen, Peter A. Balter, James D. Cox, and Ritsuko Komaki. Reduction of normal lung irradiation in locally advanced non-small-cell lung cancer patients, using ventilation images for functional avoidance. *International Journal of Radiation Oncology*Biology*Physics*, 68(2):562 – 571, 2007.

[51] Youbing Yin, Eric A. Hoffman, and Ching-Long Lin. Local tissue-weight-based nonrigid registration of lung images with application to regional ventilation. volume 7262, page 72620C. SPIE, 2009.

[52] Youbing Yin, Eric A. Hoffman, and Ching-Long Lin. Mass preserving nonrigid registration of CT lung images using cubic B-spline. *Medical Physics*, 36(9):4213–4222, 2009.

[53] Youbing Yin, Eric A. Hoffman, and Ching-Long Lin. Mass preserving nonrigid registration of CT lung images using cubic B-spline. *Medical Physics*, 36(9):4213–4222, 2009.

[54] Junan Zhang, Jinli Ma, Sumin Zhou, Jessica L. Hubbs, Terence Z. Wong, Rodney J. Folz, Elizabeth S. Evans, Ronald J. Jaszczak, Robert Clough, and Lawrence B. Marks. Radiation-induced reductions in regional lung perfusion: 0.1-12 year data from a prospective clinical study. *Int. J. Radiation Oncology Biol. Phys.*, 76:425–432, 2010.